Complex system modelling reveals oxalate homeostasis is driven by diverse oxalate-degrading bacteria

Sromona D. Mukherjee[1], Carlos A. Batagello[2], Ava Adler[3], Jose Agudelo[1], Anna Zampini[3], Mangesh Suryavanshi[1], Andrew Nguyen[4], Teri Orr[5], Denise Dearing[6], Manoj Monga[7], Aaron W. Miller[1,3#]

[1]Department of Cardiovascular and Metabolic Sciences, Cleveland Clinic, Cleveland, OH, USA

[2]Division of Urology, Hospital das Clínicas, University of Sao Paulo Medical School, Sao Paulo, Brazil.

[3]Department of Urology, Glickman Urological and Kidney Institute, Cleveland Clinic, Cleveland, OH, USA

[4]M Health Fairview Southdale Hospital, Edina, MN, USA

[5]Department of Biology, New Mexico State University, Las Cruces, NM, USA

[6]School of Biological Sciences, University of Utah, Salt Lake City, UT, USA

[7]Department of Urology, University of California San Diego, San Diego, CA, USA

#*Corresponding author.* Email: millera25@ccf.org

Phone: 1 216 444 6584
Fax: 1 216 444 9329

Running head: Oxalate metabolism within a complex system framework

Keywords: oxalate, gut microbiome, kidney stones, urinary stone disease, dietary toxins, antinutrients, complex systems, functional redundancy, homeostatic feedback, diet-mirobe-host

Summary

Decades of research have made clear that host-associated microbiomes touch all facets of health. However, effective therapies that target the microbiome have been elusive given its inherent complexity. Here, we experimentally examined diet-microbe-host interactions through a complex systems framework, centered on dietary oxalate. Using multiple, independent molecular, animal, and *in vitro* experimental models, we found that microbiome composition influenced multiple oxalate-microbe-host interfaces. Importantly, administration of the oxalate-degrading specialist, *Oxalobacter formigenes,* was only effective against a poor oxalate-degrading microbiota background and gives critical new insights into why clinical intervention trials with this species exhibit variable outcomes. Data suggest that, while heterogeneity in the microbiome impacts multiple diet-host-microbe interfaces, metabolic redundancy among diverse microorganisms in specific diet-microbe axes is a critical variable that may impact the efficacy of bacteriotherapies, which can help guide patient and probiotic selection criteria in probiotic clinical trials.

Introduction

Research into the host-associated microbiome is at an inflection point. Decades of research have revealed that host-associated microbiomes are intimately linked to host health and touch all aspects of host physiology[1,2]. The first phase of microbiome research was focused on descriptive studies that characterized differences in the microbiome by host species, body site, and disease phenotypes[3-5]. Clinical case:control metagenome wide association studies that found differences in microbiome composition between healthy and disease cohorts gave rise to the ambiguous term “dysbiosis” and much of the literature is focused on “balancing” the gut microbiota[6]. In the second, and current, phase of research, studies have moved towards gaining more mechanistic insight into specific microbe-host interactions that influence host physiology and disease[6-9]. However, it is increasingly being recognized that, given the wide variability in microbiome composition, host genetics, and lifestyles, understanding mechanisms and causal relationships between gut bacteria and host physiological responses is not enough for the development of effective bacteriotherapies that target the gut microbiota[10,11]. In fact, many probiotic clinical trials, with known mechanistic links between the probiotics and host physiology, have exhibited wide variability in results[12-15]. It is currently unclear what sources of variability may drive the response to targeted bacteriotherapies. Some variables that have been proposed include heterogeneity in microbiome composition, alcohol consumption, and bowel movement quality[10].

Complex system theory is one means to potentially constrain hypotheses and bridge the gap between mechanistic studies and effective bacteriotherapies[16,17]. Studies of the host-associated microbiome often casually acknowledge that these systems are complex and, while, there has been progress made in developing mathematical approaches to complex modelling of host-microbiome relationships[16-19], few studies have bridged the gap between experimental biology and complex system theory. Mammals and their gut microbiome, are often considered as a holobiont[20], defined as a discrete unit that exhibits collective action and evolves as a unit. Using evolutionary theory approaches, it is hypothesized that the form and function of the microbial part of the holobiont is driven primarily by host-microbe influences, but which require microbe-microbe interactions to help manage the enormous burden of microbiome constraint, which is termed an “ecosystem on a leash”[21]. Under this hypothesis, microbe-host interactions, in which host-associated microbes evolve to produce metabolic by-products for the sole benefit of the host, are necessarily rare. Essential features of complex systems include functional redundancy[21,22] and cooperation through chains of direct interactions[21-23], distinct functional nodes that process and transfer resources[22,23], fractality[22,23], and adaptability through specific homeostatic feedback mechanisms to maintain relatively consistent internal conditions given a dynamic external environment[21,24]. While considerable progress has been made in understanding the nature of complex systems, there is a lack of consensus on basic terminology and broadly applicable analytical or experimental models[25]. This limitation is due in part because complex systems necessarily transect many divergent entities in nature and is thus studied in diverse scientific disciplines[25]. Thus, while some essential features of complexity have been elucidated within specific real-world systems, such as the conversion of polysaccharides to butyrate by multiple species in the gut[26], or feedback

loops in blood pressure regulation[27], experimental evidence of multiple features of complexity within a single system is sparse, especially in microbe-host systems.

To overcome the limitations of applying complex systems theory to the microbe-host holobiont, new models and experimental frameworks are needed that balance complexity with tractability. Antinutrients, produced in plants to deter herbivory, disrupt homeostasis by targeting the function of the microbiome, host, or both[28], and provide an effective focal point to study complexity. Oxalate is an antinutrient present in many plant-based foods, which typically provides the majority of oxalate in circulation[29], but is also produced as a terminal metabolite in the liver[30]. While some host genetic mutations increase endogenous production of oxalate[31], mammals do not produce enzymes capable of degrading oxalate[32]. However, multiple oxalate-degrading bacteria exist in the gut, which degrade oxalate through one of a handful of simple metabolic pathways involving one or two genes[33-35], which isolates this function to the gut microbiota. As such, oxalate degradation as a function, exhibits a moderate amount of complexity compared to other gut microbiota functions, such as the production of trimethylamine N-oxide (TMAO), that requires host input[36]. Beyond the moderate complexity, it is known that oxalate-degrading bacteria are susceptible to antibiotics and that antibiotic use decreases oxalate degradation[37-41]. Elevated levels of oxalate induce oxidative stress, activates the inflammasome, and disrupts epithelial barrier function through tight junction proteins[42-44]. This molecule has been linked to diseases including kidney stones and chronic kidney disease[45-47], breast cancer[48], and cardiometabolic disorders such as atherosclerosis[49], obesity[50], and diabetes[50]. *Oxalobacter formigenes,* which uses oxalate as a sole carbon and energy source[33], is a well-studied oxalate-degrading species of bacteria. The negative, at times lethal, effects of oxalate, along with the identification and mechanisms of oxalate-degrading bacteria in the gut, have been worked out for several decades[33,51-54], pre-dating the current microbiome era. Despite this knowledge, clinical intervention trials involving *Oxalobacter formigenes,* which is perhaps the most effective oxalate-degrading species known, have successfully resulted in a significant reduction in urine oxalate levels in only 43% of studies[15,55]. Oxalate-degrading lactic acid bacteria have been successful in 37.5% of studies[15]. Both treatments led to a wide variability in patient responses. Given these data and the well worked out mechanisms of oxalate metabolism, it is clear that having an understanding of the mechanistic links between the gut microbiota and host physiology, alone, is demonstrably not sufficient to develop effective bacteriotherapies. Therefore, even though the history of oxalate-microbe-host interactions is much greater than most other microbe-host systems, oxalate degradation represents an accurate reflection of the challenges faced by microbiome research and is a prime candidate for complex system modelling to understand the critical variables that determine responsiveness to bacteriotherapies.

The objectives of the current study were to evaluate oxalate-microbe-host interactions, within the framework of complex systems. We used multi-omic approaches utilizing multiple independent *in vivo* and *in vitro* models to understand the critical variables that influence the gut microbiota's maintenance of oxalate homeostasis and its impact on the host. We targeted several potential oxalate-microbe-host interfaces that include the gut

144 microbiota itself, which is one of the first lines of defense against antinutrients[56,57],
145 intestinal epithelium, which is an important barrier between microbe and host[21], the liver,
146 which is important for the biotransformation of dietary or microbial metabolites[58], along
147 with the kidneys and vasculature, where calcium oxalate can potentially form calcified
148 deposits or induce inflammation[49,59-61]. Collectively, data indicate that multiple oxalate-
149 microbe-host interfaces are influenced significantly by gut microbiota composition and
150 that harboring diverse microorganisms capable of degrading oxalate can limit the impact
151 of *O. formigenes* as a probiotic. Based on results from this study, we propose a phased
152 approach for the development of bacteriotherapies whereby clinical case:control studies
153 determine whether or not a clinical phenotype is associated with the microbiome and
154 the microbial taxa/functions associated with specific phenotypes (Phase I).
155 Hypothesized taxa and/or microbial functions should be mechanistically resolved
156 through *in vitro* and germ-free animal studies (Phase II). Finally, mechanistic insights
157 should be applied to a complex systems theoretical framework to identify those
158 variables that most impact the potential success of bacteriotherapies (Phase III). Such a
159 phased approach would have broad implications for patient and probiotic selection in
160 the development of targeted bacteriotherapies.
161
162 **Results**
163
164 *Defining the oxalate-microbe-host as a complex system*
165 To use complex system modelling as a means to identify the most pertinent variables
166 that impact oxalate-microbe-host interactions, we first had to define the system as a
167 series of nodes, whereby oxalate is processed, connections, where the end-product of
168 one node is transferred to another node, and fractals, which are autonomous subunits
169 or layers that exhibit analogous, but unique, functions to other layers. For antinutrients,
170 such as oxalate, we can define four unique nodes where these molecules can either be
171 transformed or where they can transform the host. The first node is the stomach where
172 the low pH can biotransform some molecules, such as glucosinolates[62]. Some
173 proportion of the molecules can be absorbed into the circulation in the stomach.
174 Stomach contents are then transferred to the intestines, the second node, where they
175 are first exposed to high densities of gut bacteria, particularly in the colon. Within the
176 gut microbiota, there are two fractal layers that include microbial species and the genes
177 within each species. In each of these fractal layers, there are three hypotheses that can
178 be generated about how microbes can degrade oxalate or other antinutrients. These
179 include a) one species/gene, one function; b) multiple species/genes, one function; or c)
180 multiple species, multiple functions. Canonically, the hypothesis is that one single
181 species, *O. formigenes,* is primarily responsible for oxalate degradation[63], which is
182 achieved through a two gene metabolic pathway (oxalyl-CoA decarboxylase and formyl-
183 CoA transferase)[53,54]. However, more recent studies show that many species of gut
184 bacteria degrade oxalate and multiple metabolic pathways can be used to degrade
185 oxalate that comprise of one or two genes[34,35,64,65]. Furthermore, studies have shown
186 that there are broad interactions between the gut microbiota and oxalate degradation[66-
187 72]. Finally, two of the most common by-products of oxalate degradation are CO_2 and
188 formate. Importantly, these by-products can be used in downstream metabolic
189 pathways such as acetogenesis, methanogenesis, and sulfate-reduction[73-76]. Given the

190 inconsistent results in *O. formigenes* trials and the recognition that there are broad gut
191 microbiota-oxalate interactions that maintain oxalate homeostasis, we can hypothesize
192 that, instead of relying on a single species, oxalate homeostasis is maintained either by
193 diverse oxalate-degrading bacteria or by cooperative networks whereby a small number
194 of oxalate-degrading bacteria produce substrates to be used in downstream metabolic
195 pathways (i.e. multiple species, one function or multiple species, multiple functions).
196 Again, some proportion of oxalate in the intestines gets absorbed into circulation or is
197 excreted in the stool. However, oxalate can also be secreted back into the gut through
198 transporters such as SLC26a6[77,78]. Another proportion of the molecule can be
199 transported through the portal vein to the liver for hepatic biotransformation[79].
200 Importantly, for oxalate, the liver is a source, rather than a sink[32]. However, for other
201 molecules, such as trimethylamine that is produced by gut bacteria, the liver is critical
202 for converting the molecule to the more pathogenic TMAO form[36]. Some complex
203 antinutrients, such as creosote, require both the gut microbiota and the liver[80]. The liver
204 can also be divided into fractal layers based on cell type and genes. Oxalate or other
205 antinutrients that are neither excreted in the stool, nor degraded by the gut microbiota,
206 nor degraded by the liver, can impact one or more organs and interact with the host
207 through localized immune responses, with the remaining being excreted in the urine.
208 As such, this model sets up multiple testable hypotheses, which are explored in depth,
209 below.
210
211 *Constitutive and oxalate-dependent effects of the microbiome impact host hepatic gene*
212 *expression*
213 Both the gut microbiota and the liver are important organs for the neutralization of
214 antinutrients[58,81], indicative of functional redundancy, cooperation, and fractality. While
215 it is known that the liver does not degrade oxalate itself, it could still be impacted by
216 oxalate, in gut microbiota dependent ways. To determine the effects of oxalate
217 exposure and microbiome on host hepatic gene expression, we used a fecal transplant
218 model to examine different host microbiomes with the same host genetics. Specifically,
219 a five-day course of neomycin was used to suppress the native gut microbiota of Swiss-
220 Webster mice (SWM)[38], followed by fecal transplants either from SWM (allograft; SW-
221 SW) or *N. albigulia* (NALB), which has a highly effective and transferable oxalate-
222 degrading gut microbiota[68,69,72], (xenograft; SW-NALB). Subsequently, animals were
223 fed either a 0% or 1.5% oxalate diet (Evigo, Fig. 1A, Table S1). Liver tissue was
224 obtained after three weeks and processed for bulk RNAseq. The RNAseq data analyses
225 revealed constitutive microbiome and microbiome-dependent oxalate effects (Fig.
226 1B,C), whereby SW-SW mice exhibited an oxalate-dependent alteration of 219 hepatic
227 genes, with a net increase in activity, while the SW-NALB mice exhibited an oxalate-
228 dependent alteration of 21 genes with a net decrease in activity (Fig. 1C, Table S2). In
229 the SW-NALB mice, the primary response was a decrease in sulfation activity with
230 oxalate exposure, which is involved in the deactivation, detoxication, and excretion of
231 xenobiotics (Fig 1C), and suggests oxalate may be beneficial for this host-microbe
232 system[82]. The primary response in the SW-SW mice was an increase in mitochondrial
233 activity, translation, protein regulation, and ribosome biogenesis, indicative of oxalate-
234 induced hepatic stress[49,83]. Since hosts only differed by gut microbiota composition,
235 these data demonstrate causative interactions between the gut microbiota and liver

activity through oxalate-dependent and independent pathways. Within the framework of complex systems, results show microbe-host cooperation whereby oxalate effectively processed within the SW-NALB gut microbiota reduced overall liver activity, indicative of a beneficial impact. Data also suggest that both the gut microbiota and the immune system are involved in oxalate remediation (redundancy), such that if oxalate cannot be neutralized in the gut microbiota or liver, then the molecule will be processed through host immune response mechanisms (fractality), in this case indicated through an overall increase in hepatic activity and specifically in mitochondrial activity.

Constitutive and oxalate-dependent effects of the microbiome impact microbial metabolic activity in the gut

Microbe-microbe interactions are important features of the microbe-host holobiont within the conext of complex systems, both in terms of constraining the microbiome and in processing dietary components[21,22,26,56]. To assess changes to microbial metabolic output with oxalate exposure, we used the same animals as above. Following the diet trial, colon stool was collected post-necropsy and processed for untargeted metabolomics, which is a measure of total microbial metabolic output. Collectively, results are indicative of constitutive microbiome and microbiome-dependent oxalate effects (Fig. 2A,B). The SW-SW mice exhibited an alteration of 162 microbial metabolites upon oxalate exposure, with a net decrease in activity compared to the no oxalate group, whereas the SW-NALB mice exhibited an alteration of 83 microbial metabolites, with a net increase in activity compared to the no oxalate group (Fig. 2B, Table S3). In SW-NALB mice, the primary response was an increase in lipid metabolism and a shift (increase/decrease) in fatty acid, secondary metabolite, and alkaloid profiles. In the SW-SW mice, the primary response was an increase in fatty acid synthesis and phenylalanine metabolism, and a decrease in synthesis of secondary metabolites, cholesterol, and alkaloids (Fig. 2B). Therefore, while oxalate had a much greater impact on gut microbial metabolism in SW-SW mice overall, the metabolic pathways impacted were similar. Net changes in microbial metabolites produced are indicative of a negative impact of oxalate on microbial activity in SW-SW and positive impact in SW-NALB mice. Integration of host hepatic gene expression and gut metabolomic data shows that oxalate induces a small decrease in hepatic activity overall for SW-NALB mice and a large increase in hepatic activity for SW-SW mice (Fig. 2C, Table S4). From a complex systems perspective, data reflect a causative effect of oxalate for the shift in microbial metabolic output. Specifically, the SW-NALB mice exhibit hallmarks of homeostatic feedback with oxalate exposure to maintain a consistent metabolic output, defined by the relatively small, net negative, microbial metabolite-hepatic gene network compared to the large, net positive, network of SW-SW mice. Additionally, data further support the cooperation, redundancy, and fractality of the gut-liver axis. While SW-NALB exhibit a small increase in microbial metabolic activity and decrease in liver activity, the SW-SW mice saw a large decrease in microbial metabolic activity, coupled with a large increase in hepatic activity, which is reflected in the multi-omic network profiles (Fig. 2C).

Oxalate stimulates the growth of microbial populations involved in oxalate metabolism, formate metabolism, and their precursors

282 To gain a deeper understanding of microbe-microbe interactions associated with
283 oxalate exposure and to identify specific microorganisms that positively respond to
284 oxalate exposure, NALB with their native microbiota were pair-fed increasing amounts
285 of oxalate, from 0.2% to 6% (Fig. 3A). Stool was sampled after 5 days on the 0.2% and
286 6% diets and processed for shotgun metagenomics. Analysis of metagenomic data
287 revealed that oxalate had a significant impact on metagenome composition (Fig. 3B),
288 with a significant increase of 1073 gene populations and decrease of 382 gene
289 populations (Fig. 3C; Table S5). Changes in gene abundance included four oxalate
290 metabolism gene populations, a shift in 48 gene populations involved in formate
291 metabolism (32 +/16 -), and a shift in genes related to glycine and
292 glyoxylate/dicarboxylate metabolism (6+/4-), which are precursors to oxalate (Fig. 3D).
293 A total of 128 differentially abundant genes were involved in sugar metabolism. Altered
294 gene populations primarily belonged to *O. formigenes* and *Alistipes senegalensis,* with
295 many genes belonging to the *Muribaculum* genus (Fig. 3E). *Muribaculum spp* harbor
296 oxalate-degrading genes, which suggests oxalate metabolic redundancy in the gut
297 microbiota[84]. The oxalate-dependent metagenomic divergence of the NALB gut
298 microbiota (Fig. 3), combined with the lack of change in the microbial metabolomic
299 profile with oxalate exposure (Fig. 2), suggest that oxalate stimulates taxonomically
300 diverse, but metabolically redundant microorganisms, in support of maintaining
301 homeostasis. Given that data came from the same hosts sampled longitudinally, these
302 data also reflect a microbiota that is adaptive to oxalate exposure, which is another
303 important characteristic of complex systems.
304
305 *Oxalate and formate metabolism are highly redundant functions in the NALB gut*
306 To investigate the hypothesis that oxalate stimulates a taxonomically diverse,
307 metabolically redundant community, 248 full length genomes were extracted from
308 shotgun metagenomic data (Fig. S1). Genes for oxalate metabolism, formate
309 metabolism, or the formate metabolic pathways of acetogenesis, methanogenesis, and
310 sulfate reduction, were derived from the KEGG pathway database[85] and mapped to full
311 length genomes. This analysis provides a targeted assessment for metabolic
312 redundancy aimed at oxalate metabolism and pathways associated with the by-products
313 of oxalate metabolism (potential cooperation). A total of 59.3% of genomes contained
314 at least one gene associated with oxalate metabolism or handling (Fig. 4A), most
315 represented by oxalyl-CoA decarboxylase, glycerate dehydrogenase, and formyl-
316 CoA:oxalate CoA transferase (Fig. 4B). However, only 27.8% of genomes harbored a
317 complete metabolic pathway for oxalate degradation (Fig. 4C). Taxa with oxalate genes
318 were dominated by *Bacteroides, Muribaculaceae, Clostridium, Ruminococcus,* and
319 *Lachnospiraceae* (Fig. 4D). Formate metabolism genes were found in 97.18% of
320 genomes, which was dominated by serine hydroxymethyltransferase, and formate-
321 tetrahydrofolate ligase (Fig. S2A-C). Acetogenic genes were also present in 97.18% of
322 genomes, dominated by acetate kinase and formate-tetrahydrofolate ligase (Fig. S3A-
323 C). Methanogenic genes were present in 100% of genomes, dominated by
324 phosphoserine phosphatase, atp-dependent 6-phosphofructokinase, and phosphate
325 acetyltransferase (Fig. S4A-C). Sulfate-reducing genes were present in 31.05% of
326 genomes, dominated by bifunctional oligoribonuclease and PAP phosphatase, FMN
327 reductase, and cysteine synthase (Fig. S5A-C). Data show highly redundant oxalate-

328 associated metabolic pathways and thus provide evidence for very robust homeostatic
329 feedback mechanisms to handle oxalate and metabolic by-products within the NALB gut
330 microbiota. Additionally, the broad diversity of species that contain oxalate-related
331 genes suggest that the distribution of metabolic genes is somewhat independent of the
332 distribution of microbial species, which suggests that microbial genes exist in an
333 autonomous fractal layer, to some degree. This hypothesis is supported by studies
334 which show a high degree of horizontal gene transfer within the gut microbiota as a
335 means of adaptation[86].
336
337 *Oxalate metabolism is driven both by substrate availability and microbiota composition*
338 Adaptability and homeostatic feedback within complex systems is driven by the
339 convergence of system components and resource availability[24]. To examine the
340 confluence of resource availability and oxalate metabolism, a custom medium based on
341 previously published gut microbiota media[87] was modified by adding substrates
342 associated with metabolic pathways enriched by oxalate (Fig. 3C, Table S6). The
343 oxalate-degrading species *Enterococcus gallinarum,* previously isolated from NALB[70]
344 and the whole NALB community were assessed. Chosen substrates impacted oxalate
345 metabolism and the impact of oxalate on growth, particularly at the community level
346 (Fig. 5A,B). A minimal media with the same substrates added as sole carbon and
347 energy sources (Table S7) allowed for quantification of the proportion of the NALB
348 microbiota that could use each substrate as sole carbon and energy sources.
349 Culturomic data recapitulates molecular data to show a considerable amount of
350 redundancy surrounding oxalate metabolism (Fig. 5C). Isolates generated from this
351 assay were used for subsequent study (metabolic cohort; Figure 5D). Additionally, a
352 second cohort was defined and commercially purchased based both on known
353 metabolic functions and the proportion of studies that saw an increase in their
354 taxonomic population with oxalate consumption (Fig. 5D; taxonomic cohort). Where
355 possible, isolates from human sources were obtained. Cohorts, defined in the STAR
356 methods, were used to delineate hypotheses that either carbon and energy substrates
357 are sufficient to explain known effects of the oxalate-degrading microbial network or that
358 additional aspects of taxa commonly stimulated by dietary oxalate are required to
359 explain past results (taxa defined through previous meta-analysis of studies)[15]. Oxalate
360 metabolism with the metabolic and taxonomic cohorts was assessed *in vitro* in minimal
361 media with oxalate as a sole carbon and energy source (Fig. 5E,F). There were
362 considerable differences in oxalate metabolism in both cohorts, dependent on the
363 microbes present. However, significant oxalate metabolism occurred even in the
364 absence of *O. formigenes,* indicative of metabolic redundancy. Collectively, data show
365 that both resource availability and community composition impacts oxalate metabolism,
366 which helps to define the adaptive nature of the NALB gut microbiota. Additionally,
367 results further bolster evidence for redundancy surrounding oxalate metabolism.
368
369 *Severity of oxalate-induced microbe-host effects is dependent on microbial oxalate*
370 *metabolism, independent of taxonomy*
371 To delineate hypotheses of metabolic redundancy or cooperation for mitigating the
372 negative effects of oxalate on the gut microbiota and host, two independent diet trials
373 were conducted with analogous microbial communities derived from the metabolic and

374 taxonomic cohorts. Following antibiotic suppression of the gut microbiota, SWM were
375 given microbial transplants from either the metabolic or taxonomic cohorts in a
376 longitudinal, crossover experimental design with either a 0% or 3% oxalate diet (Envigo;
377 Fig. 6A, S8A; Table S1). The 0% oxalate diet was designed to test the stability of
378 oxalate-degraders since *O. formigenes* is often lost when oxalate is removed from the
379 diet[15]. Transplanted microbial communities included the same as those for *in vitro*
380 studies (Fig. 5D-F). Animal metrics and microbial were tracked over the course of the
381 trial as was urinary/fecal oxalate, urinary formate, inflammatory cytokines, and
382 creatinine. Renal calcium oxalate (CaOx) deposition, cardiac fibrosis, and colitis was
383 assessed through histopathology. CaOx deposition and cardiac fibrosis was quantified
384 through a semi-automated process, based on stain color that differentiates calcium
385 deposits (Von Kossa) or collagen (Mason's Trichrome). Colitis severity was assessed
386 by two independent reviewers in hematoxylin and eosin stained tissues through a
387 standardized, multi-factorial assessment[88].

388 Using microorganisms from the taxonomic cohort, while the change in urinary and fecal
389 oxalate levels were greatest in mice given *O. formigenes,* the change in oxalate levels
390 were significantly greater than the no bacteria controls (Group 1) even in the absence of
391 *O. formigenes,* consistent with *in vitro* results (Fig. 6B,C). Interestingly, the change in
392 urinary formate levels was not different in any microbial group for the taxonomic cohort
393 (Fig. 6D). While IL1β was below detection levels, IL6 exhibited levels consistent with
394 oxalate induction, which decreased over the course of the trial (Fig. 6B, S6A).
395 Differences in IL18 were only seen as an increase over time in the No_ox (Group 5)
396 (Fig. S6B). The only changes in urinary creatinine seen was an increase and decrease
397 in the NALB and All (Group 4) (Fig. S6C), respectively, which indicates that while the
398 NALB bacteria may induce some inflammation, the minimal community present in the
399 All (Group 4) group may limit these effects and actually improve kidney health under
400 conditions of oxalate exposure. While some differences were seen in water or food
401 metrics, these can largely be explained by batch effects of the two trials conducted (Fig.
402 S6D-G). We did see a greater increase in body mass in animals receiving the No_ox
403 (Group 5) microorganisms than when *O. formigenes* was administered alone (Group 2)
404 , which can not be explained by batch effects. Renal CaOx deposition, cardiac fibrosis,
405 and colitis severity all closely tracked oxalate levels (Fig. 6E-J, S6H-I) and did not
406 depend on *O. formigenes* if the other probiotic microbes were present. Collectively,
407 data suggest that oxalate homeostasis and oxalate-induced pathologies are mitigated
408 by the presence of diverse oxalate-degrading bacteria and that adding *O. formigenes* on
409 an already effective oxalate-degrading microbiota will not improve oxalate homeostasis.

410 The microbiota composition of colon contents from this diet trial was significantly
411 different from excreted feces (Fig. S7A). The microbiome composition in stool from
412 mice was not different based on probiotic administration (Fig. S7B), but within group
413 differences for the All (Group 4) group was significantly lower than other groups (Fig.
414 S7C), indicative of a protective effect against oxalate exposure. This conclusion is
415 corroborated by the change in alpha diversity in which the microbiota of animals given
416 the All (Group 4) group exhibited the greatest post-antibiotic recovery and is the only
417 group that saw recovery beyond a marginally significant increase in diversity, post-
418 antibiotics (Fig. S7D). In general, there was not much loss of the inoculated bacteria
419 throughout the study, in any group (Fig. S7E).

Overall, metabolic cohort transplants were less effective than the taxonomic cohort in terms of inducing oxalate metabolism, particularly in the group without bacteria (Group 1) isolated against oxalate (Figs. 6B,C, S8B,C). However, there was a much greater change in format metabolism, dependent on the microbes present (Fig. S8D). Despite the more moderate change in oxalate levels, there were similar oxalate-associated effects on renal calcium oxalate deposition (Fig. S8F,G), which was not dependent on formate levels (Fig. S8H). With the metabolic cohorts, the presence of known oxalate degraders appeared to be more important for oxalate homeostasis than the taxonomic cohort, since absence of known oxalate-degraders led to oxalate levels similar to the No_bact (Group 1) controls (Figs. 6B,C; S8B,C). Collectively, data show that while the taxa chosen for the taxonomic cohort enabled efficient oxalate even in the absence of *O. formigenes*, the bacteria present in the metabolic cohort had a greater influence on formate levels. In both diet trials, urinary oxalate, but not formate correlated with CaOx deposition (Fig. S8G,H – metabolic, data not shown - taxonomic). The effects of oxalate and transplant group differed between the two cohort studies with mice in the metabolic cohort exhibiting higher levels of IL-6 of microbial transplant groups compared to the negative controls. However, similar to the taxonomic cohort, there were no differences in IL18. Urinary creatinine increased significantly over time for all groups receiving a microbial transplant, in contrast with the taxonomic cohort (Figs. S6A-C,S9A-C). For the metabolic cohort, there similar group-based differences observed in water based metrics. However, animals in the taxonomic cohort exhibited greater positive changes in food intake and body mass than the metabolic cohort (Fig. S9D-G).

In the metabolic cohort, we did not observe the same trends in the microbiota composition, antibiotic recovery, or persistence as we did in the taxonomic trial indicative of less effective microbial communities at protecting the community as a whole (Fig. S10A-D), though probiotic bacteria were generally persistent (Fig. S10E).

Overall, data from the taxonomic and metabolic cohorts indicate that oxalate metabolism results from a defined community of microorganisms that includes redundancy in oxalate metabolism as the primary driver. Importantly, the efficacy of *O. formigenes* was apparent when administered alone, but the effect was diminished when co-inoculated with other oxalate-degrading microbes.

Discussion

While research in the last two decades have made clear that the gut microbiota is intimately tied to all facets of host health, translating those insights into actionable biotherapies has been difficult due to the inherent complexity and heterogeneity present in the microbe-host system. The study of complex systems holds enormous potential to constrain hypotheses and offer insight into effective bacteriotherapy development[23]. However, the field is limited by inconsistent terminologies, concepts, and tractable experimental frameworks[25]. The objective of the current study was to examine oxalate-microbe-host interactions within a complex systems framework. Collectively, results of the study offer quantifiable and generalizable metrics of diet-microbe-host systems that can be used to guide more effective patient and probiotic selection criteria for clinical trials involving bacteriotherapies that target the gut microbiota.

466 Microbial oxalate metabolism, which has been researched for several decades, pre-
467 dating the current microbiome era, is an ideal focal point to understand pertinent
468 variables that impact probiotic success. Here, we found that heterogeneity in
469 microbiome composition, independent of host genetics, significantly impacted multiple
470 diet-microbe-host interfaces that included hepatic activity (Figs. 1,2), gut microbiota
471 metabolism (Figs. 2,3), renal mineralization (Fig. 6E,F; S8E,F), intestinal inflammation
472 (Fig. 6H,I), and cardiac fibrosis (Fig. S6H,I). Importantly, we found that oxalate
473 degradation was highly redundant among diverse species in the gut of *N. albigula,*
474 which consumes a high oxalate diet in the wild (Fig. 4). Consistent with past studies,
475 administering *O. formigenes* led to a significant reduction in both stool and urine oxalate
476 (Fig. 6B,C). However, when co-administered with other oxalate-degrading
477 microorganisms, there was no additive effect. Oxalate-based results were similar, but
478 to a lower degree, in the metabolic cohort (Fig. S8B,C). In taxonomic cohort studies, we
479 did not see significant differences in the change in urine formate, based on microbial
480 transplant group (Fig. 6D), in contrast to metabolic cohort studies (Fig. S8D).
481 Collectively, data offer strong support for the hypothesis that metabolic redundancy
482 among diverse taxa, is the primary driver of oxalate homeostasis, rather than metabolic
483 cooperation in which the by-products of oxalate degradation are used in downstream
484 pathways such as acetogenesis, methanogenesis, and sulfate reduction. However,
485 data on the metabolic cooperation hypothesis were inconclusive and there are multiple
486 known microbe and host sources of formate, which may confound results in these
487 studies[74,89-91].
488
489 Modelling the microbe-host system through an evolutionary perspective, it has
490 previously been suggested that while host control over the microbiome is the primary
491 driver of the form and function of the gut microbiota, given the enormous biomass and
492 diversity of the gut microbiota, microbe-microbe competition is also required to constrain
493 the microbiota in mammalian microbe-host systems[21]. In the current (Figs. 2B, 5B) and
494 previous studies[33,34,64,65], we and others have found that oxalate can differentially exhibit
495 positive or negative effects on microbial growth and metabolism dependent on the
496 species and environment present. These data provide two alternative ecological
497 pressures to degrade oxalate. The first is to use oxalate as a carbon and energy source
498 for growth, as is the case with *O. formigenes*[33]. The second is to degrade oxalate to
499 remove it as a toxin, as is the case with some *Lactobacilli* and *Bifidobacteria*[64,65]. The
500 data showing oxalate degradation as a metabolically redundant function among multiple
501 diverse microorganisms that maintains oxalate homeostasis (Figs. 4, 6, S8), suggest
502 that the amount of oxalate consumed or produced by the liver is too great for a single,
503 slow-growing oxalate-degrading specialist can handle alone, in contrast to prevailing
504 hypotheses[63], and in support of the ecosystem on a leash hypothesis. Importantly, the
505 near universal presence of formate metabolism genes suggest that formate may be an
506 even greater source of ecological pressure (Figs. S2-S5). Collectively, data from the
507 current and previous studies on the effect of oxalate exposure on the gut microbiota[68,71]
508 support the hypothesis that the gut microbiota serves as an adaptive organ[92-94] in which
509 specific, metabolically redundant microbes respond to and eliminate dietary
510 components, for the benefit of themselves, but which can residually protect or harm host
511 health depending on the dietary molecules and gut microbiota composition[6,92-94].

512 Oxalate degradation, as a focal point in diet-microbe-host interactions, is a special case
513 in which the effects of oxalate on host health and the mechanisms of microbial oxalate
514 degradation have largely been worked out for decades[33,51-54]. Furthermore, oxalate
515 degradation exhibits moderate complexity, both in that it is isolated to the gut microbiota
516 and is performed through a handful of simple metabolic pathways[31-35]. Despite this
517 knowledge, clinical trials designed to reduce systemic oxalate using either *O.*
518 *formigenes* or other oxalate-degrading bacteria have exhibited a wide variety of patient
519 and trial responses[15]. However, knowledge about other diet-microbe-host links are
520 largely in their infancy. Many of the other known features exhibit much greater
521 complexity than oxalate degradation. For instance, while the production of short chain
522 fatty acids are widely viewed as beneficial for both the gut microbiota and host health[95-
523 100], many short chain fatty acids are known and are produced by a wide variety of
524 species[101,102]. Other important diet-microbe-host links, such as the production of
525 secondary bile acids or TMAO[6,36,103-105], also involve host hepatic activity, increasing the
526 complexity further. Given the complexity of diet-microbe-host interactions and the fact
527 that understanding the mechanisms through which the gut microbiota modifies the diet
528 to influence host health is demonstrably insufficient for the development of effective
529 bacteriotherapies[12-15], we propose a three-phase, pre-clinical experimental workflow for
530 the development of targeted bacteriotherapies. In the first phase of research,
531 case:control metagenome-wide studies and research into other factors that modify the
532 microbiome, such as prior antibiotic exposure, can identify disease phenotypes that are
533 influenced by the microbiome, along with the microbial taxa and genes responsible for
534 this association. In the second phase of research, hypothesized taxa and/or metabolic
535 functions can be explored through *in vitro* and germ-free animal studies, using
536 appropriate models to determine the mechanistic links that drive disease phenotypes
537 through diet-microbe-host interactions. Finally, in phase three, these mechanistic links
538 can be applied to a complex system theoretical framework, as done in the current study,
539 to identify those variables most pertinent to successfully influence specific phenotypes
540 through targeted changes to the gut microbiota. Such a phased research structure will
541 provide for much more effective probiotic and patient selection criteria prior to clinical
542 trials.
543
544 There were some important limitations to the current study. First, while we did conduct
545 one study with *N. albigula,* most animal studies here sought to eliminate host genetics
546 from the equation, as a means of simplification. Host genetics are another layer of
547 complexity that were not examined here and may have an impact on oxalate
548 homeostasis beyond the gut microbiota. Second, in animal studies with the refined
549 communities of microorganisms, the taxonomic and metabolic cohorts studies were
550 conducted separately and some batch effects are apparent, such as with the change in
551 creatinine values or urine output. Finally, it is apparent from our data and the literature
552 that there are multiple host and microbial sources of formate. As such, data pertaining
553 to formate utilization by our transplant communities are inconclusive.
554
555 In conclusion, using a complex systems theoretical framework, we examined the
556 oxalate-microbe-host interactions of multiple oxalate-microbe-host interfaces and found
557 multiple microbiome-dependent effects of oxalate. The negative effects of oxalate were

mitigated by metabolically redundant oxalate-degrading bacteria, more so than by metabolic cooperation or a single oxalate-degrading species. Critically, we found that while *O. formigenes* can lower urine oxalate when placed on a background of a poor oxalate-degrading community, as current theory predicts, this effect is lost when co-administered with other oxalate-degrading bacteria. Collectively, data help to resolve why the gut microbiota of the white throated woodrat, *Neotoma albigula,* effectively responds to and degrades even very high dietary oxalate levels[68,69,72] and offer a clear pathway for more effective patient and probiotic selection for future clinical trials to reduce urine oxalate. More importantly, the conceptual and experimental framework developed in this study, based on complex systems theory, paves the way for a phased approach to microbiome research in which clinical microbiome insights (Phase I) drive mechanistic insights between the gut microbiota and host physiology (Phase II), that can be applied to a complex system model to constrain hypotheses and identify the most pertinent variables that drive microbe-host interactions that influence host physiology and health (Phase III). Such an approach will allow for much more efficacious probiotic and patient selection criteria in clinical intervention trials.

Data availability Sequence reads from the animal study are available at the Sequence Read Archive under Accession numbers for gut microbiota genomes: PRJNA833303, Shotgun metagenomics: PRJNA839366, Liver transcriptomics: PRJNA1018952 Gut microbiota data: 16SPRJNA1018559

Acknowledgements: We would like to thank animal care facility, Metabolomics core, Microbial sequencing and analytics core, and Imaging core at Cleveland Clinic. We are thankful for the NIH funding to AWM R01 DK121689-01A1 and funding from the Cleveland Clinic Foundation to AWM.

Author contributions: SM, DD, MM and AWM conceived and designed the study. SM, CAB, AA, AN, and AWM designed and performed most *in vitro* and animal-based biological experiments. JA, MS, AZ, TO performed addtional animal and *in vitro* experiments and contributed to data analysis. SM and AWM wrote the manuscript with input from all authors. AWM supervised the study. All authors reviewed the manuscript.

Declaration of interests: The authors declare no conflict of interest

Figure titles and legends

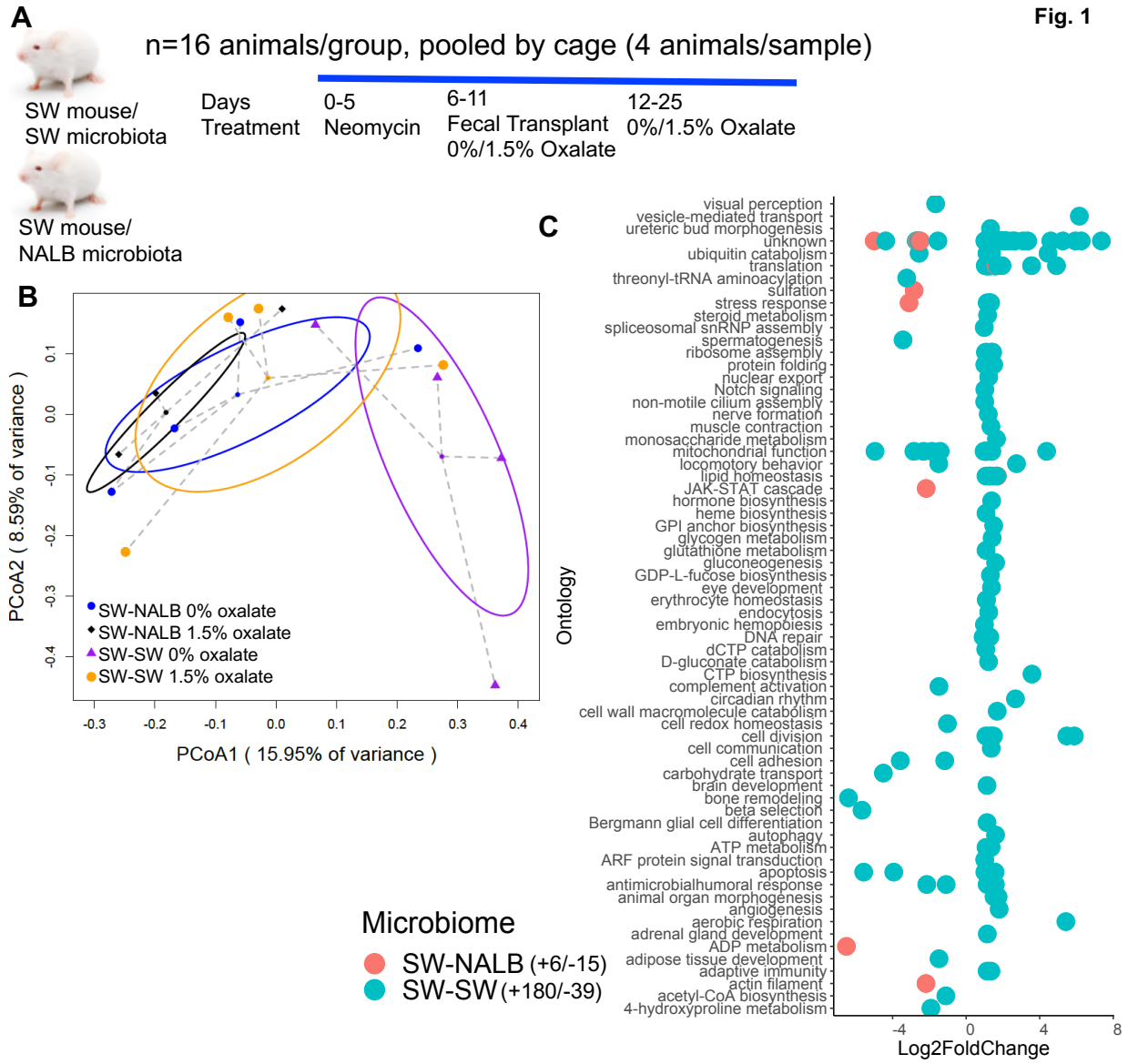

Fig. 1. Oxalate exposure impacted host hepatic activity in a microbiota dependent fashion. A) Swiss Webster mice were given neomycin, followed by an allograft (SWM) or xenograft (NALB) fecal transplant, then maintained on a 0% or 1.5% oxalate diet prior to necropsy for fecal metabolomics (Fig. 2) and hepatic transcriptomics. B) PCoA of normalized, whole-transcriptome data. p=0.02 for microbiome composition, p=0.07 for dietary oxalate content, p=0.3 in 2-way analysis; 2-way PERMANOVA. C) Total number of hepatic genes significantly stimulated or inhibited by dietary oxalate. Significant genes are plotted by Log2FoldChange. Positive values reflect genes increased with oxalate exposure and negative values are genes decreased with exposure. FDR < 0.05, Wald test. Hepatic genes are annotated to pathway (Kegg, Uniprot, PubChem,

609 Metacyc) and the total number of genes that exhibit a positive or negative shift with
610 oxalate exposure are listed in the legend. Complete gene list is in Table S2.
611

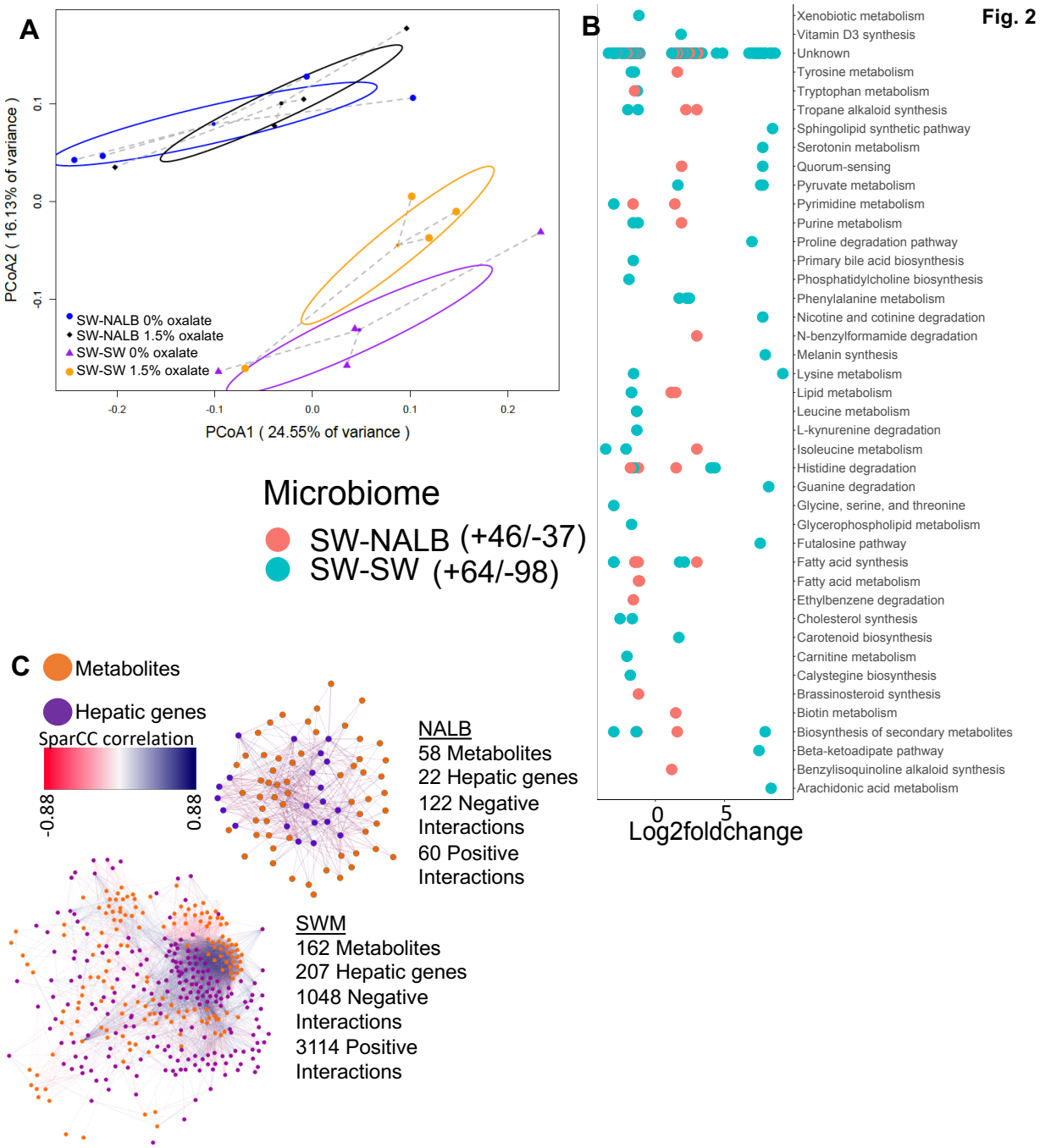

Fig. 2. Oxalate exposure impacted microbial metabolic activity in a microbiota dependent fashion. A) PCoA of protein normalized, log-transformed metabolomic data. p=0.001 for microbiome composition, p=0.1 for dietary oxalate content, p=0.3 in 2-way analysis; 2-way PERMANOVA. B) Total number of fecal metabolites significantly stimulated or inhibited by dietary oxalate. Significant metabolites are plotted by Log2FoldChange. Positive values reflect metabolites increased with oxalate exposure

621 and negative values are metabolites decreased with exposure. FDR < 0.05, Mann-
622 Whitney U or Fisher's exact test. Metabolites are annotated to pathway (Kegg, Uniprot,
623 PubChem, Metacyc) the total number of metabolites that exhibit a positive or negative
624 shift with oxalate exposure are listed in the legend. Complete list is in Table S3. C)
625 Change in the host-microbe interaction network upon exposure to oxalate, quantified as
626 hepatic gene-microbe metabolite correlations R > +/- 0.3 and FDR < 0.05 with SparCC,
627 visualized in Cytoscape. All host-microbe interactions are listed in Table S4.
628

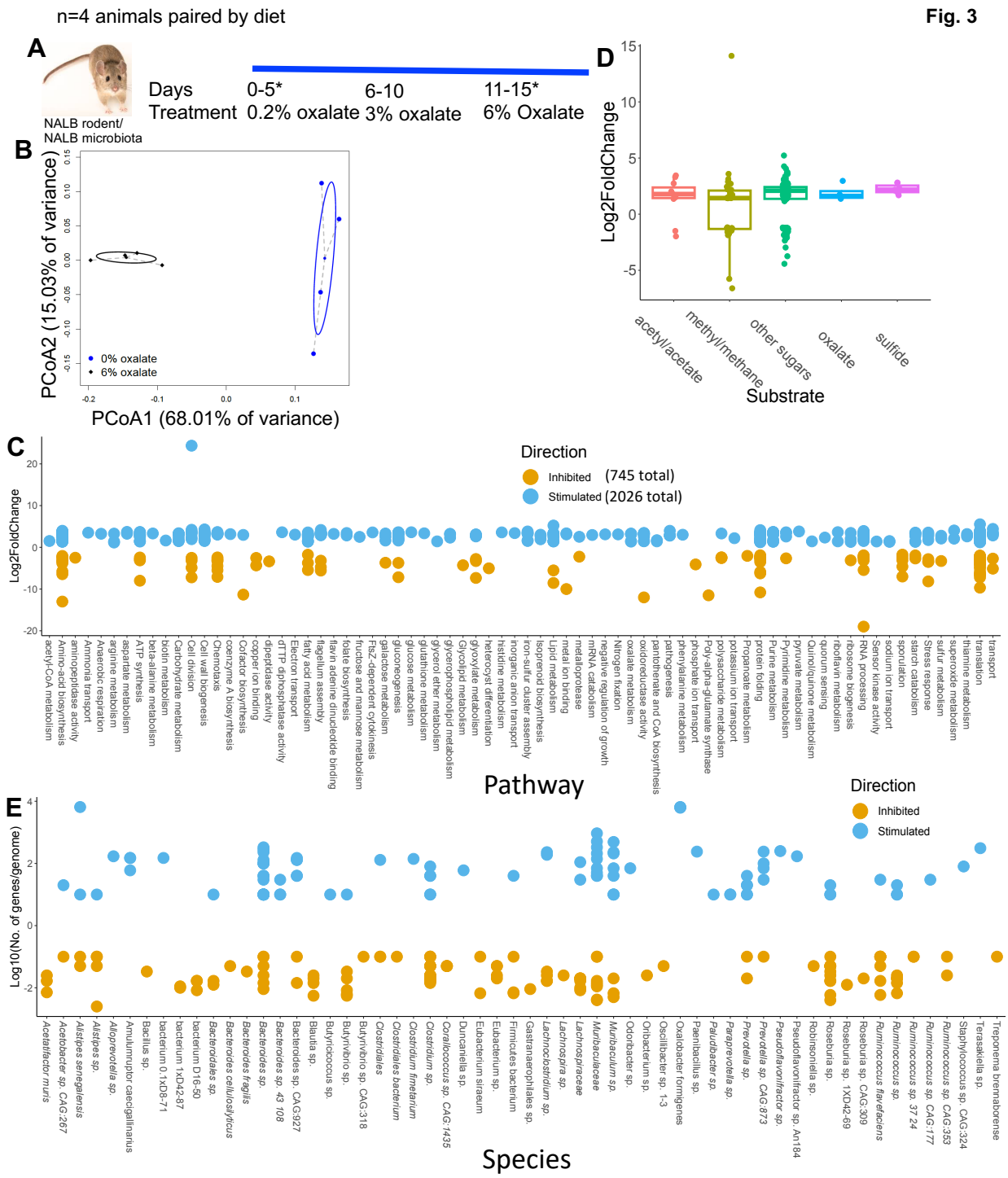

Fig. 3. Oxalate exposure stimulates taxonomically diverse microorganisms, with a few strains that dominate the response. A) *Neotoma albigula* with native microbiota were given increasing amounts of dietary oxalate up to 6% w/w. *indicates sampling

635 timepoints. B) PCoA of normalized metagenomic data. p=0.02; PERMANOVA. C) Total
636 number of microbial genes significantly stimulated or inhibited by dietary oxalate,
637 annotated to pathway (Kegg, UniProt, PubChem, Metacyc) and listed by
638 Log2FoldChange. The total number of genes stimulated or inhibited by oxalate are
639 listed in the legend. Genes with unknown annotation are not listed. The complete list of
640 annotated genes is listed in Table S5. D) Number of significantly differentiated genes
641 involved in oxalate degradation, sulfate reduction, acetogenic, methanogenic, or sugar
642 metabolic pathways or utilization of by-products of those pathways stimulated (positive)
643 or inhibited (negative) by dietary oxalate. Genes are listed by their Log2FoldChange
644 between no and high oxalate diets. FDR < 0.05, Wald test. E) The number of
645 genes/genome significantly altered by oxalate, mapped to microbial genomes extracted
646 from *N. albigula.* Number of genes/genomes are log10-transformed to show the
647 distribution more clearly. A total of 92% of genomes had at least one significantly
648 altered gene population mapped to them.
649
650
651
652
653
654

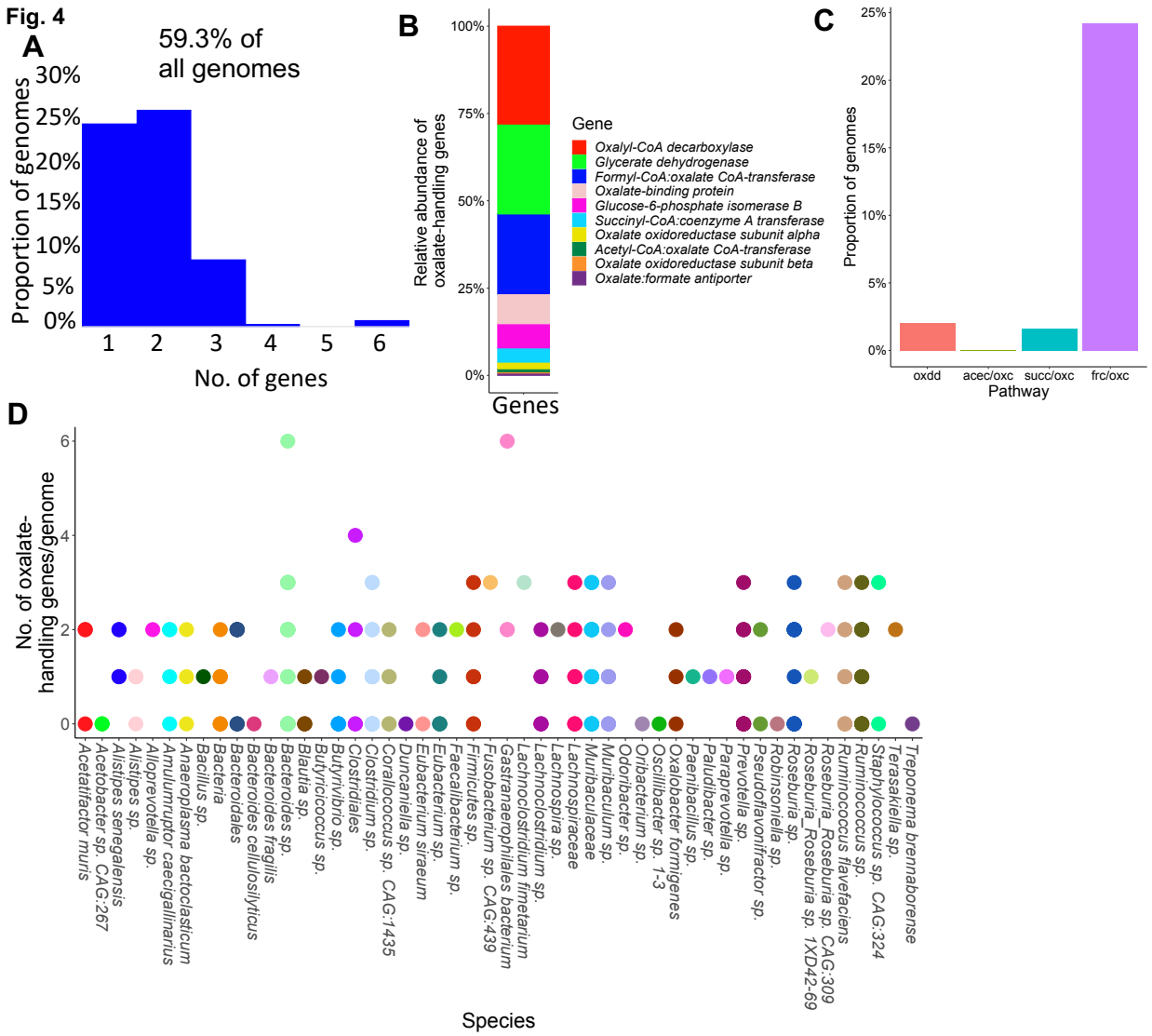

Fig. 4. Genes related to the metabolism or handling of oxalate are present in >50% of 248 full length NALB microbial genomes from the gut. A) Proportion of the genomes extracted from *N. albigula* that had at least one oxalate-related gene. B) Relative distribution of oxalate-handling genes by gene function. C) Proportion of genomes that have a complete pathway for oxalate degradation, specifically. oxdd=oxalate oxidoreductase; acec=acetyl-CoA:oxalate CoA-transferase; oxc=Oxalyl-CoA decarboxylase; succ=succinyl-CoA:coenzyme A transferase; frc=Formyl-CoA transferase; D) Number of oxalate-handling genes by genome.

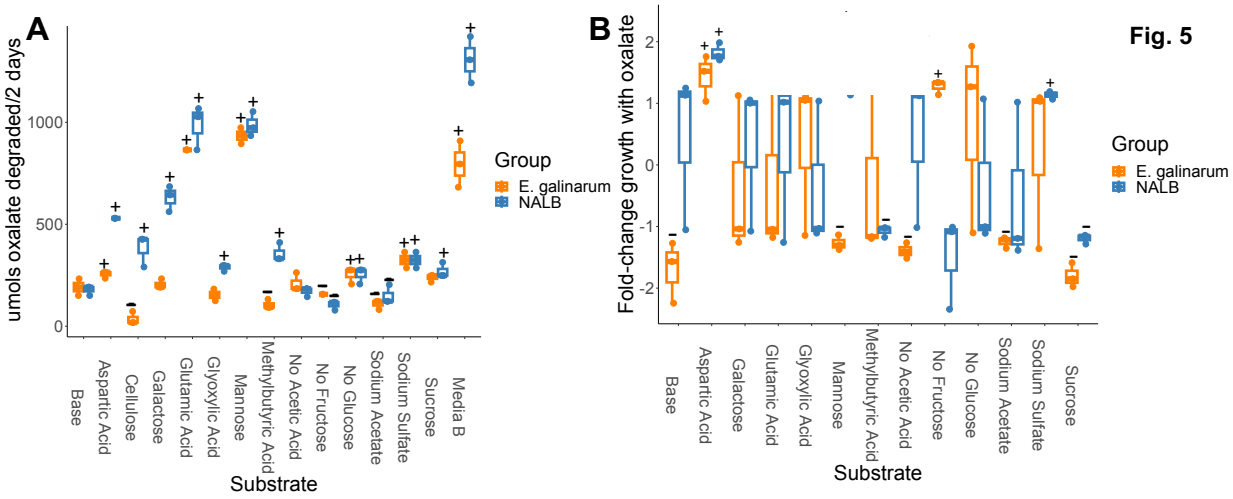

Fig. 5

C

Substrate	No. of Isolates	% of Community
Oxalate	70	14.58%
Cellulose	68	14.17%
Sucrose	65	13.54%
D-Glucose	45	9.38%
Aspartic acid	38	7.92%
Galactose	19	3.96%
Formate	16	1.67%
Mannose	12	1.25%
Fructose	10	1.04%
Acetate	7	0.73%
Methylvaric/ butyric acid	4	0.42%
Glutamic acid	1	0.10%

D

Group	Substrate usage	Metabolic cohort	Taxonomic cohort	% of studies
All, No_ox	Fructose	Ruminococcus sp.	Lactobacillus helveticus	71%
All, No_ox	Galactose	Bacteroides acidofaciens	Lactobacillus helveticus	71%
All, No_ox	Sucrose	Bacteroides acidofaciens	Bacteroides thetaiotaomicron	86%
All, No_ox, Ox_form	Formate	Enterobacter sp.	Desulfovibrio piger, Methanobrevibacter smithii, Ruminococcus gnavus	71%, 71%, 86%
All, Ox, Ox_form	Oxalate	Bacteroides vulgatus	Oxalobacter formgienes	86%
All, No_ox	Glucose	Bacteroides vulgatus	Coprococcus comes	100%
All, No_ox	Mannose	Bacteroides acidofaciens	Lactobacillus plantarum	71%
All, No_ox	Methyl	Bacteroides dorei	Bacteroides thetaiotaomicron	86%
All, No_ox	Acetate	Bacteroides dorei	Bacteroides thetaiotaomicron	86%
All, No_ox	Aspartic	Bacteroides dorei	Bacteroides thetaiotaomicron	86%

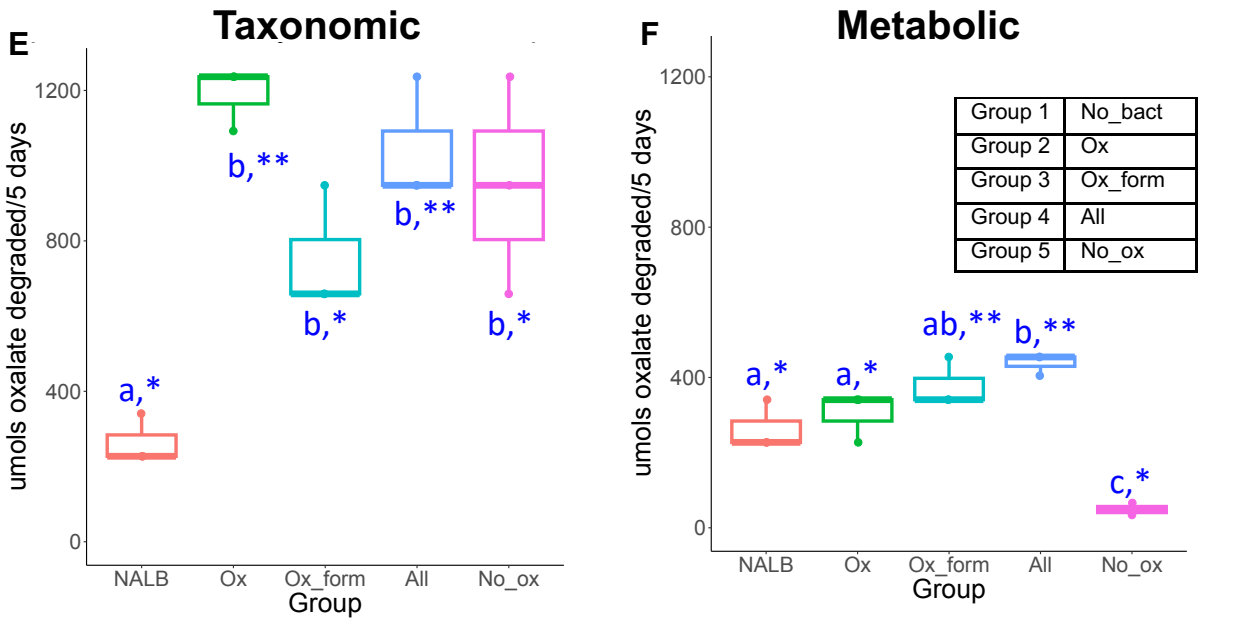

671 Fig. 5. Microbial community composition and available substrates impact oxalate
672 metabolism and the impact of oxalate on growth. A) Substrates associated with
673 metabolic pathways enriched by exposure to dietary oxalate *in vivo* differentially impact
674 oxalate metabolism. $p<0.001$ in one-way and two-way ANOVA against bacterial group
675 and substrate; +/- reflects $p<0.05$, Holm's-corrected, pairwise t-test compared to base
676 media for an increase (+) or decrease (-) in oxalate degradation. B) Substrates
677 differentially impact the influence of oxalate on microbial growth; $p<0.001$ in two-way
678 ANOVA against substrate and bacterial group, and one-way analysis against substrate;
679 +/- reflects $p<0.05$, Holm's-corrected, one-sample t-test compared 0 (no impact of
680 oxalate) for an increase (+) or decrease (-) in growth due to oxalate exposure. The
681 impact of oxalate on growth was not calculated for cellulose or Media B. C) Culture-
682 based means to quantify proportion of the NALB community that can use substrates
683 identified through shotgun metagenomics as sole carbon and energy sources. D)
684 Defined microbial communities to assess oxalate metabolism *in vitro* and *in vivo*. Listed
685 are the microbial consortia, which substrate the microbes utilize that corresponds to the
686 shotgun metagenomic data, taxonomic classification of microorganisms used in the two
687 cohorts, and the proportion of studies in which microorganisms in the taxonomic cohort
688 were stimulated by oxalate exposure. E,F) Oxalate metabolism in minimal media with
689 20mM oxalate from the microbial communities listed in 5D, in comparison to the NALB
690 community. $p<0.001$, ANOVA comparing microbial groups. *$p<0.05$, **$p<0.01$;
691 ***$p<0.001$; Holm's corrected, one sample t-tests against 0 (no oxalate metabolism).
692 Blue letters reflect statistical groups between microbial groups for oxalate metabolism.
693
694

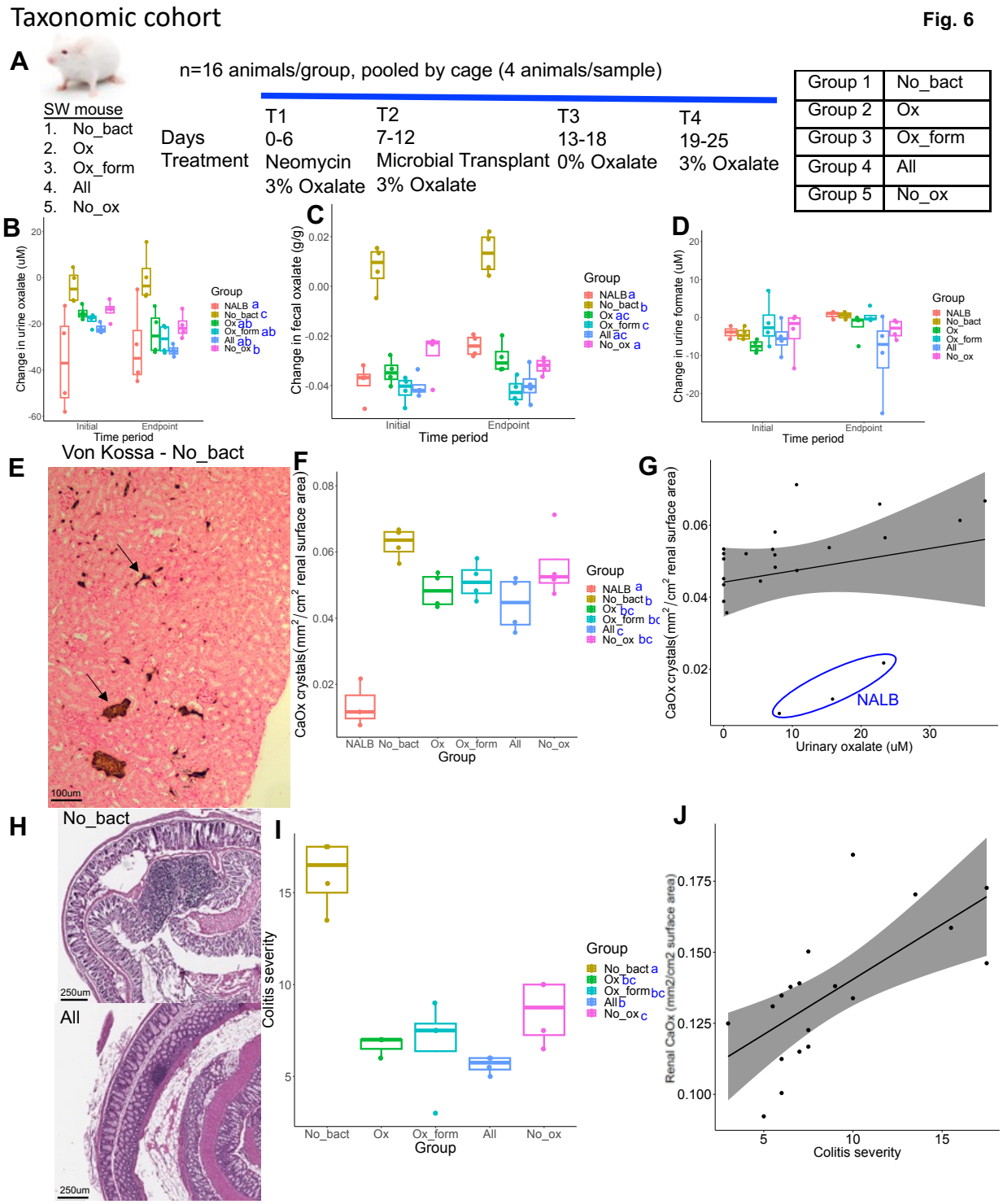

Fig. 6. Microbial community composition (taxonomic cohort) impacted the effect of exogenous oxalate on host health. A) Swiss Webster mice were given neomycin, followed by inoculation of microbial consortia that included either no bacteria or the taxonomic cohort listed in Figure 5C. B,C) The effect of microbial transplants on urinary (B) or fecal (C) oxalate levels over the course of the diet trial, compared to baseline.

ANOVA $p<0.001$ for microbial group, but was not significant by timeperiod or 2-way analyses for both B & C. D) The effect of microbial transplants on urinary formate levels over the course of the diet trial, compared to baseline. ANOVA was not significant in one-way and two-way analyses. E) Renal calcium oxalate deposition. Arrows show stained calcium deposits, which were quantified through an automated algorithm in QuPath. F) Quantification of renal calcium oxalate deposition by group. $p<0.001$, ANOVA. Blue letters reflect statistical groups between microbial groups for renal calcification by Holm's corrected paired t-tests. G) Pearson correlation between urinary oxalate and renal calcium oxalate deposition. $R=0.22$, $p=0.32$ with NALB samples included (blue circle); $R=0.7$, $p=0.001$ excluding the NALB group. H) Representative colon tissues from the No_bact (Group 1) and All (Group 4) groups, exhibiting high and low colitis severity scores, respectively. Tissues were stained with hematoxylin and eosin and scored based on standardized, multifactorial metrics. I) Quantification of colitis severity by group. $p<0.001$, ANOVA. Blue letters reflect statistical groups between microbial groups for renal calcification by Holm's corrected paired t-tests. J) Pearson correlation between colitis severity and renal calcium oxalate deposition. $R=0.7$, $p=0.002$. Colitis severity was not quantified for the NALB group.

References

1. Gomaa, E.Z. (2020). Human gut microbiota/microbiome in health and diseases: a review. Antonie Van Leeuwenhoek *113*, 2019-2040.
2. Cox, T.O., Lundgren, P., Nath, K., and Thaiss, C.A. (2022). Metabolic control by the microbiome. Genome Medicine *14*, 80.
3. Turnbaugh, P.J., Ley, R.E., Hamady, M., Fraser-Liggett, C.M., Knight, R., and Gordon, J.I. (2007). The human microbiome project. Nature *449*, 804-810.
4. Lloyd-Price, J., Mahurkar, A., Rahnavard, G., Crabtree, J., Orvis, J., Hall, A.B., Brady, A., Creasy, H.H., McCracken, C., and Giglio, M.G. (2017). Strains, functions and dynamics in the expanded Human Microbiome Project. Nature *550*, 61-66.
5. Wang, J., and Jia, H. (2016). Metagenome-wide association studies: fine-mining the microbiome. Nature Reviews Microbiology *14*, 508-522.
6. Tang, W.W., and Hazen, S.L. (2024). Unraveling the Complex Relationship Between Gut Microbiome and Cardiovascular Diseases. Circulation *149*, 1543-1545.
7. de Vos, W.M., and de Vos, E.A. (2012). Role of the intestinal microbiome in health and disease: from correlation to causation. Nutrition reviews *70*, S45-S56.
8. De Vos, W.M., Tilg, H., Van Hul, M., and Cani, P.D. (2022). Gut microbiome and health: mechanistic insights. Gut *71*, 1020-1032.
9. Zimmermann, M., Patil, K.R., Typas, A., and Maier, L. (2021). Towards a mechanistic understanding of reciprocal drug–microbiome interactions. Molecular systems biology *17*, e10116.
10. Vujkovic-Cvijin, I., Sklar, J., Jiang, L., Natarajan, L., Knight, R., and Belkaid, Y. (2020). Host variables confound gut microbiota studies of human disease. Nature *587*, 448-454.
11. Walter, J., Armet, A.M., Finlay, B.B., and Shanahan, F. (2020). Establishing or exaggerating causality for the gut microbiome: lessons from human microbiota-associated rodents. Cell *180*, 221-232.
12. Barkhidarian, B., Roldos, L., Iskandar, M.M., Saedisomeolia, A., and Kubow, S. (2021). Probiotic supplementation and micronutrient status in healthy subjects: A systematic review of clinical trials. Nutrients *13*, 3001.
13. Rogers, N.J., and Mousa, S.A. (2012). The shortcomings of clinical trials assessing the efficacy of probiotics in irritable bowel syndrome. The Journal of Alternative and Complementary Medicine *18*, 112-119.
14. Ceccherini, C., Daniotti, S., Bearzi, C., and Re, I. (2022). Evaluating the efficacy of probiotics in IBS treatment using a systematic review of clinical trials and multi-criteria decision analysis. Nutrients *14*, 2689.
15. Batagello, C.A., Monga, M., and Miller, A.W. (2018). Calcium oxalate urolithiasis: a case of missing microbes? Journal of endourology *32*, 995-1005.
16. Foster, J.A., Krone, S.M., and Forney, L.J. (2008). Application of ecological network theory to the human microbiome. Interdisciplinary perspectives on infectious diseases *2008*, 839501.

17. Layeghifard, M., Hwang, D.M., and Guttman, D.S. (2017). Disentangling interactions in the microbiome: a network perspective. Trends in microbiology *25*, 217-228.
18. Ridenhour, B.J., Brooker, S.L., Williams, J.E., Van Leuven, J.T., Miller, A.W., Dearing, M.D., and Remien, C.H. (2017). Modeling time-series data from microbial communities. The ISME journal *11*, 2526.
19. Kumar, M., Ji, B., Zengler, K., and Nielsen, J. (2019). Modelling approaches for studying the microbiome. Nature microbiology *4*, 1253-1267.
20. Richardson, L.A. (2017). Evolving as a holobiont. PLoS biology *15*, e2002168.
21. Foster, K.R., Schluter, J., Coyte, K.Z., and Rakoff-Nahoum, S. (2017). The evolution of the host microbiome as an ecosystem on a leash. Nature *548*, 43-51.
22. Palla, G., Derényi, I., Farkas, I., and Vicsek, T. (2005). Uncovering the overlapping community structure of complex networks in nature and society. nature *435*, 814-818.
23. Lambiotte, R., Rosvall, M., and Scholtes, I. (2019). From networks to optimal higher-order models of complex systems. Nature physics *15*, 313-320.
24. Cohen, A.A., Ferrucci, L., Fülöp, T., Gravel, D., Hao, N., Kriete, A., Levine, M.E., Lipsitz, L.A., Olde Rikkert, M.G., and Rutenberg, A. (2022). A complex systems approach to aging biology. Nature Aging *2*, 580-591.
25. Torres, L., Blevins, A.S., Bassett, D., and Eliassi-Rad, T. (2021). The why, how, and when of representations for complex systems. SIAM Review *63*, 435-485.
26. Roediger, W. (1980). Role of anaerobic bacteria in the metabolic welfare of the colonic mucosa in man. Gut *21*, 793-798.
27. Javorka, M., Czippelova, B., Turianikova, Z., Lazarova, Z., Tonhajzerova, I., and Faes, L. (2017). Causal analysis of short-term cardiovascular variability: state-dependent contribution of feedback and feedforward mechanisms. Medical & biological engineering & computing *55*, 179-190.
28. Kolodziejczyk, A.A., Zheng, D., and Elinav, E. (2019). Diet–microbiota interactions and personalized nutrition. Nature Reviews Microbiology *17*, 742-753.
29. Crivelli, J.J., Mitchell, T., Knight, J., Wood, K.D., Assimos, D.G., Holmes, R.P., and Fargue, S. (2021). Contribution of Dietary Oxalate and Oxalate Precursors to Urinary Oxalate Excretion. Nutrients *13*, 62.
30. Holmes, R.P., Goodman, H.O., and Assimos, D.G. (2001). Contribution of dietary oxalate to urinary oxalate excretion. Kidney international *59*, 270-276.
31. Cochat, P., and Rumsby, G. (2013). Primary hyperoxaluria. New England Journal of Medicine *369*, 649-658.
32. Hodgkinson, A. (1977). Oxalic acid in biology and medicine. London—New York.
33. Allison, M.J., Dawson, K.A., Mayberry, W.R., and Foss, J.G. (1985). Oxalobacter formigenes gen. nov., sp. nov.: oxalate-degrading anaerobes that inhabit the gastrointestinal tract. Archives of Microbiology *141*, 1-7.
34. Miller, A.W., and Dearing, D. (2013). The metabolic and ecological interactions of oxalate-degrading bacteria in the mammalian gut. Pathogens *2*, 636-652.
35. Liu, M., Devlin, J.C., Hu, J., Volkova, A., Battaglia, T.W., Ho, M., Asplin, J.R., Byrd, A., Loke, P.n., and Li, H. (2021). Microbial genetic and transcriptional

809 contributions to oxalate degradation by the gut microbiota in health and disease.
810 Elife *10*, e63642.
811 36. Tang, W.W., Wang, Z., Kennedy, D.J., Wu, Y., Buffa, J.A., Agatisa-Boyle, B., Li,
812 X.S., Levison, B.S., and Hazen, S.L. (2015). Gut microbiota-dependent
813 trimethylamine N-oxide (TMAO) pathway contributes to both development of
814 renal insufficiency and mortality risk in chronic kidney disease. Circulation
815 research *116*, 448-455.
816 37. Nazzal, L., Francois, F., Henderson, N., Liu, M., Li, H., Koh, H., Wang, C., Gao,
817 Z., Perez, G.P., and Asplin, J.R. (2021). Effect of antibiotic treatment on
818 Oxalobacter formigenes colonization of the gut microbiome and urinary oxalate
819 excretion. Scientific Reports *11*, 16428.
820 38. Miller, A.W., Orr, T., Dearing, D., and Monga, M. (2019). Loss of function
821 dysbiosis associated with antibiotics and high fat, high sugar diet. The ISME
822 journal *13*, 1379-1390.
823 39. Kharlamb, V., Schelker, J., Francois, F., Jiang, J., Holmes, R.P., and Goldfarb,
824 D.S. (2011). Oral antibiotic treatment of Helicobacter pylori leads to persistently
825 reduced intestinal colonization rates with Oxalobacter formigenes. Journal of
826 Endourology *25*, 1781-1785.
827 40. Lange, J.N., Wood, K.D., Wong, H., Otto, R., Mufarrij, P.W., Knight, J., Akpinar,
828 H., Holmes, R.P., and Assimos, D.G. (2012). Sensitivity of human strains of
829 Oxalobacter formigenes to commonly prescribed antibiotics. Urology *79*, 1286-
830 1289.
831 41. Mittal, R., Kumar, R., Bid, H., and Mittal, B. (2005). Effect of antibiotics on
832 Oxalobacter formigenes colonization of human gastrointestinal tract. Journal of
833 endourology *19*, 102-106.
834 42. Mulay, S.R., Kulkarni, O.P., Rupanagudi, K.V., Migliorini, A., Darisipudi, M.N.,
835 Vilaysane, A., Muruve, D., Shi, Y., Munro, F., and Liapis, H. (2012). Calcium
836 oxalate crystals induce renal inflammation by NLRP3-mediated IL-1β secretion.
837 The Journal of clinical investigation *123*.
838 43. Peerapen, P., and Thongboonkerd, V. (2011). Effects of calcium oxalate
839 monohydrate crystals on expression and function of tight junction of renal tubular
840 epithelial cells. Laboratory Investigation *91*, 97.
841 44. Peerapen, P., and Thongboonkerd, V. (2021). Calcium oxalate monohydrate
842 crystal disrupts tight junction via F-actin reorganization. Chem Biol Interact *345*,
843 109557. 10.1016/j.cbi.2021.109557.
844 45. Holmes, R.P., Knight, J., and Assimos, D.G. (2016). Lowering urinary oxalate
845 excretion to decrease calcium oxalate stone disease. Urolithiasis *44*, 27-32.
846 10.1007/s00240-015-0839-4.
847 46. Nazzal, L., Puri, S., and Goldfarb, D.S. (2015). Enteric hyperoxaluria: an
848 important cause of end-stage kidney disease. Nephrology Dialysis
849 Transplantation *31*, 375-382.
850 47. Waikar, S.S., Srivastava, A., Palsson, R., Shafi, T., Hsu, C.-y., Sharma, K., Lash,
851 J.P., Chen, J., He, J., and Lieske, J. (2019). Association of urinary oxalate
852 excretion with the risk of chronic kidney disease progression. JAMA internal
853 medicine *179*, 542-551.

854 48. Castellaro, A.M., Tonda, A., Cejas, H.H., Ferreyra, H., Caputto, B.L., Pucci, O.A.,
855 and Gil, G.A. (2015). Oxalate induces breast cancer. BMC Cancer *15*, 761.
856 10.1186/s12885-015-1747-2.
857 49. Liu, Y., Zhao, Y., Shukha, Y., Lu, H., Wang, L., Liu, Z., Liu, C., Zhao, Y., Wang,
858 H., Zhao, G., et al. (2021). Dysregulated oxalate metabolism is a driver and
859 therapeutic target in atherosclerosis. Cell Rep *36*, 109420.
860 10.1016/j.celrep.2021.109420.
861 50. Efe, O., Verma, A., and Waikar, S.S. (2019). Urinary oxalate as a potential
862 mediator of kidney disease in diabetes mellitus and obesity. Curr Opin Nephrol
863 Hypertens *28*, 316-320. 10.1097/MNH.0000000000000515.
864 51. James, L.F., and Butcher, J.E. (1972). Halogeton poisoning of sheep: effect of
865 high level oxalate intake. Journal of animal science *35*, 1233-1238.
866 52. Anantharam, V., Allison, M.J., and Maloney, P.C. (1989). Oxalate:formate
867 exchange. The basis for energy coupling in Oxalobacter. J Biol Chem *264*, 7244-
868 7250.
869 53. Baetz, A.L., and Allison, M.J. (1989). Purification and characterization of oxalyl-
870 coenzyme A decarboxylase from Oxalobacter formigenes. Journal of
871 bacteriology *171*, 2605-2608.
872 54. Baetz, A.L., and Allison, M.J. (1990). Purification and characterization of formyl-
873 coenzyme A transferase from Oxalobacter formigenes. Journal of bacteriology
874 *172*, 3537-3540.
875 55. Ariceta, G., Collard, L., Abroug, S., Moochhala, S.H., Gould, E., Boussetta, A.,
876 Ben Hmida, M., De, S., Hunley, T.E., and Jarraya, F. (2023). ePHex: a phase 3,
877 double-blind, placebo-controlled, randomized study to evaluate long-term efficacy
878 and safety of Oxalobacter formigenes in patients with primary hyperoxaluria.
879 Pediatric Nephrology *38*, 403-415.
880 56. Dearing, M.D., and Weinstein, S.B. (2022). Metabolic enabling and detoxification
881 by mammalian gut microbes. Annual Review of Microbiology *76*, 579-596.
882 57. Kohl, K.D., Weiss, Robert B., Cox, James, Dale, Colin, Dearing, M. Denise
883 (2014). Gut microbes of mammalian herbivores facillitate intake of plant toxins.
884 Ecology letters *17*, 1238-1246.
885 58. Grant, D. (1991). Detoxification pathways in the liver. Journal of inherited
886 metabolic disease *14*, 421-430.
887 59. Robertson, W., and Peacock, M. (1980). The cause of idiopathic calcium stone
888 disease: hypercalciuria or hyperoxaluria? Nephron *26*, 105-110.
889 60. Nishizawa, Y., Miyata, S., Tosaka, M., Hirasawa, E., Hosoda, Y., Horimoto, A.,
890 Omae, K., Ito, K., Nagano, N., and Hoshino, J. (2023). Serum oxalate
891 concentration is associated with coronary artery calcification and cardiovascular
892 events in Japanese dialysis patients. Scientific Reports *13*, 18558.
893 61. Fishbein, G.A., Micheletti, R.G., Currier, J.S., Singer, E., and Fishbein, M.C.
894 (2008). Atherosclerotic oxalosis in coronary arteries. Cardiovascular Pathology
895 *17*, 117-123.
896 62. Frandsen, H.B., Sørensen, J.C., Jensen, S.K., Markedal, K.E., Joehnke, M.S.,
897 Maribo, H., Sørensen, S., and Sørensen, H. (2019). Non-enzymatic
898 transformations of dietary 2-hydroxyalkenyl and aromatic glucosinolates in the
899 stomach of monogastrics. Food chemistry *291*, 77-86.

63. Daniel, S.L., Moradi, L., Paiste, H., Wood, K.D., Assimos, D.G., Holmes, R.P., Nazzal, L., Hatch, M., and Knight, J. (2021). Forty years of Oxalobacter formigenes, a gutsy oxalate-degrading specialist. Applied and Environmental Microbiology *87*, e00544-00521.
64. Turroni, S., Bendazzoli, C., Dipalo, S.C., Candela, M., Vitali, B., Gotti, R., and Brigidi, P. (2010). Oxalate-degrading activity in Bifidobacterium animalis subsp. lactis: impact of acidic conditions on the transcriptional levels of the oxalyl coenzyme A (CoA) decarboxylase and formyl-CoA transferase genes. Applied and environmental microbiology *76*, 5609-5620.
65. Turroni, S., Vitali, B., Bendazzoli, C., Candela, M., Gotti, R., Federici, F., Pirovano, F., and Brigidi, P. (2007). Oxalate consumption by lactobacilli: evaluation of oxalyl-CoA decarboxylase and formyl-CoA transferase activity in Lactobacillus acidophilus. Journal of applied microbiology *103*, 1600-1609.
66. Belenguer, A., Bati, M.B., Hervás, G., Toral, P.G., Yáñez-Ruiz, D.R., and Frutos, P. (2013). Impact of oxalic acid on rumen function and bacterial community in sheep. animal *7*, 940-947.
67. Miller, A.W., Choy, D., Penniston, K.L., and Lange, D. (2019). Inhibition of urinary stone disease by a multi-species bacterial network ensures healthy oxalate homeostasis. Kidney international.
68. Miller, A.W., Dale, C., and Dearing, M.D. (2017). Microbiota Diversification and Crash Induced by Dietary Oxalate in the Mammalian Herbivore Neotoma albigula. mSphere *2*. 10.1128/mSphere.00428-17.
69. Miller, A.W., Dale, C., and Dearing, M.D. (2017). The Induction of Oxalate Metabolism In Vivo Is More Effective with Functional Microbial Communities than with Functional Microbial Species. MSystems *2*, e00088-00017.
70. Miller, A.W., Kohl, K.D., and Dearing, M.D. (2014). The gastrointestinal tract of the white-throated woodrat (Neotoma albigula) harbors distinct consortia of oxalate-degrading bacteria. Applied and environmental microbiology *80*, 1595-1601.
71. Miller, A.W., Oakeson, K.F., Dale, C., and Dearing, M.D. (2016). Effect of Dietary Oxalate on the Gut Microbiota of the Mammalian Herbivore Neotoma albigula. Applied and environmental microbiology *82*, 2669-2675.
72. Miller, A.W., Oakeson, K.F., Dale, C., and Dearing, M.D. (2016). Microbial community transplant results in increased and long-term oxalate degradation. Microbial ecology *72*, 470-478.
73. Drake, H.L. (2012). Acetogenesis (Springer Science & Business Media).
74. Asanuma, N., Iwamoto, M., and Hino, T. (1999). The production of formate, a substrate for methanogenesis, from compounds related with the glyoxylate cycle by mixed ruminal microbes. Nihon Chikusan Gakkaiho *70*, 67-73.
75. Ferry, J.G. (2012). Methanogenesis: ecology, physiology, biochemistry & genetics (Springer Science & Business Media).
76. Oremland, R.S., and Polcin, S. (1982). Methanogenesis and sulfate reduction: competitive and noncompetitive substrates in estuarine sediments. Applied and Environmental Microbiology *44*, 1270-1276.
77. Freel, R.W., Hatch, M., Green, M., and Soleimani, M. (2006). Ileal oxalate absorption and urinary oxalate excretion are enhanced in Slc26a6 null mice.

American Journal of Physiology-Gastrointestinal and Liver Physiology *290*, G719-G728.

78. Hatch, M., and Freel, R.W. (2008). The roles and mechanisms of intestinal oxalate transport in oxalate homeostasis. In 2. (Elsevier), pp. 143-151.

79. Dancygier, H., and Dancygier, H. (2010). Hepatic biotransformation. Clinical Hepatology: Principles and Practice of Hepatobiliary Diseases, 127-130.

80. Kohl, K.D., and Dearing, M.D. (2011). Induced and constitutive responses of digestive enzymes to plant toxins in an herbivorous mammal. Journal of Experimental Biology *214*, 4133-4140.

81. Kohl, K.D., and Dearing, M.D. (2016). The woodrat gut microbiota as an experimental system for understanding microbial metabolism of dietary toxins. Frontiers in microbiology *7*, 1165.

82. Koppel, N., Maini Rekdal, V., and Balskus, E.P. (2017). Chemical transformation of xenobiotics by the human gut microbiota. Science *356*. 10.1126/science.aag2770.

83. Strzelecki, T., and Menon, M. (1986). The uptake of oxalate by rat liver and kidney mitochondria. J Biol Chem *261*, 12197-12201.

84. Ormerod, K.L., Wood, D.L.A., Lachner, N., Gellatly, S.L., Daly, J.N., Parsons, J.D., Dal'Molin, C.G.O., Palfreyman, R.W., Nielsen, L.K., Cooper, M.A., et al. (2016). Genomic characterization of the uncultured Bacteroidales family S24-7 inhabiting the guts of homeothermic animals. Microbiome *4*, 1-17. 10.1186/s40168-016-0181-2.

85. Okuda, S., Yamada, T., Hamajima, M., Itoh, M., Katayama, T., Bork, P., Goto, S., and Kanehisa, M. (2008). KEGG Atlas mapping for global analysis of metabolic pathways. Nucleic acids research *36*, W423-W426.

86. Groussin, M., Poyet, M., Sistiaga, A., Kearney, S.M., Moniz, K., Noel, M., Hooker, J., Gibbons, S.M., Segurel, L., and Froment, A. (2021). Elevated rates of horizontal gene transfer in the industrialized human microbiome. Cell *184*, 2053-2067. e2018.

87. Goodman, A.L., Kallstrom, G., Faith, J.J., Reyes, A., Moore, A., Dantas, G., and Gordon, J.I. (2011). Extensive personal human gut microbiota culture collections characterized and manipulated in gnotobiotic mice. Proceedings of the National Academy of Sciences *108*, 6252-6257.

88. Koelink, P.J., Wildenberg, M.E., Stitt, L.W., Feagan, B.G., Koldijk, M., van 't Wout, A.B., Atreya, R., Vieth, M., Brandse, J.F., and Duijst, S. (2018). Development of reliable, valid and responsive scoring systems for endoscopy and histology in animal models for inflammatory bowel disease. Journal of Crohn's and Colitis *12*, 794-803.

89. Hughes, E.R., Winter, M.G., Duerkop, B.A., Spiga, L., de Carvalho, T.F., Zhu, W., Gillis, C.C., Büttner, L., Smoot, M.P., and Behrendt, C.L. (2017). Microbial respiration and formate oxidation as metabolic signatures of inflammation-associated dysbiosis. Cell host & microbe *21*, 208-219.

90. Pietzke, M., Meiser, J., and Vazquez, A. (2020). Formate metabolism in health and disease. Molecular metabolism *33*, 23-37.

91. Ternes, D., Tsenkova, M., Pozdeev, V.I., Meyers, M., Koncina, E., Atatri, S., Schmitz, M., Karta, J., Schmoetten, M., and Heinken, A. (2022). The gut

microbial metabolite formate exacerbates colorectal cancer progression. Nature metabolism *4*, 458-475.

92. Scott, K.P., Gratz, S.W., Sheridan, P.O., Flint, H.J., and Duncan, S.H. (2013). The influence of diet on the gut microbiota. Pharmacological research *69*, 52-60.
93. Doré, J., and Blottière, H. (2015). The influence of diet on the gut microbiota and its consequences for health. Current opinion in biotechnology *32*, 195-199.
94. Britton, R.A., and Young, V.B. (2014). Role of the intestinal microbiota in resistance to colonization by Clostridium difficile. Gastroenterology *146*, 1547-1553.
95. Deleu, S., Machiels, K., Raes, J., Verbeke, K., and Vermeire, S. (2021). Short chain fatty acids and its producing organisms: An overlooked therapy for IBD? EBioMedicine *66*.
96. Kelly, C.J., Zheng, L., Campbell, E.L., Saeedi, B., Scholz, C.C., Bayless, A.J., Wilson, K.E., Glover, L.E., Kominsky, D.J., and Magnuson, A. (2015). Crosstalk between microbiota-derived short-chain fatty acids and intestinal epithelial HIF augments tissue barrier function. Cell host & microbe *17*, 662-671.
97. Portincasa, P., Bonfrate, L., Vacca, M., De Angelis, M., Farella, I., Lanza, E., Khalil, M., Wang, D.Q.-H., Sperandio, M., and Di Ciaula, A. (2022). Gut microbiota and short chain fatty acids: implications in glucose homeostasis. International journal of molecular sciences *23*, 1105.
98. Shimizu, H., Masujima, Y., Ushiroda, C., Mizushima, R., Taira, S., Ohue-Kitano, R., and Kimura, I. (2019). Dietary short-chain fatty acid intake improves the hepatic metabolic condition via FFAR3. Scientific reports *9*, 1-10.
99. Tian, Y., Xu, Q., Sun, L., Ye, Y., and Ji, G. (2018). Short-chain fatty acids administration is protective in colitis-associated colorectal cancer development. The Journal of Nutritional Biochemistry *57*, 103-109.
100. Vieira, A.T., Galvão, I., Macia, L.M., Vinolo, M.A.R., Garcia, C.C., Tavares, L.P., Amaral, F.A., Sousa, L.P., Martins, F.S., and Mackay, C.R. (2017). Dietary fiber and the short-chain fatty acid acetate promote resolution of neutrophilic inflammation in a model of gout in mice. Journal of leukocyte biology *101*, 275-284.
101. Fusco, W., Lorenzo, M.B., Cintoni, M., Porcari, S., Rinninella, E., Kaitsas, F., Lener, E., Mele, M.C., Gasbarrini, A., and Collado, M.C. (2023). Short-chain fatty-acid-producing bacteria: key components of the human gut microbiota. Nutrients *15*, 2211.
102. Mann, E.R., Lam, Y.K., and Uhlig, H.H. (2024). Short-chain fatty acids: linking diet, the microbiome and immunity. Nature Reviews Immunology, 1-19.
103. Chiang, J.Y. (2009). Bile acids: regulation of synthesis: thematic review series: bile acids. Journal of lipid research *50*, 1955-1966.
104. Collins, S.L., Stine, J.G., Bisanz, J.E., Okafor, C.D., and Patterson, A.D. (2023). Bile acids and the gut microbiota: Metabolic interactions and impacts on disease. Nature Reviews Microbiology *21*, 236-247.
105. Gérard, P. (2013). Metabolism of cholesterol and bile acids by the gut microbiota. Pathogens *3*, 14-24.

1038 **Supplemental information titles and legends**
1039
1040 STAR Methods
1041 Supplementary Figures and table legends
1042 Figs. S1 to S10
1043 Tables S1 and S8
1044 References (*1-56*)
1045
1046 **Star Methods**
1047
1048 **Animal studies.**
1049 *Tracking animal health*
1050 Throughout all diet trials, animals were monitored for evidence of trauma, dehydration,
1051 pain, or other forms of suffering. Additionally, water and food intake, urine output, and
1052 body mass was monitored daily (i.e., Figs. S6, S9). If animals lost >10% of their
1053 baseline body mass, they were removed from the diet trial and placed back onto
1054 standard mouse chow.
1055
1056 *Effect of oxalate on the native gut microbiota of Neotoma albigula*
1057 To determine the impact of dietary oxalate on *N. albigula* with their native microbiota, 14
1058 adult *N. albigula* woodrats were collected from Castle Valley, UT (38.63′N, 109.41′W) in
1059 September 2014, using Sherman live traps. Animals were transported to the University
1060 of Utah and housed in individual cages (48 by 27 by 20 cm) with a 12-h/12-h light/dark
1061 cycle, at 28°C and 20% humidity. Animals were initially maintained on a 0.2% oxalate,
1062 high-fiber rabbit chow (Harlan Teklad formula 2031; Envigo) for 7 months prior to
1063 experimentation. This diet reduces the overall detectable diversity of the microbiota of
1064 these animals but maintains the members of the native microbiota overall [1]. All methods
1065 were approved by the IACUC under protocol no. 12-12010.
1066
1067 Subsequently, *N. albigula* woodrats were placed in a diet trial in which the oxalate
1068 concentration of the food was gradually increased over time along a gradient from 0.2%
1069 (for days 1 to 5; herein referred to as 0%), 3% (days 6 to 10), and 6% (days 11 to 15;
1070 Fig. 3A). The oxalate concentration of the diet was adjusted by adding the appropriate
1071 amount of sodium oxalate (Fisher Scientific, Pittsburgh, PA) into the powdered rabbit
1072 chow on a dry weight basis. The schedule for each concentration of dietary oxalate was
1073 chosen to ensure that the gut microbiota had time to respond to the specific diet [2,3].
1074 During diet trials, oxalate did not have a negative impact on *N. albigula* health and
1075 neither fecal nor urinary oxalate levels increased significantly[4].
1076
1077 During the diet trial, animals were placed in metabolic cages to separate urine and
1078 feces into sterile 50-ml conical tubes. A subsample of feces was collected from each
1079 animal every 4 to 5 days on the 0% and 6% oxalate diets for shotgun metagenomic
1080 sequencing. Samples were frozen at −80°C until DNA extraction.
1081
1082 *Stool collection for bacterial isolations and fecal transplant studies*

1083 Feces for fecal transplants were collected from two sources. For the Swiss-Webster
1084 feces, 20 individual animals (Taconic Farms, female, six weeks old) were placed on a
1085 0% oxalate diet in cages with a custom-designed insert to separate urine and feces at
1086 the Cleveland Clinic (IACUC #2016-1653) [5]. For the *N. albigula* feces, 14 individual
1087 animals (mixed sex and age) were placed on a 3% oxalate diet in a metabolic chamber
1088 at the University of Utah (IACUC #12-12010) to acclimate the microbiome to oxalate
1089 metabolism[5]. After 3 days of acclimation on the respective diets, feces were collected
1090 from animals within 2 h of defecation, submerged in sterile 15% glycerol and flushed
1091 with CO_2 prior to freezing at −80 °C until use in animal studies approximately 12 months
1092 after receipt (IACUC #2016-1653) or for bacterial isolations.
1093
1094 *Microbiota-dependent effects of oxalate on liver and gut microbiota*
1095 All animal studies were approved through the Cleveland Clinic's IACUC (IACUC #'s
1096 2016-1653, 2020-2312). To examine the host-independent effects of oxalate on gut
1097 microbiota with either a low or high efficiency at degrading oxalate, two distinct host-
1098 microbe model systems were developed. For both models, equal numbers of male and
1099 female Swiss-Webster mice were used as the host. For the low oxalate-degrading gut
1100 microbiota, Swiss-Webster mice were given fecal transplants using feces from other
1101 Swiss-Webster mice (allografts), as discussed below. A 1.5% oxalate diet is sufficient to
1102 induce hyperoxaluria in Swiss-Webster mice, defined as a 50% increase in urinary
1103 oxalate excretion[6-8]. For the high oxalate-degrading gut microbiota, Swiss-Webster mice
1104 were given fecal transplants from *N. albigula* (xenografts). We have previously shown
1105 that fecal transplants from *N. albigula* are sufficient to induce significant and persistent
1106 oxalate metabolism[7,8]. During and after fecal transplants, animals were grouped four to
1107 a cage, with four cages assigned to each treatment group, for a total of 16 animals per
1108 experimental group. To minimize individual variability and eliminate any cage effect in
1109 subsequent metrics, samples and data collected from all animals in a cage were pooled
1110 together into an individual sample. To develop the two different mouse models, the
1111 conversion of the gut microbiota from the native microbiota to the grafted microbiota
1112 (allografts or xenografts) was completed in two stages. First, the native microbiota was
1113 depleted with a five-day course of neomycin (0.5g/L water, combined with 2g/L
1114 sucralose), while on a 0% oxalate diet. Mice were given *ad libitum* access to water
1115 during this time and throughout the experiment. Neomycin is a broad spectrum antibiotic
1116 that is poorly absorbed across the gut, and effectively reduces gut microbiota density by
1117 up to 90%[9]. After antibiotic depletion, mice were given the respective fecal transplants
1118 by first thawing feces, then aseptically mixing 32 g feces per kg body weight directly into
1119 powdered mouse chow. Fecal transplants were performed daily for 6 days (Fig. 1A), as
1120 previously described[5], during which animals were switched to either a 0% or 1.5%
1121 oxalate diet. All animals were maintained on their respective diets for two weeks
1122 following fecal transplants (Table S1). A total of four treatment groups were defined
1123 based on allografts/xenografts and oxalate diet.
1124
1125 Following diet trials, animals were sacrificed through CO_2 asphyxiation and cervical
1126 dislocation. Upon necropsies, liver tissue from each animal was dissected out and
1127 placed into RNAlater on ice, prior to freezing at -80ºC, within two hours of necropsies.

1128 Additionally, colon feces were collected and placed into screw-cap tubes with o-rings,
1129 on ice, prior to freezing at -80ºC.
1130
1131 *Microbial cohort-dependent effects on mitigating the systemic effects of oxalate on host*
1132 *and microbiome*
1133 To determine the effect of specific microbial cohorts at mitigating the systemic host-
1134 microbiome effects of oxalate, different combinations of two microbial cohorts were
1135 established. First, based on the metabolic pathways enriched by oxalate in the *N.*
1136 *albigula* gut microbiota (Fig. 3D,5C, Table S5), assessed through comparative shotgun
1137 metagenomics (described below), we hypothesized that microorganisms that engage in
1138 those metabolic pathways help to mitigate the systemic effects of oxalate. To test this
1139 hypothesis, we isolated bacteria from *N. albigula* stool (described below) and grouped
1140 microorganisms into four cohorts (Fig. 5D). These included oxalate-degrading bacteria
1141 alone (Ox; Group 2), microorganisms that can utilize formate or oxalate (Ox_form;
1142 Group 3), oxalate and formate users, in addition to the metabolism of selected sugars
1143 (All; Group 4), or the complete cohort except for oxalate degraders (No_ox; Group 5).
1144 Microorganisms isolated from *N. albigula* stool and used in microbial transplants were
1145 termed the "metabolic cohort". In addition to the metabolic cohort, a "taxonomic cohort"
1146 was defined by cross-referenced metabolic pathways enriched by oxalate with microbial
1147 taxa previously reported to be stimulated by oxalate (Fig. 5D)[10]. Microorganisms from
1148 this cohort were purchased commercially from the ATCC or DSMZ (Table S8). In
1149 addition to these cohorts, we also examined a negative control in which animals were
1150 inoculated with sterile media (No_bact (Group 1); Group 1), and a positive control in
1151 which animals were inoculated with the whole gut microbiota of *N. albigula,* extracted
1152 from stool by first vortexing in a 1:1 mixture of stool and sterile PBS, followed by
1153 centrifuging at 8000RPM for 2 minutes. The supernatant was inoculated into gut
1154 microbiota media with 20mM sodium oxalate (Table S6) overnight prior to microbial
1155 transplant.
1156
1157 To prepare each isolate for transplants, an overnight culture of each species was grown
1158 and mixed in equal proportions by volume for each cohort. The community was then
1159 centrifuged and supernatant was decanted. After antibiotic depletion of the native gut
1160 microbiota in Swiss-Webster mice, 38mg of pelleted bacteria of each preparation was
1161 added directly to the food and administered over the course of six days (Figs. 6, S8), as
1162 done previously[6,7]. Preparations corresponded to approximately 5 x 10^8 microorganisms
1163 for each isolate in the appropriate transplant groups. Quantification of bacterial numbers
1164 was performed through absorbance of the microbial preparations on a
1165 spectrophotometer at 600 nm, calibrated to direct microscopic counts.
1166
1167 As above, animals were grouped four to a cage, with samples from each cage pooled
1168 together prior to collection and analyses. Similarly, animals were maintained on custom
1169 inserts that mimic metabolic cage for the effective separation of urine and stool prior to
1170 collection. During the microbial transplant animal studies, stool and urine was collected
1171 daily and inserts disinfected. For oxalate and formate quantification, samples were
1172 collected at the end of the antibiotic depletion, microbial transplants, a 0% oxalate
1173 washout period, and after return to a 3% oxalate diet (Figs. 6B-D, S8B-D). Prior to

1174 biochemical assays, urine was frozen (−20°C) and feces were dried at 45°C overnight.
1175 Prior to freezing, aliquots of urine were equally divided into six fractions for each of the
1176 biochemical assays performed (discussed below). Fractions for oxalate quantification
1177 were collected into 4N HCl prior to freezing to prevent the non-enzymatic conversion of
1178 ascorbic acid into oxalate [2]. For microbial inventories, a portion of feces and colon feces
1179 (discussed below) were frozen at −80°C. All animals were maintained on a 3% oxalate
1180 diet, except during the washout period (Table S1).
1181
1182 Following diet trials, animals were sacrificed through CO_2 asphyxiation and cervical
1183 dislocation. Necropsies were performed to aseptically remove colon feces, colon,
1184 kidneys, and heart tissue. Colon tissue was longitudinally bisected, swiss-rolled, and
1185 placed into 4% paraformaldehyde overnight for fixation at 4ºC for histopathology [11].
1186 Kidney and heart tissues were placed into 4% paraformaldehyde overnight for fixation at
1187 4ºC prior to histopathology. Hearts were first perfused with paraformaldehyde solution
1188 prior to immersion.
1189
1190 After fixation, colon, kidney, and heart tissue were placed in 70% ethanol at 4ºC prior to
1191 paraffin embedding, serial sectioning, and staining. To quantify colitis, colon tissue was
1192 stained with hematoxylin and eosin and imaged with light microscopy (Fig. 6H). Whole
1193 colons were scored for colitis by two blinded, independent reviewers using a semi-
1194 quantitative protocol that considers inflammatory infiltrates, goblet cell loss, crypt
1195 density, crypt hyperplasia, muscle thickening, submucosal inflammation, crypt
1196 abcesses, and ulcerations[12]. To quantify calcium oxalate deposition, kidney tissue was
1197 stained with Von Kossa staining[13], which turns calcium deposits black and the
1198 remaining tissue pink (Figs. 6E, S8E). Kidneys were imaged under light microscopy
1199 and calcium oxalate deposition was quantified using an automated process in QuPath,
1200 based on stain color. The area of the black calcium oxalate deposits was normalized to
1201 total kidney area. To quantify cardiac fibrosis, heart tissue was stained with Masson's
1202 trichrome stain, which stains collagen fibrosis blue and the remaining tissue red (Fig.
1203 S6H). Hearts were imaged under light microscopy and fibrosis was quantified with an
1204 automated process in QuPath, quantifying the blue and red stained areas[14]. Fibrosis
1205 was normalized to total heart surface area.
1206
1207 **Biochemical assays.**
1208 Urinary creatinine (Fisher Scientific), formate (VWR), IL-6 (R&D Systems), IL-18 (Fisher
1209 Scientific), and IL-1β (R&D Systems) were quantified with ELISA-based assays,
1210 following manufacturer's instructions. Positive controls that included a known amount of
1211 substrate along with no substrate negative controls were included in all batches of
1212 ELISA assays. Samples, standards and controls were all run in duplicate and values
1213 averaged. Urinary and fecal oxalate were quantified with an ELISA-based assay
1214 (Sigma-Aldrich), with a modified protocol, as follows. Upon initial testing of oxalate and
1215 formate assays using solutions of sodium oxalate and sodium formate in water, it was
1216 discovered that while formate assays only had affinity for formate, the oxalate assays
1217 had equal affinity for both oxalate and formate (Figs. S11A). Specifically, when oxalate
1218 alone was added to solution, the quantified concentration of oxalate matched the
1219 amount added. However, when oxalate and formate was added at equal

1220 concentrations, the quantified oxalate was approximately twice as high as what was
1221 added (Fig. S11B). Furthermore, when adding 300uM of formate or oxalate to human
1222 urine specimens, the amount of oxalate quantified was approximately 300uM higher
1223 than urine without any modifications (Fig. S11C). To eliminate the formate
1224 contamination on oxalate measurements, oxalate was extracted by first acidifying to pH
1225 3 with 3M HNO_3. Acidified urine was centrifuged, and supernatant collected. The pH
1226 was then brought up to 7 with NaOH. Subsequently, 5M $CaCl_2$ was added to solution to
1227 precipitate calcium oxalate. The precipitates were extracted by centrifugation and
1228 decanting. Finally, calcium oxalate solution was acidified in 1:4 parts of 4N HCl prior to
1229 enzymatic assay, as previously described[2]. When oxalate was extracted from urine
1230 specimens in this way, prior to quantification, we saw a significant decrease in
1231 quantified oxalate (Fig. S11C), as expected given the assay affinity for formate. When
1232 solutions containing formate alone went through the extraction process, no oxalate was
1233 quantified. Given these results, urinary and fecal oxalate was extracted prior to ELISA-
1234 based assays using the manufacturer's recommendations, post-extraction. For fecal
1235 oxalate, samples were acidified with 6N H_2SO_4 to solubilize oxalate prior to following the
1236 extraction protocol above. For creatinine, cytokines, and oxalate, values generated on
1237 a 0% oxalate diet were substracted from all other values, matched by cage, with the
1238 assumption that this would isolate oxalate-induced molecule generation. For urinary
1239 formate, this substraction was not done since formate can come from multiple sources
1240 other than oxalate degradation and values on a 0% oxalate diet were not clearly lower
1241 than on a 3% oxalate diet. For all values, data are presented as the change from
1242 baseline. Data were statistically compared with two-way analyses and post-hoc,
1243 Holm's-corrected, paired t-tests.
1244
1245 **Culturomic assays.**
1246 All assays were conducted under strict anaerobic conditions (90% N_2, 5% H_2, 5% CO_2)
1247 in an anaerobic chamber (Bactron 300).
1248
1249 The stool from *N. albigula* were used to determine the impact of environmental factors
1250 on oxalate metabolism *in vitro* and to isolate bacteria for the metabolic cohort.
1251 *Enterococcus gallinarum,* an oxalate-degrading species previously isolated from *N.*
1252 *albigula,* was also used in culturomic assays to determine the impact of environmental
1253 factors on oxalate metabolism[15]. To test environmental factors on oxalate metabolism,
1254 gut microbiota media, previously designed to support a broad array of gut bacteria[16],
1255 was used as a base media. From there, compounds were added to the media based on
1256 metabolic pathways enriched by dietary oxalate in the *N. albigula* gut microbiota (Fig.
1257 3D, Table S6). Concentrations of added chemicals were based on previously published
1258 media recipes where necessary. To assess oxalate metabolism in different culture
1259 conditions, oxalate was quantified by extracting oxalate and quantification through
1260 titration with $KMnO_4$, as we have done previously[15].
1261
1262 To isolate bacteria for the metabolic cohort and to validate the metabolic redundancy of
1263 oxalate metabolism and other pathways stimulated by oxalate, a minimal media with the
1264 same substrates from above were added as sole carbon and energy sources (Table
1265 S7). In this medium, oxalate was added at 50mM to specifically select for bacteria that

1266 can use oxalate as a carbon and energy source. Subsequently, the NALB microbiota
1267 from the stool was first diluted to ~1 bacterium/100ul and then inoculated into 5 or 10
1268 96-well plates, depending on the rarity of positive hits, and quantifying growth through
1269 spectrophotometry. Wells in which the absorbance values at 600nm for greater than
1270 one standard deviation above the average for all well were considered positive for
1271 growth. Wells with positive growth had bacteria isolated by streaking on rich media,
1272 transferred to broth cultures, and had stocks made in 15% glycerol that were frozen at -
1273 80ºC until needed. Those isolates grown in oxalate or formate containing media were
1274 subsequently enriched in the minimal media and oxalate or formate degradation was
1275 validated through broth cultures and ELISA-based assays.
1276
1277 **Metabolomics.**
1278 For untargeted metabolomic assays, fecal samples were re-suspended in Optima
1279 LC/MS grade water (50mg stool to 150ul water. The samples were then placed briefly in
1280 a water bath at 37°C and placed on dry ice. An aliquot of each sample was taken out for
1281 protein concentration measurement. Then, 150 µL of chilled acetonitrile containing
1282 internal standards (Betaine-d9, Carnitine-d9, Orinithine-d6, Valine-13C3, Tyrosine-13C,
1283 15N, Estrone-13C3, and Cholesterol-13C3) was added to the remaining samples
1284 followed by centrifugation at 14,000g for 10 minutes to precipitate out the protein pellet.
1285 The supernatants were recovered and transferred to fresh tubes. The samples were
1286 dried briefly and re-suspended in 2% acetonitrile and 0.1% formic acid for subsequent
1287 LCMS analysis. One-microliter aliquots taken from each sample were pooled and this
1288 QC standard was analyzed every 10 injections. The untargeted metabolomics was
1289 performed by injecting 0.5uL of each sample onto a 10 cm C18 column (Thermo Fisher
1290 CA) coupled to a Vanquish UHPLC running at 0.35mL/min using water and 0.1% formic
1291 acid as solvent A and acetonitrile and 0.1% formic acid as solvent B. The 15-min
1292 gradient used is given below. The Orbitrap Q Exactive HF was operated in positive and
1293 negative electrospray ionization modes in different LC-MS runs over a mass range of
1294 50-750 Da using full MS at 120,000 resolution. The data dependent acquisitions were
1295 obtained on the pooled QC sample. The DDA acquisition (DDA) include MS full scans at
1296 a resolution of 120,000 and HCD MS/MS scans taken on the top 10 most abundant ions
1297 at a resolution of 30,000 with dynamic exclusion of 4.0 seconds and the apex trigger set
1298 at 2.0 to 4.0 seconds. The resolution of the MS2 scans were taken at a stepped NCE
1299 energy of 20.0, 30.0 and 45.0.
1300
1301 XCMS was used to deconvolute the data using 5 ppm consecutive scan error, 7 to 75
1302 seconds as minimum and maximum peak width, S/N threshold of 10, and span of 0.2 in
1303 positive and negative electrospray ionization modes for retention time correction. The
1304 resulting peak table was normalized to total protein concentration and further analyzed
1305 via MetaboLyzer [17]. Briefly, the ion presence threshold was set at 0.7 in each study
1306 group. Data were then log-transformed and analyzed for statistical significance via non-
1307 parametric Mann-Whitney U test. Ions present in just a subset of samples were to be
1308 analyzed as categorical variables for presence status via Fisher's exact test. All p-
1309 values were set to be corrected via the Benjamini-Hochberg step-up procedure for false
1310 discovery rate (FDR < 0.05). The data could then be utilized for PCA, putative
1311 identification assignment, and pathway enrichment analysis via KEGG[18], HMDB[19],

1312 LIPIDMAPS[20], and BioCyc[21] databases. In addition to differential abundance analysis
1313 provided by MetaboLyzer, whole metabolome comparisons were made as a Binomial
1314 dissimilarity matrix, which is optimal for metabolomic datasets[22], with statistical analysis
1315 provided by PERMANOVA with 999 permutations and a principal component
1316 visualization in Vegan[23].
1317
1318 **Transcriptomics.**
1319 For transcriptomic analysis, RNA was extracted from liver tissue with a TRIzol RNA
1320 purification kit (Invitrogen), following manufacturer's recommendations. Extracted RNA
1321 was converted to cDNA using a cDNA synthesis kit (Fisher Scientific) and stored at -
1322 20ºC. The cDNA quality was checked on a bioanalyzer and libraries were prepared with
1323 the TruSeq stranded mRNA library prep kit. Sequencing occurred on an Illumina HiSeq
1324 2500 at the Genomics Core (Cleveland Clinic) for paired 100bp sequencing.
1325
1326 The raw sequencing files, with 33.5 million +/- 950,000 reads per sample, were pre-
1327 processed using an established protocol[24]. Specifically, FastQC and SortMeRNA was
1328 used to remove low quality reads, remove rRNA reads, and merge paired reads[25,26].
1329 Subsequently, trimmomatic was used to remove adapter sequences[27] and the
1330 remaining high quality reads were mapped to the mm10 mouse reference genome for
1331 annotation, using HISAT[28,29]. The annotated gene counts were normalized to fragments
1332 per kilobase of transcript per million mapped reads. Comparative whole transcriptome
1333 analyses were conducted as a Bray-Curtis dissimilarity index and principal components
1334 visualization with statistical analysis provided by PERMANOVA with 999 permutations,
1335 in the Vegan package of R statistical software[23,30]. Differential abundance analysis was
1336 conducted in Cuffdiff2, with significance defined at a false discovery rate <0.05 [31].
1337 Sequences mapping to mouse genes were annotated to metabolic pathway with the
1338 gene ontology database[32].
1339
1340 To integrate transcriptomic and metabolomic data, the normalized metabolite
1341 concentrations and normalized transcript counts of metabolites and genes that were
1342 significantly different between the SWM-SWM and SWM-NALB groups were correlated,
1343 within each group, using SPARCC correlations in R[33]. Significant positive and negative
1344 correlations were calculated at an R greater or less than 0.4 or -0.4, respectively and an
1345 FDR <0.05. Significant correlations were visualized in Cytoscape version 3.3.0[34].
1346
1347 **Shotgun metagenomics.**
1348 For shotgun metagenomic analysis, DNA from *N. albigula* stool was extracted with the
1349 QIAmp DNA stool minikit (Qiagen). The extracted DNA was submitted to Argonne
1350 National Laboratory (Chicago, IL) for 150bp paired-end shotgun metagenomic
1351 sequencing on an Illumina HiSeq 2500. The low quality reads were trimmed from raw
1352 sequencing data and paired ends were merged using default parameters in BBMerge[35].
1353 Reads were first mapped to the *Neotoma* genome [36] with BWA mem with default
1354 settings[37], and removed. Paired, non-rodent sequences were assembled in
1355 MetaSpades with default parameters[38].
1356

1357 Full-length microbial genes were extracted and annotated from the assembled contigs
1358 using PROKKA software[39]. Gene annotation was achieved by mapping to the UniProt
1359 and Hamap protein databases[40,41]. To dereplicate genes, ensure common
1360 nomenclature across samples, and build a reference gene catalog for the quantification
1361 of gene counts, full-length genes were clustered at 90% homology in CD-hit[42]. After the
1362 creation of a non-redundant gene catalogue, high quality reads for each sample were
1363 mapped to the annotated gene catalog to generate gene-level count tables with BWA
1364 mem.
1365
1366 Gene count tables were normalized and differential abundance analysis was conducted
1367 with a negative binomial Wald test in DESeq2[43]. Significantly different genes were
1368 considered at an FDR <0.05. The normalized count tables were also used to generate a
1369 weighted Bray–Curtis dissimilarity matrix in the Vegan R package, with statistical
1370 comparisons with a PERMANOVA at 999 permutations[23]. To annotate differentially
1371 abundant genes to taxonomy, genes were mapped to full length genomes extracted
1372 directly from the shotgun metagenomic data, as described below.
1373
1374 de novo *genome construction and calculation of metabolic redundancy*
1375 For the *de novo* construction of genomes, the metaspades assembled contigs were
1376 binned to genomes with Autometa software[44], as previously described[45]. The Autometa
1377 algorithm takes assembled contigs as input, bins the data to genomes using contig
1378 coverage values, GC content, and the Barnes-Hut t-Distributed Stochastic Neighbor
1379 Embedding (BH t-SNE) distribution of the contigs. Taxonomy is assigned based on the
1380 consensus classification of all contigs in a genomic bin. Completeness and purity
1381 calculations are based on the presence of known, unique universal single copy genes in
1382 Autometa. After genomic binning, the contigs were oriented and scaffolded in CSAR[46],
1383 which compares the genomic bins to reference genomes of close relatives. Gaps within
1384 the genomes were filled with Abyss-Sealer[47] using the original raw sequencing reads as
1385 input. The completeness and purity of genomes were recalculated and taxonomic
1386 assignment was validated through phylogenetic analysis of the *de novo* constructed
1387 genomes in comparison with all complete NCBI genomes (Fig S1), achieved through
1388 Phylophlan, using the "—accurate" parameter which considers more phylogenetic
1389 positions at the cost of computational speed[48]. Phylophlan allows for the phylogenetic
1390 analysis of bacteria and archaea using complete genomes rather than gene amplicons,
1391 which provides greater resolution on phylogenetic analysis. Collectively, we extracted
1392 248 high quality, full length genomes, defined as being >80% complete and >90% pure,
1393 based on current standards[49].
1394
1395 To quantify the proportion of the *N. albigula* microbiota that contained genes related to
1396 oxalate metabolism, formate metabolism, acetogenesis, methanogenesis, or sulfate
1397 reduction, all genes that contribute to those metabolic pathways were extracted from the
1398 KEGG database[50]. Subsequently, PROKKA[39] was run on the 248 full length genomes
1399 to extract and annotate full length genes. The PROKKA extracted genes were then
1400 cross-referenced with the gene databases from KEGG to determine the proportion of
1401 genomes that contained at least one gene in the target pathways and determine which
1402 taxa had those genes.

1403
1404 **16S rRNA metagenomics.**
1405 Fecal DNA from mice in the SWM-NALB and SWM-SWM studies, underwent DNA
1406 extraction through a semi-automated protocol on a KingFisher Duo Prime System
1407 (Thermo Scientific) following the manufacturer's protocol for stool. The protocol
1408 includes mechanical lysis with bead-beating, piston driven lysis, and proteinase K
1409 chemical lysis. The extracted DNA, which attaches to magnetic beads in a proprietary
1410 salt solution, is removed from solution and eluted in buffer. Duplicate samples of a
1411 commercial DNA positive of known composition (Zymboiomcs, USA) were included as
1412 positive controls, as well as the DNA reagents that went through the entire workflow,
1413 sterile water, and a PCR negative as negative controls.
1414
1415 The fecal DNA was submitted to the Microbial Sequencing and Analytics Core at
1416 Cleveland Clinic for high throughput sequencing of the 16S rRNA gene on an Illumina
1417 MiSeq. The DNA was first PCR amplified with the 515F and 806R primers that target
1418 the V4 hypervariable region of the 16S gene. The DNA concentrations were quantified
1419 before and after PCR amplification on a Qubit and normalized prior to library prep with
1420 the Illumina Nextera XT library prep kit. The sequence run was conducted to generate
1421 150bp, paired-end sequences.
1422
1423 The raw sequencing data were processed in the R statistical package (4.2.0)[30]. Quality
1424 control, removal of bimeras, and assignment of amplicon sequence variants (ASV) were
1425 completed in dada2[51]. For ASV taxonomic assignment, a combined, non-redundant
1426 database of the Silva 138 SSURef and NCBI 16S rRNA databases were used[52]. Taxa
1427 assigned to mitochondria or chloroplasts were removed from subsequent analysis. The
1428 resulting ASV's were aligned in MSA[53] and arranged into a maximum likelihood
1429 phylogeny in phangorn[54]. The resulting phylogenetic tree and ASV table were merged
1430 with sample data for loading into PhyloSeq[55]. The sequencing depth threshold required
1431 to adequately capture microbial diversity was calculated with a rarefaction analysis in
1432 Vegan[23]. Non-control samples below the depth threshold were removed from further
1433 analysis.
1434
1435 The raw count table of 16S rRNA sequences was normalized with the DESeq2
1436 algorithm and α-diversity was calculated as phylogenetic diversity in Phyloseq, along
1437 with beta-diversity as a weighted UniFrac distance[56]. Alpha diversity was analyzed with
1438 a paired t-test with a Holm's correction where applicable, while beta-diversity analyses
1439 were conducted with a PERMANOVA after 999 permutations.
1440
1441
1442 **Supplementary figure legends:**
1443
1444 Fig. S1. Phylogeny of genomes extracted from the *N. albigula* metagenome, in
1445 comparison to >3000 full length microbial genomes. Stars indicate taxonomic
1446 placement of extracted genomes. All other points indicate reference genomes.
1447

1448 Fig. S2. Representation of formate metabolism genes in the NALB metagenome derived
1449 from 248 full length genomes. A) Proportion of the genomes extracted from *N. albigula*
1450 that had at least one formate metabolism gene. B) Representation of formate
1451 metabolism genes among the metagenome, broken down by gene function and
1452 proportion of total formate metabolism genes. C) Representation of formate metabolism
1453 genes broken down by taxon.
1454
1455 Fig. S3. Representation of acetogenic genes in the NALB metagenome derived from
1456 248 full length genomes. A) Proportion of the genomes extracted from *N. albigula* that
1457 had at least one acetogenic gene. B) Representation of acetogenic genes among the
1458 metagenome, broken down by gene function and proportion of total acetogenic genes.
1459 C) Representation of acetogenic genes broken down by taxon.
1460
1461 Fig. S4. Representation of methanogenic genes in the NALB metagenome derived from
1462 248 full length genomes. A) Proportion of the genomes extracted from *N. albigula* that
1463 had at least one methanogenic gene. B) Representation of methanogenic genes
1464 among the metagenome, broken down by gene function and proportion of total
1465 methanogenic genes. C) Representation of methanogenic genes broken down by
1466 taxon.
1467
1468 Fig. S5. Representation of sulfate-reducing genes in the NALB metagenome derived
1469 from 248 full length genomes. A) Proportion of the genomes extracted from *N. albigula*
1470 that had at least one sulfate-reducing gene. B) Representation of sulfate-reducing
1471 genes among the metagenome, broken down by gene function and proportion of total
1472 sulfate-reducing genes. C) Representation of sulfate-reducing genes broken down by
1473 taxon.
1474
1475 Fig. S6. Microbial transplant composition impact on urinary inflammation, renal health,
1476 and overall mouse health for the taxonomic cohort. A-G) The effect of microbial
1477 transplants on urinary IL-6 (A), IL-18 (B), and creatinine (C) levels, along with water
1478 intake (D), urine output (E), food intake (F) and body mass (G). H) Masson's Trichrome
1479 staining of heart tissue reveals fibrosis. Shown are representative images from the
1480 No_bact (Group 1) and All (Group 4) groups. I) Quantification of cardiac fibrosis from
1481 different microbial transplant groups. Statistical significance - 2-way ANOVA (shown on
1482 charts) and post-hoc, Holm's corrected, paired t-tests. Blue letters reflect statistical
1483 groups between microbial transplants and *$p<0.05$, **$p<0.01$; ***$p<0.001$ for longitudinal
1484 comparisons within each microbial transplant group.
1485
1486 Fig. S7. Effect of microbial transplants on microbial community composition for the
1487 taxonomic cohort. A,B) Beta-diversity analysis based on a weighted UniFrac
1488 dissimilarity matrix of colon feces collected at the end of the study period vs. stool (A; .
1489 $p=0.006$, PERMANOVA) or in the endpoint stool samples by group (B; no significant
1490 differences). Similar results for (B) were obtained with colon feces. Statistical
1491 differences shown by blue letters in legend. C) Within group beta-diversity distance of
1492 colon feces. $p=0.006$, one-way ANOVA. Blue letters represent statistical groups, based
1493 on post-hoc, Holm's corrected, paired t-tests. Similar results were found with endpoint

stool samples. D) Change in phylogenetic diversity of stool for each microbial transplant group. Stats, shown on graph, are based on Pearson correlations. E) Normalized counts of transplanted microorganisms in the stool across timepoints and in the colon feces at the end of the diet trial.

Fig. S8. Microbial community composition (metabolic cohort) impacted the effect of exogenous oxalate on kidney health. A) Experimental design. Swiss Webster mice were given neomycin, followed by inoculation of one of five microbial consortia that included either no bacteria, the NALB community, or the metabolic cohort listed in Figure 5C. Animals were maintained on a 3% oxalate diet throughout the trial except for a 0% oxalate washout period after the microbial transplant period. B,C) The effect of microbial transplants on urinary (B) or fecal (C) oxalate levels over the course of the diet trial, compared to baseline. ANOVA $p<0.001$ for microbial group (B&C), and $p<0.01$ for both timeperiod and in 2-way analysis for (B only). D) The effect of microbial transplants on urinary formate levels over the course of the diet trial. ANOVA $p<0.001$ for microbial group and timeperiod. E) Renal calcium oxalate deposition based on Von Kossa staining of renal tissue sections. Arrows show calcium deposits stained black, which were quantified through an automated algorithm in QuPath. F) Quantification of renal calcium oxalate deposition by group. $p=0.014$; ANOVA. G,H) Pearson correlation between urinary oxalate ($R=0.7$, $p<0.001$) (G) or formate ($R=0.026$, $p=0.9$) (H) and renal calcium oxalate deposition. Where applicable, statistical significance was assessed through an ANOVA and post-hoc, Holm's corrected, paired t-tests. Statistical groups shown by blue letters.

Fig. S9. Microbial transplant composition impact on urinary inflammation, renal health, and overall mouse health for the metabolic cohort. A-G) The effect of microbial transplants on urinary IL-6 (A), IL-18 (B), and creatinine (C) levels, along with water intake (D), urine output (E), food intake (F) and body mass (G). Statistical significance - 2-way ANOVA (shown on charts) and post-hoc, Holm's corrected, paired t-tests. Blue letters reflect statistical groups between microbial transplants and $*p<0.05$, $**p<0.01$; $***p<0.001$ for longitudinal comparisons within each microbial transplant group.

Fig. S10. Effect of microbial transplants on microbial community composition for the metabolic cohort. A,B) Beta-diversity analysis based on a weighted UniFrac dissimilarity matrix of colon feces collected at the end of the study period vs. stool (A; . $p=0.006$, PERMANOVA) or in the endpoint stool samples by group (B; no significant differences). Similar results for (B) were obtained with colon feces. Statistical differences shown by blue letters in legend. C) Within group beta-diversity distance of colon feces. $p=0.006$, one-way ANOVA. Blue letters represent statistical groups, based on post-hoc, Holm's corrected, paired t-tests. Similar results were found with endpoint stool samples. D) Change in phylogenetic diversity of stool for each microbial transplant group. Stats, shown on graph, are based on Pearson correlations. E) Normalized counts of transplanted microorganisms in the stool across timepoints and in the colon feces at the end of the diet trial.

Fig. S11. Effect of oxalate and formate on oxalate quantification using an enzymatic, ELISA-based assay. A) Correlation between oxalate or oxalate + formate, added to water, on oxalate concentration quantified through the enzymatic kit. B) Ratio of the calculated oxalate vs. the added concentration of oxalate and formate. C) The effect of adding oxalate or formate to urine, or of extracting oxalate from urine. R values and p-values (A) or p-values from one-way ANOVA (B,C) shown on chart. Blue letters represent statistical groups, based on pairwise t-tests.

1549 **Supplementary legends**
1550
1551 Table S1. Diets used in animal studies.
1552
1553 Table S2. The number of host hepatic genes in each metabolic pathway that exhibited
1554 a significant increase (positive numbers) or decrease (negative numbers) in expression
1555 upon consumption of a 1.5% oxalate diet.
1556
1557 Table S3. The number of microbial metabolites in each metabolic pathway that
1558 exhibited a significant increase (positive numbers) or decrease (negative numbers) in
1559 expression upon consumption of a 1.5% oxalate diet by the host.
1560
1561 Table S4. The significant positive and negative correlations between microbial
1562 metabolites and host hepatic gene expression for those metabolites/genes significantly
1563 altered by 1.5% oxalate consumption. Data are listed with the host microbiome,
1564 metabollite and gene ID, long with correlation values and false discovery rate corrected
1565 p-values.
1566
1567 Table S5. The number of microbial genes in each metabolic pathway that exhibited a
1568 significant increase (positive numbers) or decrease (negative numbers) in abundance
1569 upon consumption of a 6% oxalate diet by the host.
1570
1571 Table S6. Media recipe used to test the impact of substrates on oxalate metabolism.
1572
1573 Table S7. Media recipe used to test the proportion of the NALB community that can
1574 utilize substrates as sole carbon and energy sources.

Supplementary Figures

Fig. S1

A: Bacteroidetes
B: Firmicutes
C: Proteobacteria
D: Synergistetes
E: Tenericutes
F: Actinobacteria
G: Actinobacteria
H: Thermotogae
I: Thermotogae
J: Spirochaetes
K: Spirochaetes
L: Chrysiogenetes
M: Chrysiogenetes
N: Thermi
O: Thermi
P: Thermodesulfobacteria
Q: Thermodesulfobacteria
R: Deferribacteres
S: Deferribacteres
T: Cyanobacteria
U: Caldithrix
V: Caldithrix
W: Chloroflexi
X: Chloroflexi
Y: Fusobacteria
Z: Fusobacteria
a: Aquificae
b: Aquificae
c: Verrucomicrobia
d: Planctomycetes
e: Acidobacteria
f: Acidobacteria
g: Chlamydiae
h: Chlamydiae
i: Deinococcus-Thermus
j: Chlorobi
k: Lentisphaerae
l: Lentisphaerae
m: WWE1
n: Elusimicrobia
o: Elusimicrobia
p: TM7
q: Dictyoglomi
r: Nitrospirae
s: Gemmatimonadetes
t: Gemmatimonadetes
u: Fibrobacteres
v: Fibrobacteres
w: Euryarchaeota
x: Crenarchaeota
y: Nanoarchaeota

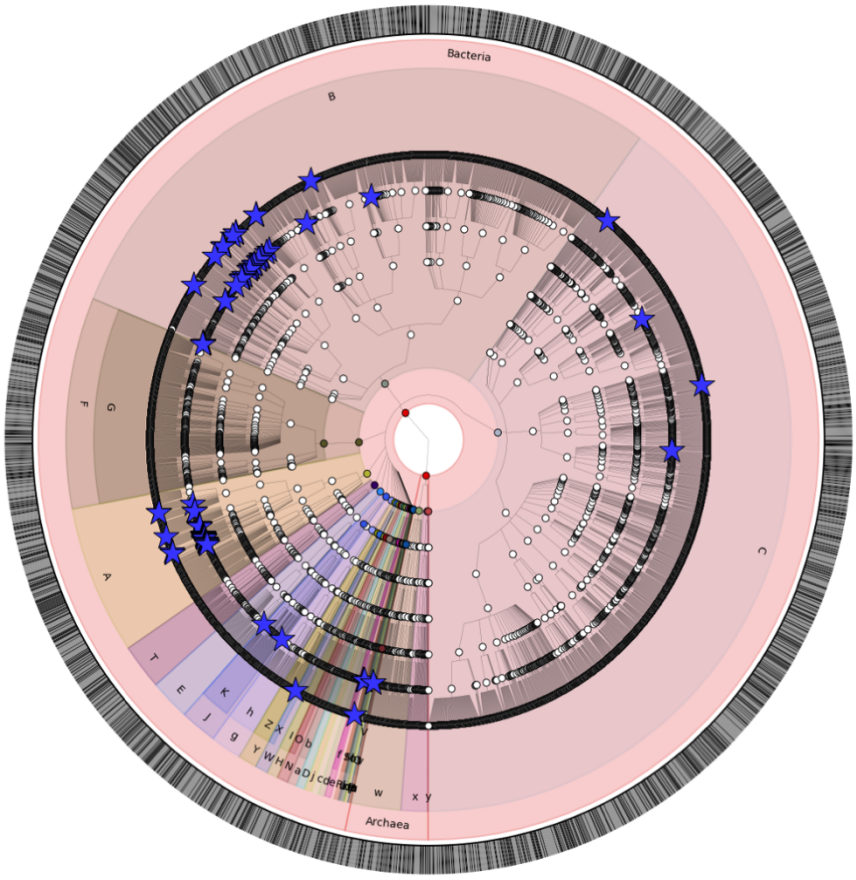

.

Fig. S2

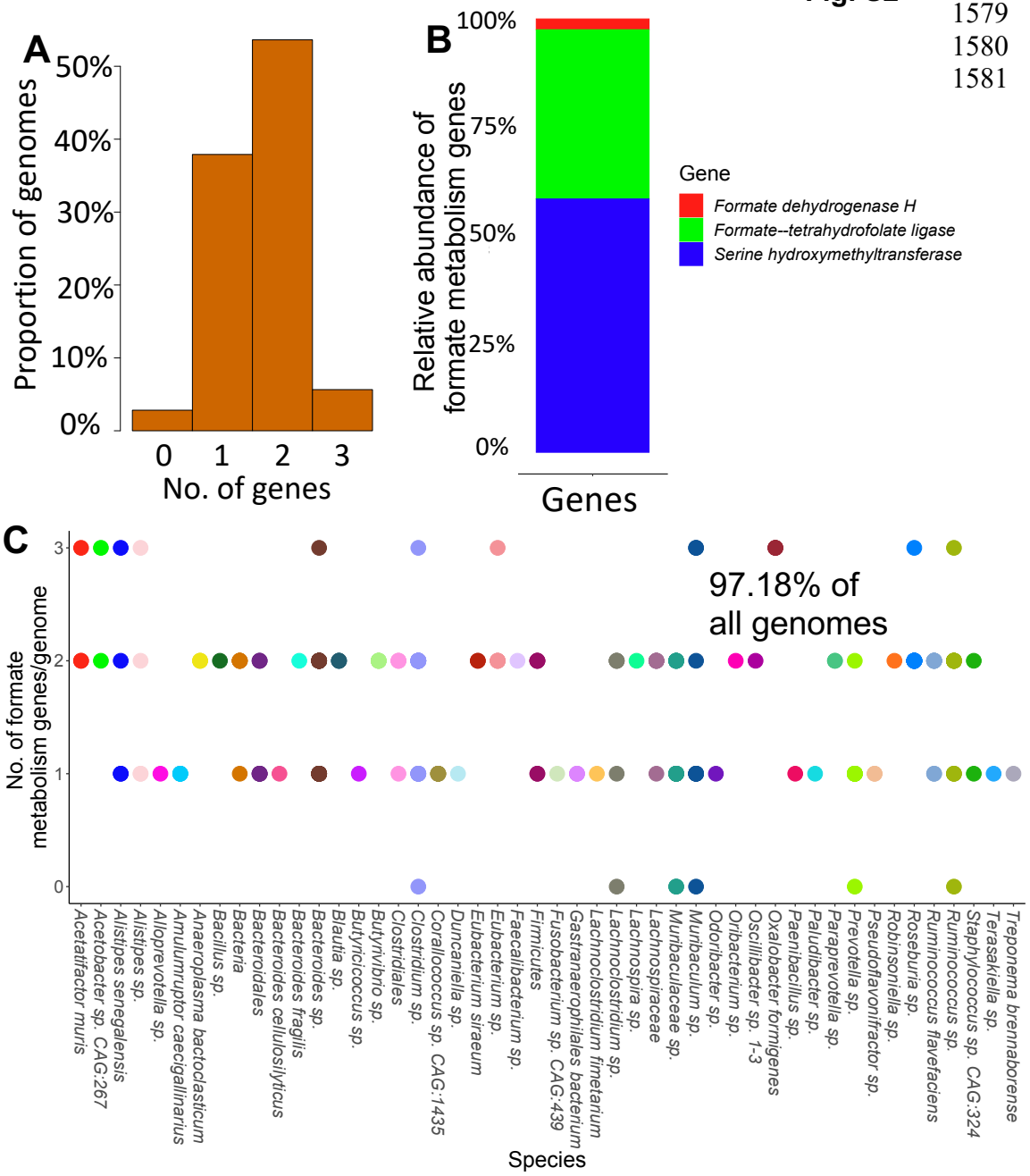
A
Proportion of genomes
50%
40%
30%
20%
10%
0%
0
1
2
3
No. of genes
B
Relative abundance of formate metabolism genes
100%
75%
50%
25%
0%
Genes
Gene
Formate dehydrogenase H
Formate--tetrahydrofolate ligase
Serine hydroxymethyltransferase
C
No. of formate metabolism genes/genome
97.18% of all genomes
Acetatifactor muris
Acetobacter sp. CAG:267
Alistipes senegalensis
Alistipes sp.
Alloprevotella sp.
Amulumruptor caecigallinarius
Anaeroplasma bactoclasticum
Bacillus sp.
Bacteria
Bacteroidales
Bacteroides cellulosilyticus
Bacteroides fragilis
Bacteroides sp.
Blautia sp.
Butyricicoccus sp.
Butyrivibrio sp.
Clostridiales
Clostridium sp.
Coprococcus sp. CAG:1435
Duncaniella sp.
Eubacterium siraeum
Eubacterium sp.
Faecalibacterium sp.
Firmicutes
Fusobacterium sp. CAG:439
Gastranaerophilales bacterium
Lachnoclostridium fimetarium
Lachnoclostridium sp.
Lachnospira sp.
Lachnospiraceae
Muribaculum sp.
Muribaculaceae sp.
Odoribacter sp.
Oribacterium sp.
Oscillibacter sp. 1-3
Oxalobacter formigenes
Paenibacillus sp.
Paludibacter sp.
Paraprevotella sp.
Prevotella sp.
Pseudoflavonifractor sp.
Robinsoniella sp.
Roseburia sp.
Ruminococcus flavefaciens
Ruminococcus sp.
Staphylococcus sp. CAG:324
Terasakiella sp.
Treponema brennaborense
Species

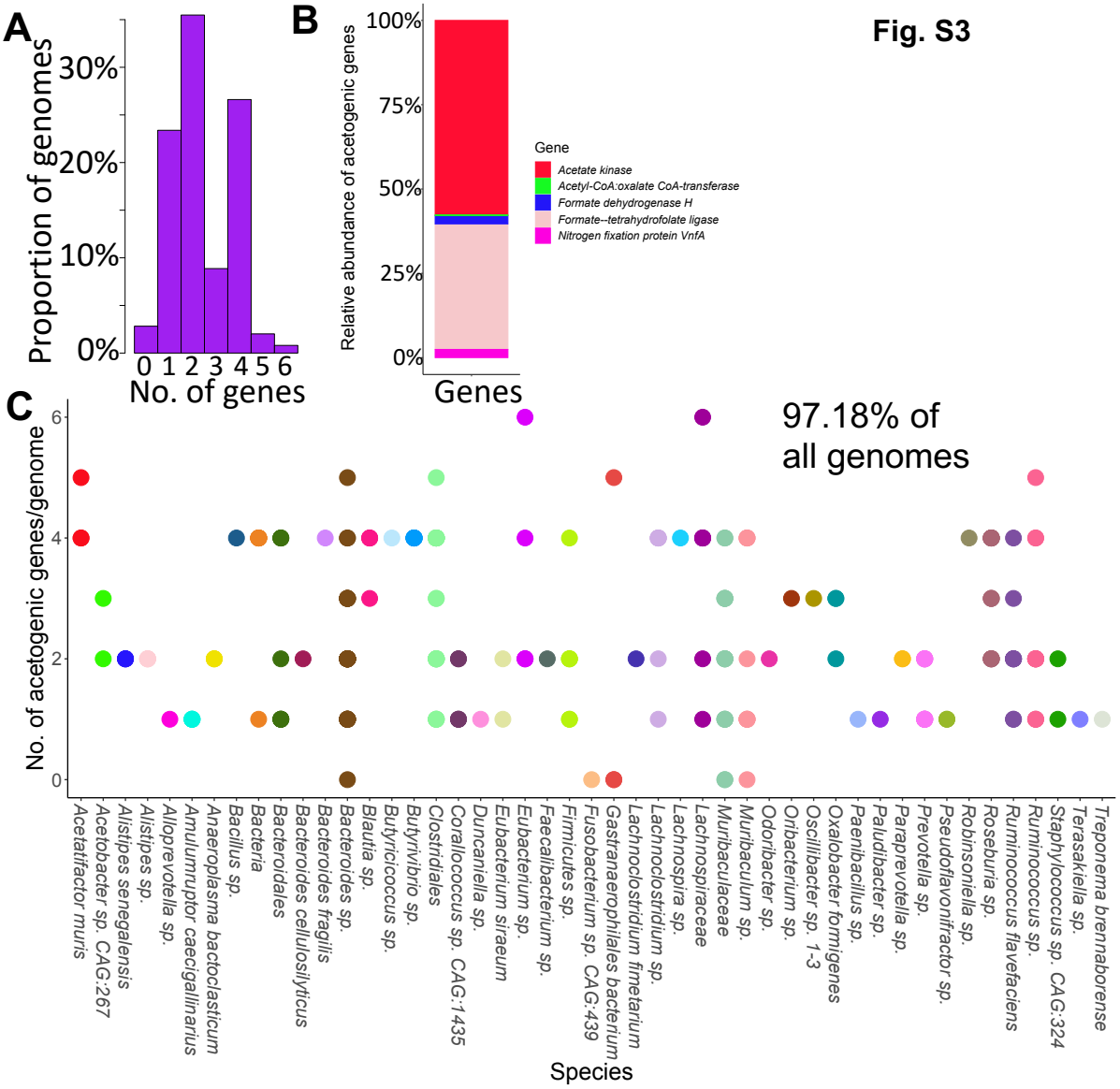
A
Proportion of genomes
30%
20%
10%
0%
0 1 2 3 4 5 6
No. of genes
B
Relative abundance of acetogenic genes
100%
75%
50%
25%
0%
Genes
Gene
Acetate kinase
Acetyl-CoA:oxalate CoA-transferase
Formate dehydrogenase H
Formate--tetrahydrofolate ligase
Nitrogen fixation protein VnfA
C
No. of acetogenic genes/genome
97.18% of
all genomes
Acetatifactor muris
Acetobacter sp. CAG:267
Alistipes senegalensis
Alistipes sp.
Alloprevotella sp.
Amulumruptor caecigallinarius
Anaeroplasma bactoclasticum
Bacillus sp.
Bacteria
Bacteroidales
Bacteroides cellulosilyticus
Bacteroides fragilis
Bacteroides sp.
Blautia sp.
Butyricicoccus sp.
Butyrivibrio sp.
Clostridiales
Coprococcus sp. CAG:1435
Duncaniella sp.
Eubacterium siraeum
Eubacterium sp.
Faecalibacterium sp.
Firmicutes sp.
Fusobacterium sp. CAG:439
Gastranaerophilales bacterium
Lachnoclostridium firmetarium
Lachnoclostridium sp.
Lachnospira sp.
Lachnospiraceae
Muribaculum sp.
Muribaculaceae
Odoribacter sp.
Oribacterium sp.
Oscillibacter sp. 1-3
Oxalobacter formigenes
Paludibacter sp.
Paenibacillus sp.
Paraprevotella sp.
Prevotella sp.
Pseudoflavonifractor sp.
Robinsoniella sp.
Roseburia sp.
Ruminococcus flavefaciens
Ruminococcus sp.
Staphylococcus sp. CAG:324
Terasakiella sp.
Treponema brennaborense
Species

Fig. S3

1582

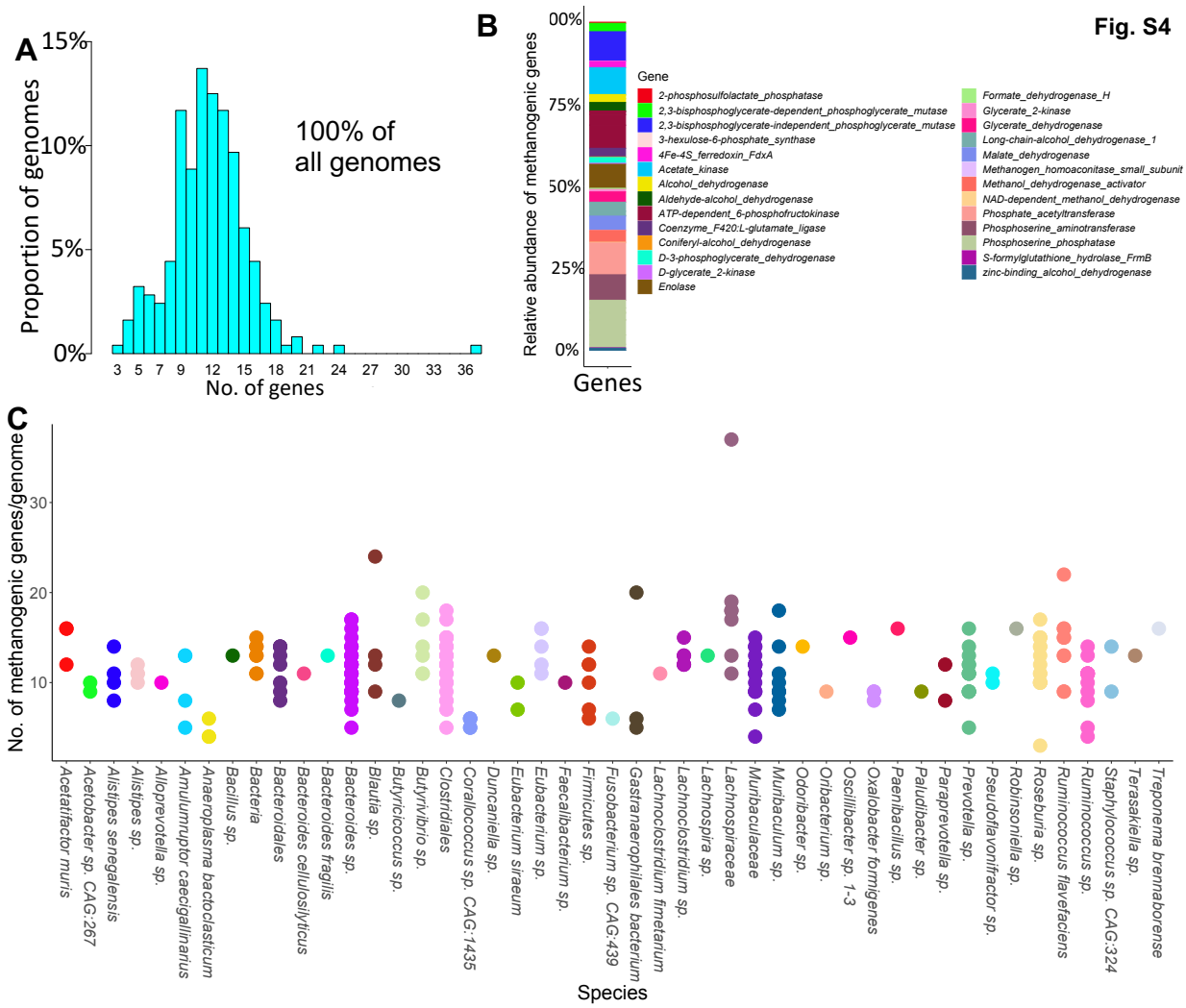
Fig. S4
A
Proportion of genomes
15%
10%
5%
0%
100% of
all genomes
3 5 7 9 12 15 18 21 24 27 30 33 36
No. of genes
B
Relative abundance of methanogenic genes
00%
75%
50%
25%
0%
Genes
Gene
2-phosphosulfolactate_phosphatase
2,3-bisphosphoglycerate-dependent_phosphoglycerate_mutase
2,3-bisphosphoglycerate-independent_phosphoglycerate_mutase
3-hexulose-6-phosphate_synthase
4Fe-4S_ferredoxin_FdxA
Acetate_kinase
Alcohol_dehydrogenase
Aldehyde-alcohol_dehydrogenase
ATP-dependent_6-phosphofructokinase
Coenzyme_F420:L-glutamate_ligase
Coniferyl-alcohol_dehydrogenase
D-3-phosphoglycerate_dehydrogenase
D-glycerate_2-kinase
Enolase
Formate_dehydrogenase_H
Glycerate_2-kinase
Glycerate_dehydrogenase
Long-chain-alcohol_dehydrogenase_1
Malate_dehydrogenase
Methanogen_homoaconitase_small_subunit
Methanol_dehydrogenase_activator
NAD-dependent_methanol_dehydrogenase
Phosphate_acetyltransferase
Phosphoserine_aminotransferase
Phosphoserine_phosphatase
S-formylglutathione_hydrolase_FrmB
zinc-binding_alcohol_dehydrogenase
C
No. of methanogenic genes/genome
30
20
10
Acetatifactor muris
Acetobacter sp. CAG:267
Alistipes senegalensis
Alistipes sp.
Alloprevotella sp.
Amulumruptor caecigallinarius
Anaeroplasma bactoclasticum
Bacillus sp.
Bacteria
Bacteroidales
Bacteroides cellulosilyticus
Bacteroides fragilis
Bacteroides sp.
Blautia sp.
Butyrivibrio sp.
Butyricicoccus sp.
Clostridiales
Coprococcus sp. CAG:1435
Duncaniella sp.
Eubacterium siraeum
Eubacterium sp.
Faecalibacterium sp.
Firmicutes sp.
Fusobacterium sp. CAG:439
Gastranaerophilales bacterium
Lachnoclostridium fimetarium
Lachnoclostridium sp.
Lachnospira sp.
Lachnospiraceae
Muribaculum sp.
Muribaculaceae
Odoribacter sp.
Oribacterium sp.
Oscillibacter sp. 1-3
Oxalobacter formigenes
Paenibacillus sp.
Paludibacter sp.
Parapreotella sp.
Prevotella sp.
Pseudoflavonifractor sp.
Robinsoniella sp.
Roseburia sp.
Ruminococcus flavefaciens
Ruminococcus sp.
Staphylococcus sp. CAG:324
Terasakiella sp.
Treponema brennaborense
Species

1583

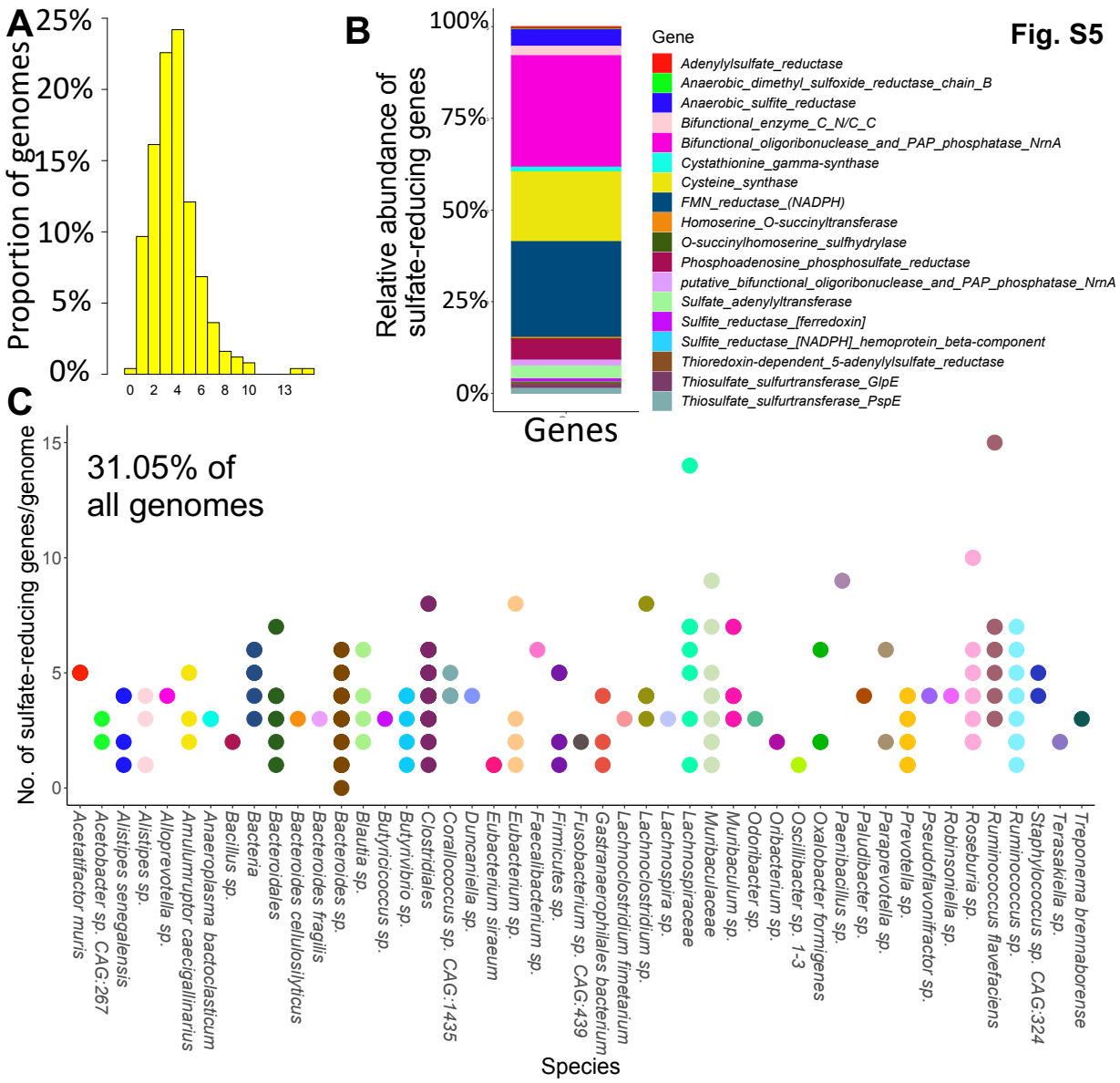
Fig. S5
A
Proportion of genomes
25%
20%
15%
10%
5%
0%
0 2 4 6 8 10 13
B
Relative abundance of sulfate-reducing genes
100%
75%
50%
25%
0%
Genes
Gene
Adenylylsulfate_reductase
Anaerobic_dimethyl_sulfoxide_reductase_chain_B
Anaerobic_sulfite_reductase
Bifunctional_enzyme_C_N/C_C
Bifunctional_oligoribonuclease_and_PAP_phosphatase_NrnA
Cystathionine_gamma-synthase
Cysteine_synthase
FMN_reductase_(NADPH)
Homoserine_O-succinyltransferase
O-succinylhomoserine_sulfhydrylase
Phosphoadenosine_phosphosulfate_reductase
putative_bifunctional_oligoribonuclease_and_PAP_phosphatase_NrnA
Sulfate_adenylyltransferase
Sulfite_reductase_[ferredoxin]
Sulfite_reductase_[NADPH]_hemoprotein_beta-component
Thioredoxin-dependent_5-adenylylsulfate_reductase
Thiosulfate_sulfurtransferase_GlpE
Thiosulfate_sulfurtransferase_PspE
C
No. of sulfate-reducing genes/genome
15
10
5
0
31.05% of
all genomes
Acetatifactor muris
Acetobacter sp. CAG:267
Alistipes senegalensis
Alistipes sp.
Alloprevotella sp.
Amulumruptor caecigallinarius
Anaeroplasma bactoclasticum
Bacillus sp.
Bacteria
Bacteroidales
Bacteroides cellulosilyticus
Bacteroides fragilis
Bacteroides sp.
Blautia sp.
Butyricicoccus sp.
Butyrivibrio sp.
Clostridiales
Coprococcus sp. CAG:1435
Duncaniella sp.
Eubacterium siraeum
Eubacterium sp.
Faecalibacterium sp.
Firmicutes sp.
Fusobacterium sp. CAG:439
Gastranaerophilales bacterium
Lachnoclostridium fimetarium
Lachnoclostridium sp.
Lachnospira sp.
Lachnospiraceae
Muribaculaceae
Muribaculum sp.
Odoribacter sp.
Oribacterium sp.
Oscillibacter sp. 1-3
Oxalobacter formigenes
Paenibacillus sp.
Paludibacter sp.
Paraprevotella sp.
Prevotella sp.
Pseudoflavonifractor sp.
Robinsoniella sp.
Roseburia sp.
Ruminococcus flavefaciens
Ruminococcus sp.
Staphylococcus sp. CAG:324
Terasakiella sp.
Treponema brennaborense
Species

1584

1585

Taxonomic cohort

Fig. S6

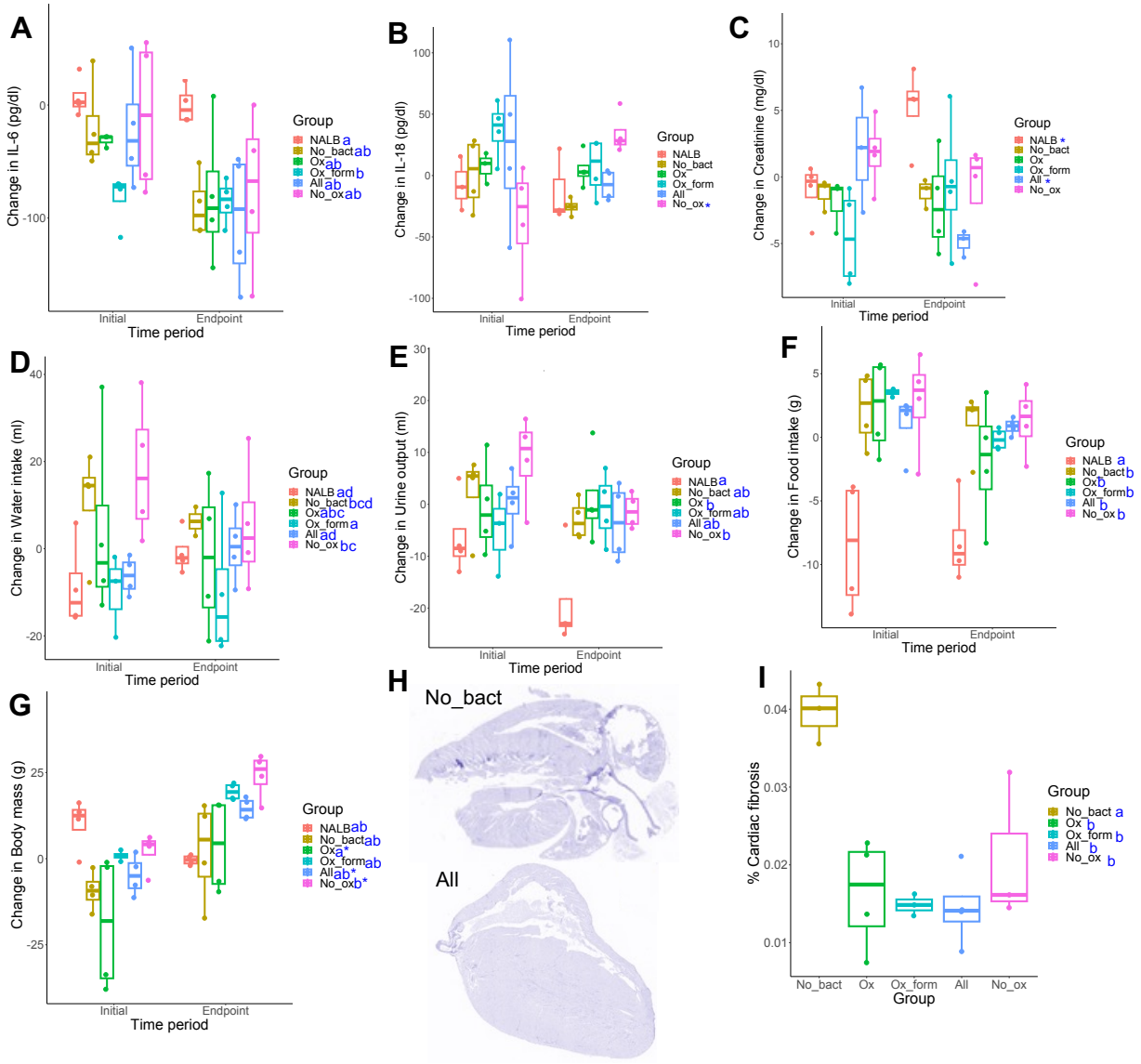

Group 1	No_bact
Group 2	Ox
Group 3	Ox_form
Group 4	All
Group 5	No_ox

1586
1587

Taxonomic cohort

Fig. S7

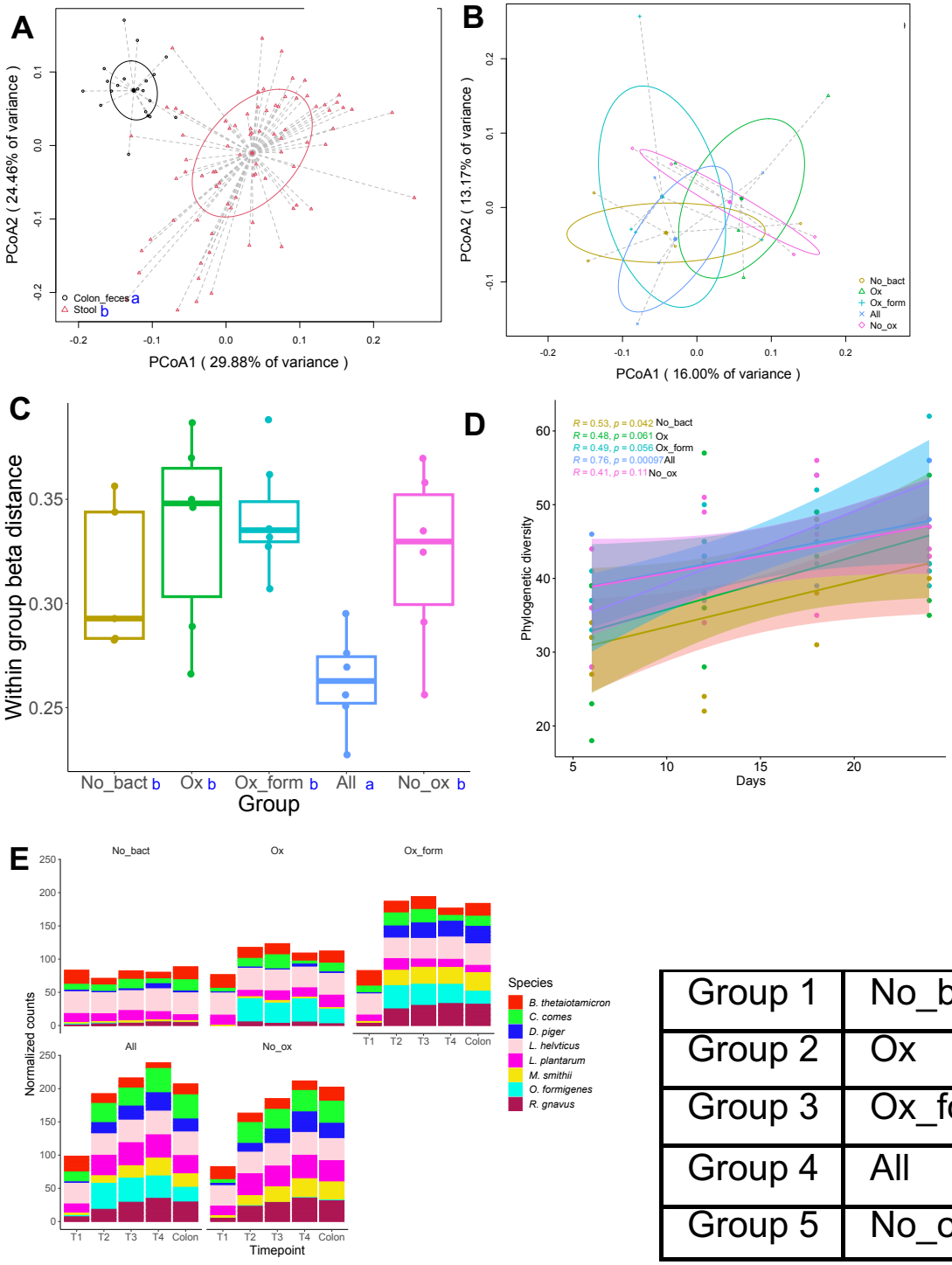

Group 1	No_bact
Group 2	Ox
Group 3	Ox_form
Group 4	All
Group 5	No_ox

1588

1589

Metabolic cohort

Fig. S8

A

n=16 animals/group, pooled by cage (4 animals/sample)

SW mouse
1. NALB
2. Ox
3. Ox_form
4. All
5. No_ox

	T1	T2	T3	T4
Days	0-6	7-12	13-18	19-25
Treatment	Neomycin 3% Oxalate	Microbial Transplant 3% Oxalate	0% Oxalate	3% Oxalate

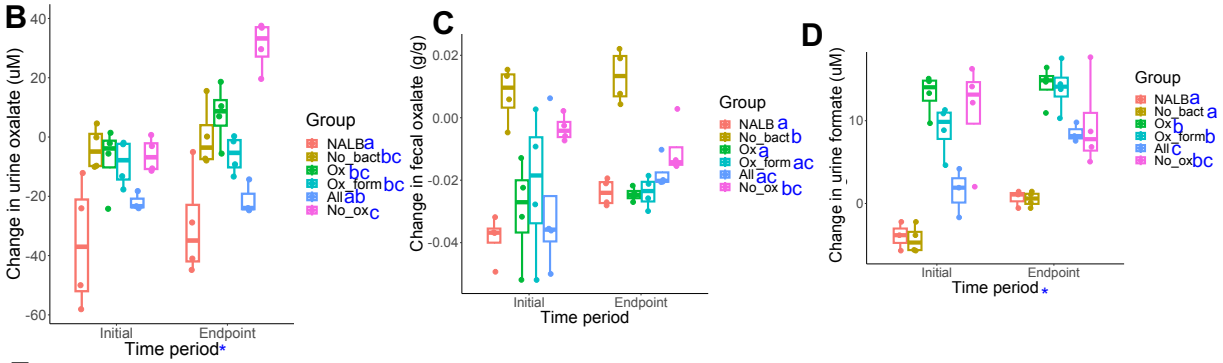

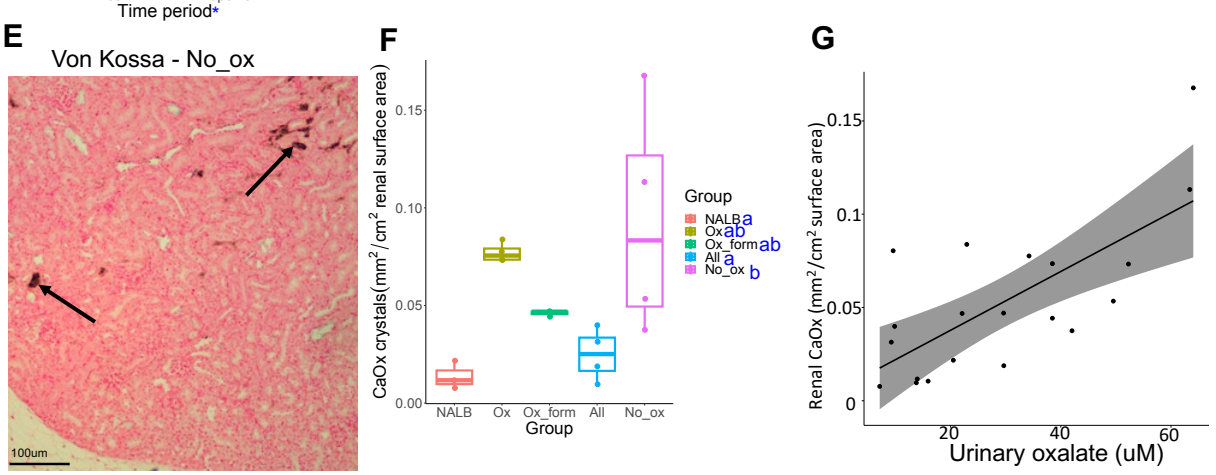

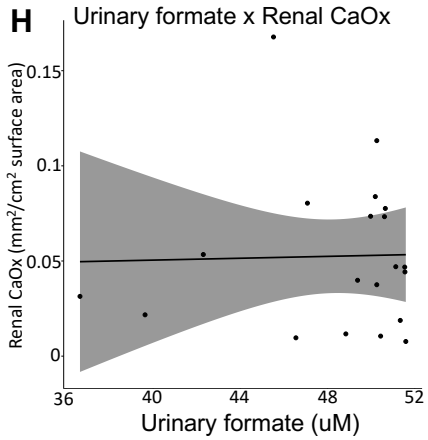

Group 1	No_bact
Group 2	Ox
Group 3	Ox_form
Group 4	All
Group 5	No_ox

1590

Metabolic cohort

Fig. S9

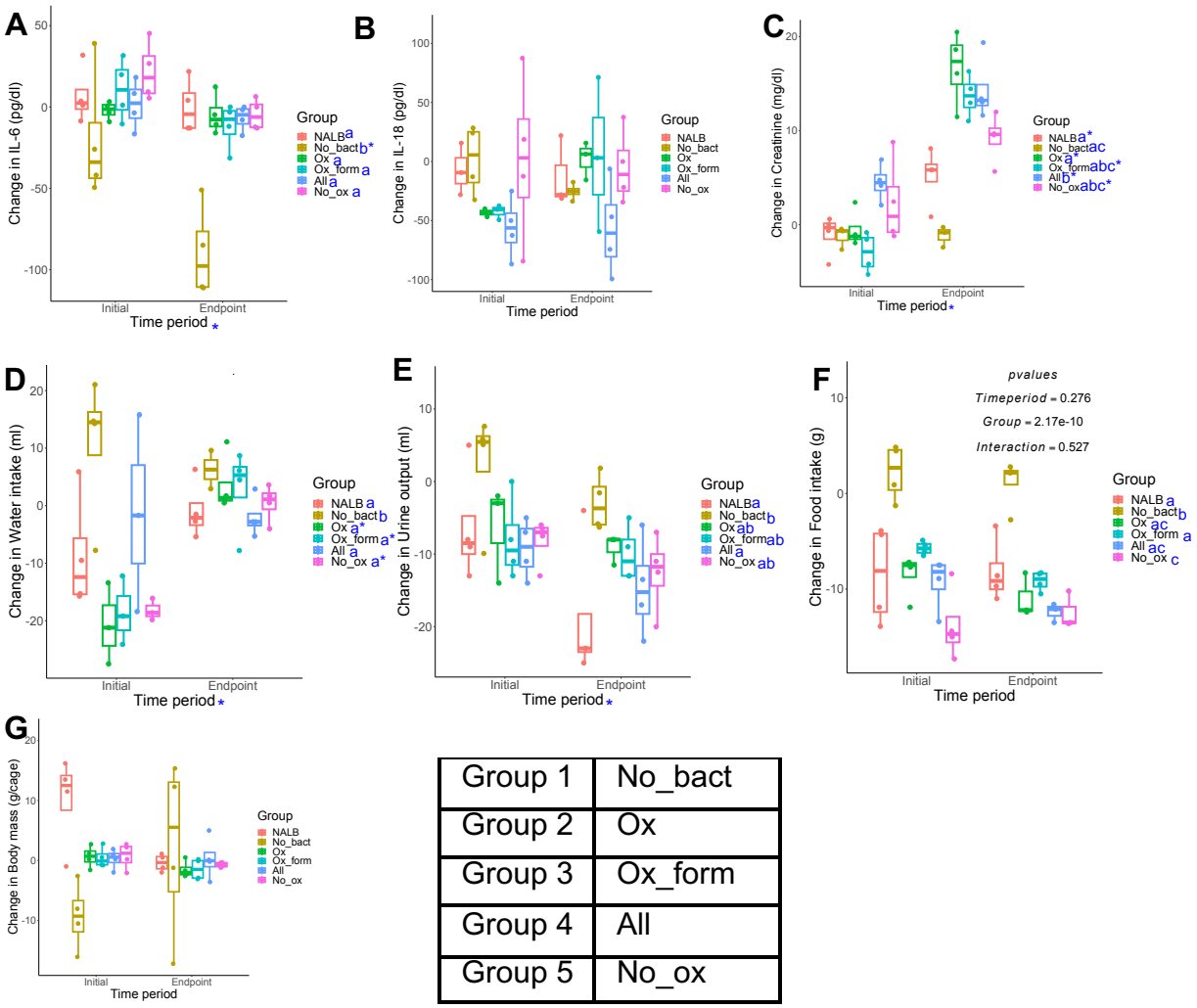

Group 1	No_bact
Group 2	Ox
Group 3	Ox_form
Group 4	All
Group 5	No_ox

Metabolic cohort

Fig. S10

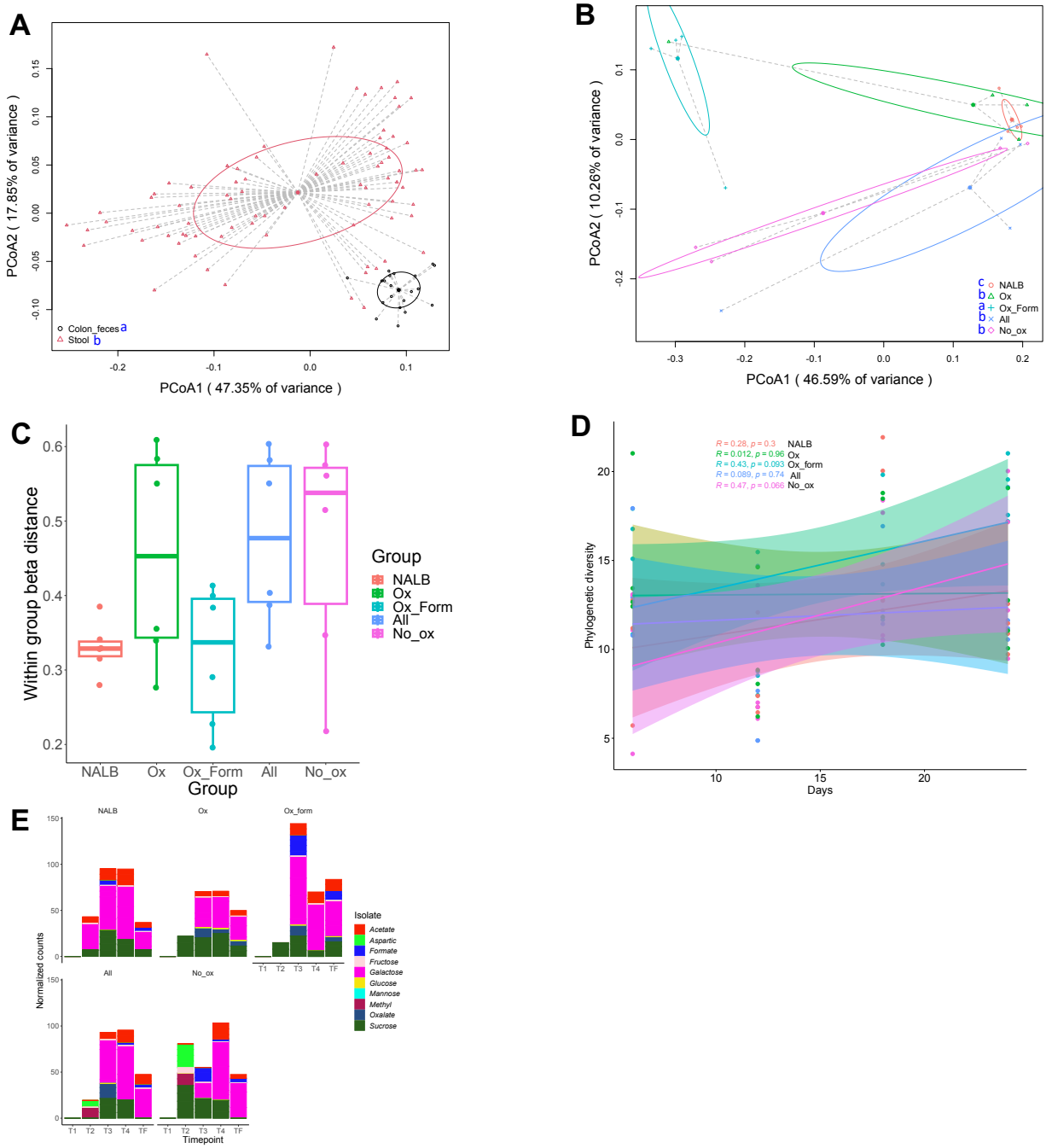

1593
1594

1595

Fig. S11

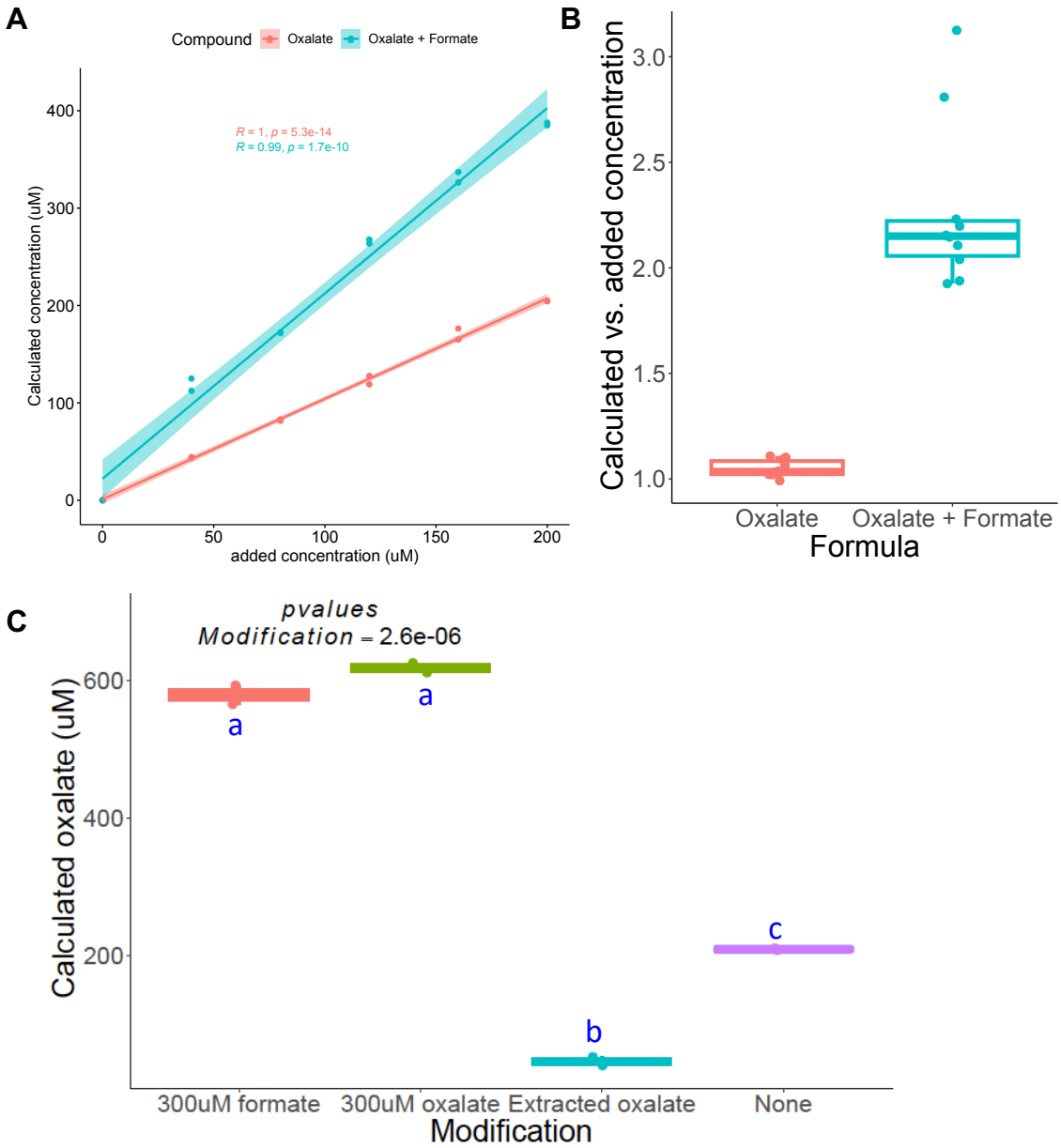

1596
1597
1598
1599
1600
1601
1602
1603
1604
1605
1606

1607
1608 **Supplementary Tables**

Table S1. Composition of the diets used in the diet trials.

Ingredients	0% oxalate (g/Kg)	1.5% oxalate (g/Kg)	3% oxalate (g/Kg)
Casein	200	200	200
L-Cysteine	3	3	3
Corn Starch	285.5	NA	NA
Maltodextrin	120	120	120
Sucrose	100	185.4	185.4
Anhydrous Milkfat	NA	200	200
Soybean Oil	70	70	70
Cellulose	150	150	150
Mineral Mix	42	42	42
Vitamin Mix	12	12	12
Choline Bitartrate	2.5	2.5	2.5
TBHQ, antioxidant	0.014	0.054	0.054
Sodium Oxalate	0	15	30

1609

Table S2. The number of host hepatic genes in each metabolic pathway that exhibited a significant increase or decrease in expression upon consumption of 1.5% oxalate

Microbiome	tracking_id	gene	locus	Sum of Reads	Ave 1.5% Oxalate	log2(fold_change)	test_stat	p_value	FDR	direction	Protein	Gene ontology (biological process)	Gene ontology (cellular component)	Gene ontology (molecular function)
SWM	XLOC_000746	Spp2	2:27307748-27576096	1,89744	0,096197	-4,39858	-0,335453	1,00E-05	5,91E-03	Down	Secreted phosphoprotein 24 (Fragment)	bone remodeling	extracellular region	unknown
SWM	XLOC_000242	Zwp70	12:11175888-11181873	12,0101	0,68188	-4,46017	-0,536216	1,00E-05	5,91E-03	Down	Tyrosine-protein kinase ZAP-70 (Fragment)	beta selection	cell-cell junction	ATP binding
SWM	XLOC_020691	Cd5l	6:127123965-127212611	2,02486	0,0425156	-5,5734	-0,561689	1,00E-05	5,91E-03	Down	CD5 antigen-like (Apoptosis inhibitor expressed by macrophages) (mAIM) (Apoptosis inhibitory 6) (SP-alpha)	apoptotic process	cytoplasm	scavenger receptor activity
SWM	XLOC_012270	Ndufb11	17:58206642-57384668	14,9499	1,76651	-4,69065	-0,03937	1,00E-05	5,91E-03	Down	NADH dehydrogenase (ubiquinone) 1 beta subcomplex subunit 11, mitochondrial (Complex I-X1kD) (CI-X1kD)	mitochondrial respiratory chain complex I ass	integral component of membrane	unknown
SWM	XLOC_014654	Hft1	7:119760922-119840850	1,29615	0,0571921	-4,52227	-0,263954	1,00E-05	5,91E-03	Down	Protein HFT1 homolog	carbohydrate transport	endoplasmic reticulum membrane	lipid transporter activity
SWM	XLOC_040594	Gm1075	11:16367836-16369047	11,5821	0,517754	-4,37617	-1,1958	1,00E-05	5,91E-03	Down	unknown	unknown	unknown	unknown
SWM	XLOC_041694	Tars2	3:152239945-152278995	1,02634	0,109071	-3,23617	-0,490847	1,00E-05	5,91E-03	Down	Probable threonine--tRNA ligase 2, cytoplasmic (EC 6.1.1.3) (Threonyl-tRNA synthetase) (TrRS) (Threonyl-tR	threonyl-tRNA aminoacylation	cytoplasm	ATP binding
SWM	XLOC_010254	Fam25c	11:115117249-115179467	2,88844	0,599092	-2,73874	-0,614947	1,00E-05	5,91E-03	Down	Protein FAM25C	unknown	unknown	unknown
SWM	XLOC_008130	Serp2	17:55648850-55727720	8,2091	1,85957	-2,14326	-1,46723	1,00E-05	5,91E-03	Down	Liver-expressed antimicrobial peptide 2 (LEAP-2)	defense response to bacterium	extracellular region	unknown
SWM	XLOC_051271	Prdx4	11:26367766-26368140	26,6287	2,75021	-1,91782	-1,26498	1,00E-05	5,91E-03	Down	Peroxiredoxin-4	4-hydroxyproline metabolic process	cytosol	antioxidant activity
SWM	XLOC_007693	Mrpl12	X:107057175-107069437	72,276	19,8756	-1,86252	-2,2074	1,00E-05	5,91E-03	Down	39S ribosomal protein L12, mitochondrial (L12mt) (MRP-L12)	mitochondrial transcription	mitochondrial large ribosomal subunit	structural constituent of ribosome
SWM	XLOC_049391	Cnrip1	X:108177038-108184025	53,2437	18,9519	-1,49027	-1,52067	1,00E-05	5,91E-03	Down	G1/S-specific cyclin-D2 (Fragment)	adult locomotory behavior	cyclin D2-CDK4 complex	unknown
SWM	XLOC_035338	Aacs	5:125475564-125517847	44,7957	16,0942	-1,47682	-2,34974	1,00E-05	5,91E-03	Down	Acetoacetyl-CoA synthetase (EC 6.2.1.16)	adipose tissue development	cytosol	acetoacetate-CoA ligase activity
SWM	XLOC_046096	Ankrd37	8:69375527-69385677	2,40561	0	NA	NA	1,00E-05	5,91E-03	Down	Ankyrin repeat domain-containing protein 37	unknown	cytoplasm	unknown
SWM	XLOC_010285	Slc10a47	8:48623412-48662298	1,22321	0	NA	NA	1,00E-05	5,91E-03	Down	Solute carrier family 25 member 47	unknown	integral component of membrane	unknown
SWM	XLOC_031741	Ubl3ENSMUSG00000029580	8:69805052-69805622	7,72747	0	NA	NA	1,00E-05	5,91E-03	Down	RHEB GTPase (ENSMUSG00000029580)	unknown	unknown	unknown
SWM	XLOC_002201	Tpw5	12:98920573-98983238	1,11262	0	NA	NA	1,00E-05	5,91E-03	Down	tRNA wybutosine-synthesizing protein 5 (EC 1.14.11.42) (tRNAPhe) (7-(3-amino-3-carboxypropyl)wyosine) (e	wybutosine biosynthetic process	unknown	unknown
SWM	XLOC_018898	-	2:127107573-91071619	1,30154	0	NA	NA	1,00E-05	5,91E-03	Down	unknown	unknown	unknown	iron ion binding
SWM	XLOC_047059	-	5:87322395-87323857	2,19854	0	NA	NA	1,00E-05	5,91E-03	Down	unknown	unknown	unknown	unknown
SWM	XLOC_053554	-	1:179810152-179819968	1,41818	0	NA	NA	1,00E-05	5,91E-03	Down	unknown	unknown	unknown	unknown
SWM	XLOC_056298	-	1:194667979-194683521	73,0843	0	NA	NA	1,00E-05	5,91E-03	Down	unknown	unknown	unknown	unknown
SWM	XLOC_020119	-	2:103663266-103664457	121,302	0	NA	NA	1,00E-05	5,91E-03	Down	unknown	unknown	unknown	unknown
SWM	XLOC_020135	-	16:70998867-70999115	287,223	0	NA	NA	1,00E-05	5,91E-03	Down	unknown	unknown	unknown	unknown
SWM	XLOC_022356	Rps14	17:75268627-75268852	444,001	951,25	1,09026	1,8632	1,00E-05	5,91E-03	Up	40S ribosomal protein S14	erythrocyte differentiation	cytosolic small ribosomal subunit	mRNA 5'-UTR binding
SWM	XLOC_011648	Xrcc1	11:83746939-83752642	663,108	1421,64	1,10024	2,00737	1,00E-05	5,91E-03	Up	DNA repair protein XRCC1 (X-ray repair cross-complementing protein 1)	DNA repair	cytoplasm	ATP binding
SWM	XLOC_017404	Galectin1	3:115010739-115019188	192,239	417,359	1,11839	1,86221	1,00E-05	5,91E-03	Up	Galectin-1 (Gal-1) (14 kDa lectin) (Beta-galactoside-binding lectin 1-16-1) (Galaptin) (Lactose-binding lectin	apoptotic process	cytosol	S-lactoylglutathione binding
SWM	XLOC_009066	Eifka2	2:28971371-28981864	123,61	272,874	1,14244	1,94689	1,00E-05	5,91E-03	Up	Eukaryotic initiation factor 4A-II	cellular response to leukemia inhibitory facto	cytosol	ATP-dependent RNA helicase activity
SWM	XLOC_041396	Eif3k	4:126610559-126600548	101,57	227,731	1,16486	2,03649	1,00E-05	5,91E-03	Up	Eukaryotic translation initiation factor 3 subunit K	regulation of translational initiation	eukaryotic translation initiation factor 3 complex	unknown
SWM	XLOC_026412	Robejek	11:70525366-70527958	213,219	710,628	1,68	2,05546	1,00E-05	5,91E-03	Up	Roblk-effector protein with leitch motifs	unknown	endosome membrane	unknown
SWM	XLOC_012145	Gm11861	4:89475527-89476962	493,411	1102,1	1,19861	2,07501	1,00E-05	5,91E-03	Up	MCU1671	translation	ribosome	RNA binding
SWM	XLOC_008282	Epn2	8:41569774-41647594	115,903	266,464	1,22612	2,08014	1,00E-05	5,91E-03	Up	Epsin-2	endocytosis	clathrin coat of endocytic vesicle	unknown
SWM	XLOC_010861	Nenf	19:28087602-28127937	185,926	426,086	1,22774	2,11908	1,00E-05	5,91E-03	Up	Nuclear export mediator factor Nenf (Serologically defined colon cancer antigen 1 homolog)	nucleocytoplasmic transport	cytosol	nucleus
SWM	XLOC_031257	Psme1ks	11:97703368-97713500	176,08	413,427	1,2314	2,07886	1,00E-05	5,91E-03	Up	Proteasome subunit beta type-1 (EC 3.4.25.1) (Macropain epsilon chain) (Multicatalytic endopeptidase com	proteasome-mediated ubiquitin-dependent p	centrosome	peptidase activity
SWM	XLOC_019542	Map3k2	2:128499658-128499645	458,305	1105,62	1,26017	2,11044	1,00E-05	5,91E-03	Up	Mitotic-spindle organizing protein 2 (Mitotic-spindle organizing protein associated with a ring of gamma-tu	unknown	centrosome	unknown
SWM	XLOC_046096	Uxs1	8:110606939-110570297	697,802	1691,95	1,2795	2,21921	1,00E-05	5,91E-03	Up	Vesicle transport protein USE1	unknown	endoplasmic reticulum	unknown
SWM	XLOC_054419	Rps16-ps3	X:71126609-71126961	121,931	296,177	1,2804	2,19922	1,00E-05	5,91E-03	Up	unknown	unknown	unknown	unknown
SWM	XLOC_040030	Rpl32	1:39367841-39478755	638,388	1064,89	1,28042	2,16979	1,00E-05	5,91E-03	Up	60S ribosomal protein L32	cellular response to dexamethasone stimulus	cytosolic large ribosomal subunit	structural constituent of ribosome
SWM	XLOC_040769	Tpx1	9:64946285-64949516	166,842	405,629	1,28862	2,16341	1,00E-05	5,91E-03	Up	60S ribosomal protein S3 (Cleaved into: 40S ribosomal protein S3, N-terminally processed)	regulation of translational fidelity	cytosolic small ribosomal subunit	mRNA binding
SWM	XLOC_028744	5100a10	2:90511033-90524581	256,241	634,127	1,30772	2,1224	1,00E-05	5,91E-03	Up	Uncharacterized protein	cellular response to leukemia inhibitory facto	unknown	calcium ion binding
SWM	XLOC_018276	Tcs1	4:61052027-61082114	44,9318	112,069	1,31844	2,02819	1,00E-05	5,91E-03	Up	GDP-L-fucose synthase (EC 1.1.1.271) (GDP-4-keto-6-deoxy-D-mannose-3,5-epimerase-4-reductase) (Protein	de novo GDP-L-fucose biosynthesis process	cytosol	unknown
SWM	XLOC_041146	Rps16	10:80920452-80929114	1452,2	3648,55	1,32908	2,13151	1,00E-05	5,91E-03	Up	40S ribosomal protein S16	cellular response to leukemia inhibitory facto	cytosolic small ribosomal subunit	RNA binding
SWM	XLOC_026128	Myl6	11:104175552-104184185	59,7209	151,478	1,34664	2,1995	1,00E-05	5,91E-03	Up	Myosin light polypeptide 6 (17 kDa myosin light chain) (LC17) (Myosin light chain 3) (MLC-3) (Myosin light c	muscle contraction	brush border	actin depolymerization factor activity
SWM	XLOC_052377	Rpl39	11:116648523-116672331	497,073	1278,42	1,36306	2,34675	1,00E-05	5,91E-03	Up	60S ribosomal protein L39	antibacterial humoral response	cytosolic large ribosomal subunit	RNA binding
SWM	XLOC_051432	Gjb2	1:74009284-74010341	105,166	270,153	1,36392	2,1596	1,00E-05	5,91E-03	Up	Gap junction protein	cell communication	connexon complex	unknown
SWM	XLOC_050803	Bhlh5	1:137865848-137991543	784,532	2036,25	1,37601	2,07246	1,00E-05	5,91E-03	Up	99 domain-containing protein 1 (Fragment)	cornea rigor and development	membrane	hedgehog receptor activity
SWM	XLOC_033148	Dsc1	18:20568658-20569259	302,4565	241,311	1,38537	2,17823	1,00E-05	5,91E-03	Up	Desmocollin-1	homophilic cell adhesion via plasma membrane	desmosome	calcium ion binding
SWM	XLOC_046164	Ndufb7	X:20615126-20615901	281,881	740,298	1,39302	2,19891	1,00E-05	5,91E-03	Up	NADH dehydrogenase [ubiquinone] 1 beta subcomplex subunit 7 (Complex I-B18) (CI-B18) (NADH-ubiquinone	mitochondrial respiratory chain complex I ass	mitochondrial inner membrane	NADH dehydrogenase (ubiquinone) activity
SWM	XLOC_006270	Gm13996	X:39730991-39733165	1354,15	3561,57	1,39513	2,35491	1,00E-05	5,91E-03	Up	unknown	unknown	unknown	unknown
SWM	XLOC_008515	Rpl23a	11:98001507-98009002	861,151	2264,01	1,41164	2,20907	1,00E-05	5,91E-03	Up	60S ribosomal protein L23a	ribosomal large subunit assembly	cytosolic large ribosomal subunit	large ribosomal subunit rRNA binding
SWM	XLOC_007579	Rpl38	9:104585452-104588062	363,08	708,445	1,42915	2,41673	1,00E-05	5,91E-03	Up	60S ribosomal protein L38	60S preribosome assembly	cytosolic large ribosomal subunit	RNA binding
SWM	XLOC_018261	9030619P08Rik	4:134629415-134631288	319,601	324,737	1,4684	2,21874	1,00E-05	5,91E-03	Up	Uncharacterized protein	unknown	unknown	unknown
SWM	XLOC_023011	Fau	14:34351697-34352842	153,404	308,165	1,49223	2,25368	1,00E-05	5,91E-03	Up	Ubiquitin-like protein FUBI (Monoclonal non-specific suppressor factor beta) (MNSF-beta)	antibacterial humoral response	cytosolic small ribosomal subunit	unknown
SWM	XLOC_009749	Gm12513	8:105629497-105635598	16,2926	40,6855	1,49384	2,12124	1,00E-05	5,91E-03	Up	unknown	unknown	unknown	unknown
SWM	XLOC_020823	Rpl36	2:38896712-38916557	402,631	1099,28	1,49894	1,99129	1,00E-05	5,91E-03	Up	60S ribosomal protein L36	cytoplasmic translation	cytosolic large ribosomal subunit	RNA binding
SWM	XLOC_007453	Cst3	2:148919788-148919922	31,62	87,0833	1,46231	2,00219	1,00E-05	5,91E-03	Up	Cystatin-C (Fragment)	angiogenesis	extracellular region	cysteine endopeptidase inhibitor activity
SWM	XLOC_023974	Usmg5	X:71368847-71368969	80,1252	223,859	1,48226	2,41739	1,00E-05	5,91E-03	Up	Up-regulated during skeletal muscle growth protein 5 (Diabetes-associated protein in insulin-sensitive tissue	unknown	integral component of membrane	unknown
SWM	XLOC_020647	Dpm3	4:62705664-62707109	27,1984	76,7989	1,49778	2,62329	1,00E-05	5,91E-03	Up	Dolichol-phosphate mannosyltransferase subunit 3 (Dolichol-phosphate mannose synthase subunit 3) (DPM	GPI anchor biosynthetic process	dolichol-phosphate mannose synthase complex	dolichyl-phosphate beta-D-mannosyltransferase activity
SWM	XLOC_045780	Zdhhc2	1:36761797-36782918	11,3833	32,1737	1,49935	2,09276	1,00E-05	5,91E-03	Up	Palmitoyltransferase ZDHHC2 (EC 2.3.1.225) (Zinc finger DHHC domain-containing protein 2) (DHHC-2)	protein palmitoylation	endoplasmic reticulum	palmitoyltransferase activity
SWM	XLOC_035288	Thwd	7:62444888-62763913	49,567	141,638	1,51651	2,08914	1,00E-05	5,91E-03	Up	T-box transcription factor TWIST-like protein (Fragment)	animal organ morphogenesis	nucleus	DNA binding transcription factor activity
SWM	XLOC_010234	Serpina3k	12:104028768-104044443	6,22892	18,0525	1,53514	2,39542	1,00E-05	5,91E-03	Up	Serine (Or cysteine) peptidase inhibitor, clade A, member 3C	unknown	extracellular space	unknown
SWM	XLOC_039142	5100a6	11:77012284-77013406	361,121	1,16843	2,78965	1,01E-05	5,91E-03	Up	Protein S100-A1 (S- 100 protein alpha chain) (S-100 protein subunit alpha) (S100 calcium-binding protein A1)	negative regulation of transcription by RNA p	nucleus	ATPase binding	unknown
SWM	XLOC_048544	Rpa2Th	2:90215251-90215631	2306,64	6860,25	1,57036	2,60527	1,00E-05	5,91E-03	Up	40S ribosomal protein S27-like	activation of cysteine-type endopeptidase act	cytosolic small ribosomal subunit	cysteine-type endopeptidase activator activity involved in apoptotic proce
SWM	XLOC_037164	Rpl31	17:28126970-28131205	493,661	1477,62	1,58168	2,17486	1,00E-05	5,91E-03	Up	60S ribosomal protein L31	cytoplasmic translation	cytosolic large ribosomal subunit	5S rRNA binding
SWM	XLOC_006123	Rpl41	X:37082514-37085402	162,611	486,862	1,58209	2,41288	1,00E-05	5,91E-03	Up	60S ribosomal protein L41	cytoplasmic translation	cytosolic large ribosomal subunit	mRNA 5'-UTR binding
SWM	XLOC_007256	Sugt1a	9:108962947-108973829	315,7	948,264	1,58764	2,29677	1,00E-05	5,91E-03	Up	SGT1 homolog, U5/U11snRNP-specific (SNU18) (Suppressor of Ty 4A)	regulation of transcription from RNA polymer	nucleus	unknown
SWM	XLOC_024885	Metazip1d	16:45152238-45162660	141,202	426,959	1,59624	2,27192	1,00E-05	5,91E-03	Up	Methionine aminopeptidase 1D, mitochondrial (MAP 1D) (MetAP 1D) (EC 3.4.11.18) (Methionyl aminopeptid	intracellular membrane-bounded org	mitochondrial inner membrane	NADH dehydrogenase (ubiquinone) activity
SWM	XLOC_046417	Tmem208	8:121620796-121669897	99,984	302B,31	1,59851	2,29918	1,00E-05	5,91E-03	Up	Transmembrane protein 208	embryogenesis	endoplasmic reticulum membrane	unknown
SWM	XLOC_011368	Serpina12	11:16257733-16308484	103,765	314,816	1,60147	2,28737	1,00E-05	5,91E-03	Up	Serpin A12 (Visceral adipose tissue-derived serine protease inhibitor) (Vaspin) (Visceral adipose-specific ser	negative regulation of gluconeogenesis	extracellular space	serine-type endopeptidase inhibitor activity
SWM	XLOC_048845	Hbqa	9:48504164-48577739	764,991	2453,72	1,64564	2,48707	1,00E-05	5,91E-03	Up	Hemoglobin subunit alpha (Hemoglobin alpha-1/2) (Hemoglobin alpha-1/2 chain) (Hemoglobin alpha-1/2 globin)	oxygen transport	cell body	alpha-type hemoglobin
SWM	XLOC_012728	Gm6149	7:91610931-91618832	363,08	708,445	1,67015	2,41673	1,00E-05	5,91E-03	Up	60S ribosomal protein L38	60S preribosome assembly	cytosolic large ribosomal subunit	RNA binding
SWM	XLOC_018261	9030619P08Rik	4:134629415-134631288	319,601	324,737	1,4684	2,21874	1,00E-05	5,91E-03	Up	Uncharacterized protein	unknown	unknown	unknown
SWM	XLOC_023011	Fau	14:34351697-34352842	153,404	308,165	1,49223	2,25368	1,00E-05	5,91E-03	Up	Ubiquitin-like protein FUBI (Monoclonal non-specific suppressor factor beta) (MNSF-beta)	antibacterial humoral response	cytosolic small ribosomal subunit	unknown
SWM	XLOC_009749	Gm12513	8:105629497-105635598	16,2926	40,6855	1,49384	2,12124	1,00E-05	5,91E-03	Up	unknown	unknown	unknown	unknown
SWM	XLOC_020823	Rpl36	2:38896712-38916557	402,631	1099,28	1,49894	1,99129	1,00E-05	5,91E-03	Up	60S ribosomal protein L36	cytoplasmic translation	cytosolic large ribosomal subunit	RNA binding
SWM	XLOC_007453	Cst3	2:148919788-148919922	31,62	87,0833	1,46231	2,00219	1,00E-05	5,91E-03	Up	Cystatin-C (Fragment)	angiogenesis	extracellular region	cysteine endopeptidase inhibitor activity
SWM	XLOC_023974	Usmg5	X:71368847-71368969	80,1252	223,859	1,48226	2,41739	1,00E-05	5,91E-03	Up	Up-regulated during skeletal muscle growth protein 5 (Diabetes-associated protein in insulin-sensitive tissue	unknown	integral component of membrane	unknown
SWM	XLOC_020647	Dpm3	4:62705664-62707109	27,1984	76,7989	1,49778	2,62329	1,00E-05	5,91E-03	Up	Dolichol-phosphate mannosyltransferase subunit 3 (Dolichol-phosphate mannose synthase subunit 3) (DPM	GPI anchor biosynthetic process	dolichol-phosphate mannose synthase complex	dolichyl-phosphate beta-D-mannosyltransferase activity
SWM	XLOC_045780	Zdhhc2	1:36761797-36782918	11,3833	32,1737	1,49935	2,09276	1,00E-05	5,91E-03	Up	Palmitoyltransferase ZDHHC2 (EC 2.3.1.225) (Zinc finger DHHC domain-containing protein 2) (DHHC-2)	protein palmitoylation	endoplasmic reticulum	palmitoyltransferase activity
SWM	XLOC_035288	Thwd	7:62444888-62763913	49,567	141,638	1,51651	2,08914	1,00E-05	5,91E-03	Up	T-box transcription factor TWIST-like protein (Fragment)	animal organ morphogenesis	nucleus	DNA binding transcription factor activity
SWM	XLOC_010234	Serpina3k	12:104028768-104044443	6,22892	18,0525	1,53514	2,39542	1,00E-05	5,91E-03	Up	Serine (Or cysteine) peptidase inhibitor, clade A, member 3C	unknown	extracellular space	unknown
SWM	XLOC_039142	5100a6	11:77012284-77013406	361,121	1,16843	2,78965	1,01E-05	5,91E-03	Up	Protein S100-A1 (S- 100 protein alpha chain) (S-100 protein subunit alpha) (S100 calcium-binding protein A1)	negative regulation of transcription by RNA p	nucleus	ATPase binding	unknown
SWM	XLOC_048544	Rpa2Th	2:90215251-90215631	2306,64	6860,25	1,57036	2,60527	1,00E-05	5,91E-03	Up	40S ribosomal protein S27-like	activation of cysteine-type endopeptidase act	cytosolic small ribosomal subunit	cysteine-type endopeptidase activator activity involved in apoptotic proce
SWM	XLOC_037164	Rpl31	17:28126970-28131205	493,661	1477,62	1,58168	2,17486	1,00E-05	5,91E-03	Up	60S ribosomal protein L31	cytoplasmic translation	cytosolic large ribosomal subunit	5S rRNA binding
SWM	XLOC_006123	Rpl41	X:37082514-37085402	162,611	486,862	1,58209	2,41288	1,00E-05	5,91E-03	Up	60S ribosomal protein L41	cytoplasmic translation	cytosolic large ribosomal subunit	mRNA 5'-UTR binding
SWM	XLOC_007256	Sugt1a	9:108962947-108973829	315,7	948,264	1,58764	2,29677	1,00E-05	5,91E-03	Up	SGT1 homolog, U5/U11snRNP-specific (SNU18) (Suppressor of Ty 4A)	regulation of transcription from RNA polymer	nucleus	unknown
SWM	XLOC_024885	Metazip1d	16:45152238-45162660	141,202	426,959	1,59624	2,27192	1,00E-05	5,91E-03	Up	Methionine aminopeptidase 1D, mitochondrial (MAP 1D) (MetAP 1D) (EC 3.4.11.18) (Methionyl aminopeptid	intracellular membrane-bounded org	mitochondrial inner membrane	NADH dehydrogenase (ubiquinone) activity
SWM	XLOC_046417	Tmem208	8:121620796-121669897	99,984	302B,31	1,59851	2,29918	1,00E-05	5,91E-03	Up	Transmembrane protein 208	embryogenesis	endoplasmic reticulum membrane	unknown
SWM	XLOC_011368	Serpina12	11:16257733-16308484	103,765	314,816	1,60147	2,28737	1,00E-05	5,91E-03	Up	Serpin A12 (Visceral adipose tissue-derived serine protease inhibitor) (Vaspin) (Visceral adipose-specific ser	negative regulation of gluconeogenesis	extracellular space	serine-type endopeptidase inhibitor activity
SWM	XLOC_048845	Hbqa	9:48504164-48577739	764,991	2453,72	1,64564	2,48707	1,00E-05	5,91E-03	Up	Hemoglobin subunit alpha (Hemoglobin alpha-1/2) (Hemoglobin alpha-1/2 chain) (Hemoglobin alpha-1/2 globin)	oxygen transport	cell body	alpha-type hemoglobin
SWM	XLOC_012728	Gm6149	7:91610931-91618832	363,08	708,445	1,67015	2,41673	1,00E-05	5,91E-03	Up	unknown	unknown	unknown	unknown
SWM	XLOC_005575	Lyz1	15:78926724-78930661	30,8477	99,4577	1,68814	2,48384	1,00E-05	5,91E-03	Up	Lysozyme C (EC 3.2.1.17) (1,4-beta-N-acetylmuramidase C) (Lysozyme C type M)	cell wall macromolecule catabolic process	cytoplasm	hydrolase activity, acting on glycosyl bonds
SWM	XLOC_042797	Mrpl23	4:151802877-151809975	64,8571	210,734	1,70009	2,33899	1,00E-05	5,91E-03	Up	39S ribosomal protein L23, mitochondrial	translation	ribosome	structural constituent of ribosome
SWM	XLOC_019159	Srfn201	11:83767227-73790937	160,765	620,638	1,70234	2,54113	1,00E-05	5,91E-03	Up	unknown	unknown	mitochondrion	mitochondrial endopeptidase inhibitor activity
SWM	XLOC_021510	Grip2	3:107077218-107898846	20,2969	67,5885	1,73598	2,43171	1,00E-05	5,91E-03	Up	Glutamate S-transferase P 1 (Gst P1) (EC 2.5.1.18) (GST YF-YF) (GST class-pi) (GST-pi) (Prostaglandin pros	animal organ regeneration	cytoplasm	dextrorsyl-trans sulfoxide
SWM	XLOC_021660	Myd88	9:119470576-119476136	46,1031	159,883	1,79456	2,27763	1,00E-05	5,91E-03	Up	Myeloid-derived growth factor (MYDGF) (Interleukin-25) (IL-25) (Stromal cell-derived growth factor SF2/B)	angiogenesis	endoplasmic reticulum-Golgi intermediate	growth factor activity
SWM	XLOC_053255	Gm6472	16:89372388-89372865	158,294	568,245	1,84391	2,03377	1,00E-05	5,91E-03	Up	unknown	unknown	unknown	unknown
SWM	XLOC_009125	Gm16418	2:158966-161618	575,417	2094,16	1,86383	2,80284	1,00E-05	5,91E-03	Up	Cytochrome and glycine-rich protein 2 (Fragment)	unknown	unknown	unknown
SWM	XLOC_004295	Rps15	18:60774650-60800944	492,493	1902,12	1,94943	2,87863	1,00E-05	5,91E-03	Up	40S ribosomal protein S15	translation	small ribosomal subunit	RNA binding
SWM	XLOC_038129	Rpl4a-ps1	9:79175352-79175633	121,165	471,672	1,96105	2,93502	1,00E-05	5,91E-03	Up	unknown	unknown	unknown	unknown
SWM	XLOC_008862	Rpsa-ps10	X:79195696-79195448	20,3222	157,383	2,00013	3,31129	1,00E-05	5,91E-03	Up	unknown	unknown	unknown	unknown
SWM	XLOC_017518	Gm16895	17:56448896-56451171	24,7146	932,559	2,11857	2,98756	1,00E-05	5,91E-03	Up	unknown	unknown	unknown	unknown
SWM	XLOC_022991	Mgat4b-ps	2:103812519-103813996	113,169	496,085	2,12211	2,28664	1,00E-05	5,91E-03	Up	unknown	unknown	unknown	unknown
SWM	XLOC_003457	-	7:61316489-61316647	14,2934	64,7037	2,18397	1,75227	1,00E-05	5,91E-03	Up	unknown	unknown	unknown	unknown
SWM	XLOC_010237	Serpina1j	12:104146381-104153870	1671,69	8229,85	2,46339	2,70333	1,00E-05	5,91E-03	Up	MGC64087 (Serine (or cysteine) peptidase inhibitor, clade A (alpha-1 antiproteinase, antitrypsin), member 3	unknown	extracellular space	serine-type endopeptidase inhibitor activity
SWM	XLOC_000867	Gm15427	1:167103165-167106053	19,2857	113,477	2,65152	1,52498	1,00E-05	5,91E-03	Up	unknown	unknown	unknown	unknown
SWM	XLOC_038671	Bhlhe40	11:61505143-61512931	1,73841	11,1536	2,68161	1,46537	1,00E-05	5,91E-03	Up	Class E basic helix-loop-helix protein 40	circadian regulation of gene expression	nucleus	E-box binding
SWM	XLOC_012868	Muptl8	4:61416786-61450763	20,1632	138,441	2,72714	2,70349	1,00E-05	5,91E-03	Up	Major urinary protein 18	behavior	extracellular region	pheromone binding
SWM	XLOC_017264	AC168777.2	15:82687719-82707357	11,227	95,8239	2,93941	2,19919	1,00E-05	5,91E-03	Up	unknown	unknown	unknown	unknown
SWM	XLOC_009647	Cyrp2	1:110073688-110081681	2,42958	28,732	3,8476	1,93205	1,00E-05	5,91E-03	Up	Cysteine and glycine-rich protein 2 (Fragment)	unknown	extracellular space	unknown
SWM	XLOC_047600	Adrt1	8:119468869-119492202	1,15568	13,5883	3,55551	3,32278	1,00E-05	5,91E-03	Up	tRNA-specific adenosine deaminase 1 (mADAT1) (EC 3.5.4.33) (tRNA-specific adenosine-37 deaminase)	tRNA processing	unknown	metal ion binding
SWM	XLOC_000652	Psme4	1:188872483-189053813	1,13629	24,9011	4,6138	2,16284	1,00E-05	5,91E-03	Up	Proteasome subunit beta type-4 (EC 3.4.25.1)	proteasome-mediated ubiquitin-dependent p	cytoplasm	threonine-type endopeptidase activity
SWM	XLOC_050062	Ifn7hs	1:190117767-190219846	10,9962	266,797	4,60093	4,45315	1,00E-05	5,91E-03	Up	unknown	unknown	unknown	unknown
SWM	XLOC_008646	Ism1	1:136085459-136089855	11,6073	352,627	4,91881	3,24445	1,00E-05	5,91E-03	Up	Integrator complex subunit 2 (Int2)	unknown	unknown	unknown
SWM	XLOC_045957	Tmem192	1:127205214-127774092	2,09566	80,2515	5,29912	4,09201	1,00E-05	5,91E-03	Up	Transmembrane protein 192 (Fragment)	unknown	integral component of membrane	unknown
SWM	XLOC_012180	Sdhb	8:88027234-88068283	5,05258	216,928	5,42377	2,96264	1,00E-05	5,91E-03	Up	Succinate dehydrogenase [ubiquinone] iron-sulfur subunit, mitochondrial (EC 1.3.5.1) (Iron-sulfur subunit of	aerobic respiration	mitochondrial inner membrane	iron-sulfur cluster binding
SWM	XLOC_020793	Kat2b	11:118026689-118061998	2,18465	97,1023	5,47617	3,89022	1,00E-05	5,91E-03	Up	Histone acetyltransferase KAT2B (EC 2.3.1.48) (Histone acetyltransferase PCAF) (Histone acetylase PCAF) (L	cell cycle	A band	acetyltransferase activity
SWM	XLOC_021523	Slc22a7	19:8600429-8602022	1,08826	83,4606	6,26088	5,05642	1,00E-05	5,91E-03	Up	Solute carrier family 22 member 7	unknown	integral component of membrane	organic anion transmembrane transporter activity
SWM	XLOC_024328	Tacc3	16:36556859-36562948	0	49,788	inf	nan	5,00E-05	5,91E-03	Up	Transforming acidic coiled-coil-containing protein 3 (AINT-interacting protein)	astral microtubule organization	centrosome	protein domain specific binding
SWM	XLOC_021670	2410015M02	X:125839346-125840629	0	2,45882	inf	nan	5,00E-05	5,91E-03	Up	Sr106 protein (Fragment)	unknown	unknown	unknown
SWM	XLOC_007946

Table 13. The number of microbial metabolites that exhibited a significant increase or decrease in expression upon consumption of 1.5% oxalate by the host.

Microbiome	Molecular mass	Retention time	Direction	qvalue	Bun Rho	Dual/bar	5.5% Dis	p-value	FDR	Log2 fold ch	Direction	HMDB ident	KEGG ident	LIPIDMAPS	KEGCpc ident	Consensus_id
NAIA	316.101	0.4	Positive	-0.956	1.073	0	0	-0.168	Down	0/0	0/0	0	0		0	0
NAIA	256.228	1.022	Positive	-0.594	-0.738	0	0	-0.209	Down	0/0	0/0	0	0		0	0
NAIA	125.108	0.288	Positive	-0.565	-0.701	0	0	-0.268	Down	0/0	0/0	1/1,0	C6H6O2		0	0/1,0,Benzylamine
NAIA	227.160	0.885	Positive	-0.505	-0.872	0	0	-0.32	Down	0/0	0/0	0	0		0	0
NAIA	57.035	0.305	Positive	-0.262	-0.604	0	0	-0.216	Down	0/0	0/0	0	0		0	0
NAIA	152.118	0.286	Positive	-0.435	-0.55	0	0	-0.152	Down	0/0	0/0	0	0		0	0
NAIA	126.101	0.286	Positive	-0.411	-0.835	0	0	-0.511	Down	2/2,0	Meth/1/2,0	C00127			0/1,0/0	M0371/2,0/1,Methylhistamine
NAIA	538.102	12.075	Positive	-0.32	-0.69	0	0	-0.798	Down	0/0	0/0	0	0		0	0
NAIA	256.227	1.022	Positive	-0.32	-0.69	0	0	-0.798	Down	0/0	0/0	0	0		0	0
NAIA	359.242	5.209	Positive	-0.205	-0.379	0	0	-0.589	Down	0/0	0/0	0	0		0	0
NAIA	105.076	9.166	Positive	-0.186	-1.101	0	0	-1.839	Down	2/2,0	Pipen/1/1,0	C18796			0	0
NAIA	307.021	9.583	Positive	-0.262	0.051	0	0	-0.916	Down	2/2,0	cis-5-Tetradecenoyl	C14082	5,LMFA0		0/1,0	cis-5-Tetradecenoylcarnitine/,trans-2-Tetradecenoylcarnitine/
NAIA	456.282	3.679	Positive	0.353	0.057	0	0	-0.655	Down	0/0	0/0	0	0		0	0
NAIA	439.362	3.402	Positive	0.428	0.15	0	0	-0.766	Down	1/1,0	Ch/1/1,0	C14076	1,LMST0102		0/1,0	C14076: Testosterone / ,C15776: Tetradecenal /
NAIA	328.021	7.731	Positive	0.905	0.191	0	0	-1.05	Down	0/1,0	Dioxo/1/1,0	C16526	2,LGAL0006		0/1,0	5,Dioxopiperlonaloxal/,N,N-Dimethylsphingosine/,Bruceanol acid/
NAIA	362.058	9.159	Positive	0.977	-0.364	0	0	-1.916	Down	0/0	0/0	0	0		0	0
NAIA	160.097	3.021	Positive	1.095	0.724	0	0	-0.669	Down	0/0,2	Meth/1/1,0	C00087	2,LMFA0102		0/0,1	2,Methylhexylglycine/,Dialanylglycine/,Valerylglycine/,N-Isohydroxal/,N-Dehydrocarnitine/,N-Acetanilidoacetate/
NAIA	146.058	2.021	Positive	1.095	0.724	0	0	-0.669	Down	0/0,2	Meth/1/1,0	C00021	1,LSP-0001,1,LSP-0002,1,LSP-0003,1,LSP-0004,1,LSP-0005,1,LSP-0006,1,LSP-0007,1,LSP-0008,1,LSP-0009,1,LSP-0010,1,LSP-0011,1,LSP-0012,1,LSP-0013,1,LSP-0014,1,LSP-0015,1,LSP-0016,1,LSP-0017,1,LSP-0018,1,LSP-0019,1,LSP-0020,1,LSP-0021,1,LSP-0022,1,LSP-0023,1,LSP-0024,1,LSP-0025,1,LSP-0026,1,LSP-0027,1,LSP-0028,1,LSP-0029,1,LSP-0030,1,LSP-0031,1,LSP-0032,1,LSP-0033,1,LSP-0034,1,LSP-0035,1,LSP-0036,1,LSP-0037,1,LSP-0038,1,LSP-0039,1,LSP-0040,1,LSP-0041,1,LSP-0042,1,LSP-0043,1,LSP-0044,1,LSP-0045,1,LSP-0046,1,LSP-0047,1,LSP-0048,1,LSP-0049,1,LSP-0050,1,LSP-0051,1,LSP-0052,1,LSP-0053,1,LSP-0054,1,LSP-0055,1,LSP-0056,1,LSP-0057,1,LSP-0058,1,LSP-0059,1,LSP-0060,1,LSP-0061,1,LSP-0062,1,LSP-0063,1,LSP-0064,1,LSP-0065,1,LSP-0066,1,LSP-0067,1,LSP-0068,1,LSP-0069,1,LSP-0070,1,LSP-0071,1,LSP-0072,1,LSP-0073,1,LSP-0074,1,LSP-0075,1,LSP-0076,1,LSP-0077,1,LSP-0078,1,LSP-0079,1,LSP-0080,1,LSP-0081,1,LSP-0082,1,LSP-0083,1,LSP-0084,1,LSP-0085,1,LSP-0086,1,LSP-0087,1,LSP-0088,1,LSP-0089,1,LSP-0090,1,LSP-0091,1,LSP-0092,1,LSP-0093,1,LSP-0094,1,LSP-0095,1,LSP-0096,1,LSP-0097,1,LSP-0098,1,LSP-0099,1,LSP-0100,1,LSP-0101,1,LSP-0102,1,LSP-0103,1,LSP-0104,1,LSP-0105,1,LSP-0106,1,LSP-0107,1,LSP-0108,1,LSP-0109,1,LSP-0110,1,LSP-0111,1,LSP-0112,1,LSP-0113,1,LSP-0114,1,LSP-0115,1,LSP-0116,1,LSP-0117,1,LSP-0118,1,LSP-0119,1,LSP-0120,1,LSP-0121,1,LSP-0122,1,LSP-0123,1,LSP-0124,1,LSP-0125,1,LSP-0126,1,LSP-0127,1,LSP-0128,1,LSP-0129,1,LSP-0130,1,LSP-0131,1,LSP-0132,1,LSP-0133,1,LSP-0134,1,LSP-0135,1,LSP-0136,1,LSP-0137,1,LSP-0138,1,LSP-0139,1,LSP-0140,1,LSP-0141,1,LSP-0142,1,LSP-0143,1,LSP-0144,1,LSP-0145,1,LSP-0146,1,LSP-0147,1,LSP-0148,1,LSP-0149,1,LSP-0150,1,LSP-0151,1,LSP-0152,1,LSP-0153,1,LSP-0154,1,LSP-0155,1,LSP-0156,1,LSP-0157,1,LSP-0158,1,LSP-0159,1,LSP-0160,1,LSP-0161,1,LSP-0162,1,LSP-0163,1,LSP-0164,1,LSP-0165,1,LSP-0166,1,LSP-0167,1,LSP-0168,1,LSP-0169,1,LSP-0170,1,LSP-0171,1,LSP-0172,1,LSP-0173,1,LSP-0174,1,LSP-0175,1,LSP-0176,1,LSP-0177,1,LSP-0178,1,LSP-0179,1,LSP-0180,1,LSP-0181,1,LSP-0182,1,LSP-0183,1,LSP-0184,1,LSP-0185,1,LSP-0186,1,LSP-0187,1,LSP-0188,1,LSP-0189,1,LSP-0190,1,LSP-0191,1,LSP-0192,1,LSP-0193,1,LSP-0194,1,LSP-0195,1,LSP-0196,1,LSP-0197,1,LSP-0198,1,LSP-0199,1,LSP-0200,1,LSP-0201,1,LSP-0202,1,LSP-0203,1,LSP-0204,1,LSP-0205,1,LSP-0206,1,LSP-0207,1,LSP-0208,1,LSP-0209,1,LSP-0210,1,LSP-0211,1,LSP-0212,1,LSP-0213,1,LSP-0214,1,LSP-0215,1,LSP-0216,1,LSP-0217,1,LSP-0218,1,LSP-0219,1,LSP-0220,1,LSP-0221,1,LSP-0222,1,LSP-0223,1,LSP-0224,1,LSP-0225,1,LSP-0226,1,LSP-0227,1,LSP-0228,1,LSP-0229,1,LSP-0230,1,LSP-0231,1,LSP-0232,1,LSP-0233,1,LSP-0234,1,LSP-0235,1,LSP-0236,1,LSP-0237,1,LSP-0238,1,LSP-0239,1,LSP-0240,1,LSP-0241,1,LSP-0242,1,LSP-0243,1,LSP-0244,1,LSP-0245,1,LSP-0246,1,LSP-0247,1,LSP-0248,1,LSP-0249,1,LSP-0250,1,LSP-0251,1,LSP-0252,1,LSP-0253,1,LSP-0254,1,LSP-0255,1,LSP-0256,1,LSP-0257,1,LSP-0258,1,LSP-0259,1,LSP-0260,1,LSP-0261,1,LSP-0262,1,LSP-0263,1,LSP-0264,1,LSP-0265,1,LSP-0266,1,LSP-0267,1,LSP-0268,1,LSP-0269,1,LSP-0270,1,LSP-0271,1,LSP-0272,1,LSP-0273,1,LSP-0274,1,LSP-0275,1,LSP-0276,1,LSP-0277,1,LSP-0278,1,LSP-0279,1,LSP-0280,1,LSP-0281,1,LSP-0282,1,LSP-0283,1,LSP-0284,1,LSP-0285,1,LSP-0286,1,LSP-0287,1,LSP-0288,1,LSP-0289,1,LSP-0290,1,LSP-0291,1,LSP-0292,1,LSP-0293,1,LSP-0294,1,LSP-0295,1,LSP-0296,1,LSP-0297,1,LSP-0298,1,LSP-0299,1,LSP-0300,1,LSP-0301,1,LSP-0302,1,LSP-0303,1,LSP-0304,1,LSP-0305,1,LSP-0306,1,LSP-0307,1,LSP-0308,1,LSP-0309,1,LSP-0310,1,LSP-0311,1,LSP-0312,1,LSP-0313,1,LSP-0314,1,LSP-0315,1,LSP-0316,1,LSP-0317,1,LSP-0318,1,LSP-0319,1,LSP-0320,1,LSP-0321,1,LSP-0322,1,LSP-0323,1,LSP-0324,1,LSP-0325,1,LSP-0326,1,LSP-0327,1,LSP-0328,1,LSP-0329,1,LSP-0330,1,LSP-0331,1,LSP-0332,1,LSP-0333,1,LSP-0334,1,LSP-0335,1,LSP-0336,1,LSP-0337,1,LSP-0338,1,LSP-0339,1,LSP-0340,1,LSP-0341,1,LSP-0342,1,LSP-0343,1,LSP-0344,1,LSP-0345,1,LSP-0346,1,LSP-0347,1,LSP-0348,1,LSP-0349,1,LSP-0350,1,LSP-0351,1,LSP-0352,1,LSP-0353,1,LSP-0354,1,LSP-0355,1,LSP-0356,1,LSP-0357,1,LSP-0358,1,LSP-0359,1,LSP-0360,1,LSP-0361,1,LSP-0362,1,LSP-0363,1,LSP-0364,1,LSP-0365,1,LSP-0366,1,LSP-0367,1,LSP-0368,1,LSP-0369,1,LSP-0370,1,LSP-0371,1,LSP-0372,1,LSP-0373,1,LSP-0374,1,LSP-0375,1,LSP-0376,1,LSP-0377,1,LSP-0378,1,LSP-0379,1,LSP-0380,1,LSP-0381,1,LSP-0382,1,LSP-0383,1,LSP-0384,1,LSP-0385,1,LSP-0386,1,LSP-0387,1,LSP-0388,1,LSP-0389,1,LSP-0390,1,LSP-0391,1,LSP-0392,1,LSP-0393,1,LSP-0394,1,LSP-0395,1,LSP-0396,1,LSP-0397,1,LSP-0398,1,LSP-0399,1,LSP-0400,1,LSP-0401,1,LSP-0402,1,LSP-0403,1,LSP-0404,1,LSP-0405,1,LSP-0406,1,LSP-0407,1,LSP-0408,1,LSP-0409,1,LSP-0410,1,LSP-0411,1,LSP-0412,1,LSP-0413,1,LSP-0414,1,LSP-0415,1,LSP-0416,1,LSP-0417,1,LSP-0418,1,LSP-0419,1,LSP-0420,1,LSP-0421,1,LSP-0422,1,LSP-0423,1,LSP-0424,1,LSP-0425,1,LSP-0426,1,LSP-0427,1,LSP-0428,1,LSP-0429,1,LSP-0430,1,LSP-0431,1,LSP-0432,1,LSP-0433,1,LSP-0434,1,LSP-0435,1,LSP-0436,1,LSP-0437,1,LSP-0438,1,LSP-0439,1,LSP-0440,1,LSP-0441,1,LSP-0442,1,LSP-0443,1,LSP-0444,1,LSP-0445,1,LSP-0446,1,LSP-0447,1,LSP-0448,1,LSP-0449,1,LSP-0450,1,LSP-0451,1,LSP-0452,1,LSP-0453,1,LSP-0454,1,LSP-0455,1,LSP-0456,1,LSP-0457,1,LSP-0458,1,LSP-0459,1,LSP-0460,1,LSP-0461,1,LSP-0462,1,LSP-0463,1,LSP-0464,1,LSP-0465,1,LSP-0466,1,LSP-0467,1,LSP-0468,1,LSP-0469,1,LSP-0470,1,LSP-0471,1,LSP-0472,1,LSP-0473,1,LSP-0474,1,LSP-0475,1,LSP-0476,1,LSP-0477,1,LSP-0478,1,LSP-0479,1,LSP-0480,1,LSP-0481,1,LSP-0482,1,LSP-0483,1,LSP-0484,1,LSP-0485,1,LSP-0486,1,LSP-0487,1,LSP-0488,1,LSP-0489,1,LSP-0490,1,LSP-0491,1,LSP-0492,1,LSP-0493,1,LSP-0494,1,LSP-0495,1,LSP-0496,1,LSP-0497,1,LSP-0498,1,LSP-0499,1,LSP-0500,1,LSP-0501,1,LSP-0502,1,LSP-0503,1,LSP-0504,1,LSP-0505,1,LSP-0506,1,LSP-0507,1,LSP-0508,1,LSP-0509,1,LSP-0510,1,LSP-0511,1,LSP-0512,1,LSP-0513,1,LSP-0514,1,LSP-0515,1,LSP-0516,1,LSP-0517,1,LSP-0518,1,LSP-0519,1,LSP-0520,1,LSP-0521,1,LSP-0522,1,LSP-0523,1,LSP-0524,1,LSP-0525,1,LSP-0526,1,LSP-0527,1,LSP-0528,1,LSP-0529,1,LSP-0530,1,LSP-0531,1,LSP-0532,1,LSP-0533,1,LSP-0534,1,LSP-0535,1,LSP-0536,1,LSP-0537,1,LSP-0538,1,LSP-0539,1,LSP-0540,1,LSP-0541,1,LSP-0542,1,LSP-0543,1,LSP-0544,1,LSP-0545,1,LSP-0546,1,LSP-0547,1,LSP-0548,1,LSP-0549,1,LSP-0550,1,LSP-0551,1,LSP-0552,1,LSP-0553,1,LSP-0554,1,LSP-0555,1,LSP-0556,1,LSP-0557,1,LSP-0558,1,LSP-0559,1,LSP-0560,1,LSP-0561,1,LSP-0562,1,LSP-0563,1,LSP-0564,1,LSP-0565,1,LSP-0566,1,LSP-0567,1,LSP-0568,1,LSP-0569,1,LSP-0570,1,LSP-0571,1,LSP-0572,1,LSP-0573,1,LSP-0574,1,LSP-0575,1,LSP-0576,1,LSP-0577,1,LSP-0578,1,LSP-0579,1,LSP-0580,1,LSP-0581,1,LSP-0582,1,LSP-0583,1,LSP-0584,1,LSP-0585,1,LSP-0586,1,LSP-0587,1,LSP-0588,1,LSP-0589,1,LSP-0590,1,LSP-0591,1,LSP-0592,1,LSP-0593,1,LSP-0594,1,LSP-0595,1,LSP-0596,1,LSP-0597,1,LSP-0598,1,LSP-0599,1,LSP-0600,1,LSP-0601,1,LSP-0602,1,LSP-0603,1,LSP-0604,1,LSP-0605,1,LSP-0606,1,LSP-0607,1,LSP-0608,1,LSP-0609,1,LSP-0610,1,LSP-0611,1,LSP-0612,1,LSP-0613,1,LSP-0614,1,LSP-0615,1,LSP-0616,1,LSP-0617,1,LSP-0618,1,LSP-0619,1,LSP-0620,1,LSP-0621,1,LSP-0622,1,LSP-0623,1,LSP-0624,1,LSP-0625,1,LSP-0626,1,LSP-0627,1,LSP-0628,1,LSP-0629,1,LSP-0630,1,LSP-0631,1,LSP-0632,1,LSP-0633,1,LSP-0634,1,LSP-0635,1,LSP-0636,1,LSP-0637,1,LSP-0638,1,LSP-0639,1,LSP-0640,1,LSP-0641,1,LSP-0642,1,LSP-0643,1,LSP-0644,1,LSP-0645,1,LSP-0646,1,LSP-0647,1,LSP-0648,1,LSP-0649,1,LSP-0650,1,LSP-0651,1,LSP-0652,1,LSP-0653,1,LSP-0654,1,LSP-0655,1,LSP-0656,1,LSP-0657,1,LSP-0658,1,LSP-0659,1,LSP-0660,1,LSP-0661,1,LSP-0662,1,LSP-0663,1,LSP-0664,1,LSP-0665,1,LSP-0666,1,LSP-0667,1,LSP-0668,1,LSP-0669,1,LSP-0670,1,LSP-0671,1,LSP-0672,1,LSP-0673,1,LSP-0674,1,LSP-0675,1,LSP-0676,1,LSP-0677,1,LSP-0678,1,LSP-0679,1,LSP-0680,1,LSP-0681,1,LSP-0682,1,LSP-0683,1,LSP-0684,1,LSP-0685,1,LSP-0686,1,LSP-0687,1,LSP-0688,1,LSP-0689,1,LSP-0690,1,LSP-0691,1,LSP-0692,1,LSP-0693,1,LSP-0694,1,LSP-0695,1,LSP-0696,1,LSP-0697,1,LSP-0698,1,LSP-0699,1,LSP-0700,1,LSP-0701,1,LSP-0702,1,LSP-0703,1,LSP-0704,1,LSP-0705,1,LSP-0706,1,LSP-0707,1,LSP-0708,1,LSP-0709,1,LSP-0710,1,LSP-0711,1,LSP-0712,1,LSP-0713,1,LSP-0714,1,LSP-0715,1,LSP-0716,1,LSP-0717,1,LSP-0718,1,LSP-0719,1,LSP-0720,1,LSP-0721,1,LSP-0722,1,LSP-0723,1,LSP-0724,1,LSP-0725,1,LSP-0726,1,LSP-0727,1,LSP-0728,1,LSP-0729,1,LSP-0730,1,LSP-0731,1,LSP-0732,1,LSP-0733,1,LSP-0734,1,LSP-0735,1,LSP-0736,1,LSP-0737,1,LSP-0738,1,LSP-0739,1,LSP-0740,1,LSP-0741,1,LSP-0742,1,LSP-0743,1,LSP-0744,1,LSP-0745,1,LSP-0746,1,LSP-0747,1,LSP-0748,1,LSP-0749,1,LSP-0750,1,LSP-0751,1,LSP-0752,1,LSP-0753,1,LSP-0754,1,LSP-0755,1,LSP-0756,1,LSP-0757,1,LSP-0758,1,LSP-0759,1,LSP-0760,1,LSP-0761,1,LSP-0762,1,LSP-0763,1,LSP-0764,1,LSP-0765,1,LSP-0766,1,LSP-0767,1,LSP-0768,1,LSP-0769,1,LSP-0770,1,LSP-0771,1,LSP-0772,1,LSP-0773,1,LSP-0774,1,LSP-0775,1,LSP-0776,1,LSP-0777,1,LSP-0778,1,LSP-0779,1,LSP-0780,1,LSP-0781,1,LSP-0782,1,LSP-0783,1,LSP-0784,1,LSP-0785,1,LSP-0786,1,LSP-0787,1,LSP-0788,1,LSP-0789,1,LSP-0790,1,LSP-0791,1,LSP-0792,1,LSP-0793,1,LSP-0794,1,LSP-0795,1,LSP-0796,1,LSP-0797,1,LSP-0798,1,LSP-0799,1,LSP-0800,1,LSP-0801,1,LSP-0802,1,LSP-0803,1,LSP-0804,1,LSP-0805,1,LSP-0806,1,LSP-0807,1,LSP-0808,1,LSP-0809,1,LSP-0810,1,LSP-0811,1,LSP-0812,1,LSP-0813,1,LSP-0814,1,LSP-0815,1,LSP-0816,1,LSP-0817,1,LSP-0818,1,LSP-0819,1,LSP-0820,1,LSP-0821,1,LSP-0822,1,LSP-0823,1,LSP-0824,1,LSP-0825,1,LSP-0826,1,LSP-0827,1,LSP-0828,1,LSP-0829,1,LSP-0830,1,LSP-0831,1,LSP-0832,1,LSP-0833,1,LSP-0834,1,LSP-0835,1,LSP-0836,1,LSP-0837,1,LSP-0838,1,LSP-0839,1,LSP-0840,1,LSP-0841,1,LSP-0842,1,LSP-0843,1,LSP-0844,1,LSP-0845,1,LSP-0846,1,LSP-0847,1,LSP-0848,1,LSP-0849,1,LSP-0850,1,LSP-0851,1,LSP-0852,1,LSP-0853,1,LSP-0854,1,LSP-0855,1,LSP-0856,1,LSP-0857,1,LSP-0858,1,LSP-0859,1,LSP-0860,1,LSP-0861,1,LSP-0862,1,LSP-0863,1,LSP-0864,1,LSP-0865,1,LSP-0866,1,LSP-0867,1,LSP-0868,1,LSP-0869,1,LSP-0870,1,LSP-0871,1,LSP-0872,1,LSP-0873,1,LSP-0874,1,LSP-0875,1,LSP-0876,1,LSP-0877,1,LSP-0878,1,LSP-0879,1,LSP-0880,1,LSP-0881,1,LSP-0882,1,LSP-0883,1,LSP-0884,1,LSP-0885,1,LSP-0886,1,LSP-0887,1,LSP-0888,1,LSP-0889,1,LSP-0890,1,LSP-0891,1,LSP-0892,1,LSP-0893,1,LSP-0894,1,LSP-0895,1,LSP-0896,1,LSP-0897,1,LSP-0898,1,LSP-0899,1,LSP-0900,1,LSP-0901,1,LSP-0902,1,LSP-0903,1,LSP-0904,1,LSP-0905,1,LSP-0906,1,LSP-0907,1,LSP-0908,1,LSP-0909,1,LSP-0910,1,LSP-0911,1,LSP-0912,1,LSP-0913,1,LSP-0914,1,LSP-0915,1,LSP-0916,1,LSP-0917,1,LSP-0918,1,LSP-0919,1,LSP-0920,1,LSP-0921,1,LSP-0922,1,LSP-0923,1,LSP-0924,1,LSP-0925,1,LSP-0926,1,LSP-0927,1,LSP-0928,1,LSP-0929,1,LSP-0930,1,LSP-0931,1,LSP-0932,1,LSP-0933,1,LSP-0934,1,LSP-0935,1,LSP-0936,1,LSP-0937,1,LSP-0938,1,LSP-0939,1,LSP-0940,1,LSP-0941,1,LSP-0942,1,LSP-0943,1,LSP-0944,1,LSP-0945,1,LSP-0946,1,LSP-0947,1,LSP-0948,1,LSP-0949,1,LSP-0950,1,LSP-0951,1,LSP-0952,1,LSP-0953,1,LSP-0954,1,LSP-0955,1,LSP-0956,1,LSP-0957,1,LSP-0958,1,LSP-0959,1,LSP-0960,1,LSP-0961,1,LSP-0962,1,LSP-0963,1,LSP-0964,1,LSP-0965,1,LSP-0966,1,LSP-0967,1,LSP-0968,1,LSP-0969,1,LSP-0970,1,LSP-0971,1,LSP-0972,1,LSP-0973,1,LSP-0974,1,LSP-0975,1,LSP-0976,1,LSP-0977,1,LSP-0978,1,LSP-0979,1,LSP-0980,1,LSP-0981,1,LSP-0982,1,LSP-0983,1,LSP-0984,1,LSP-0985,1,LSP-0986,1,LSP-0987,1,LSP-0988,1,LSP-0989,1,LSP-0990,1,LSP-0991,1,LSP-0992,1,LSP-0993,1,LSP-0994,1,LSP-0995,1,LSP-0996,1,LSP-0997,1,LSP-0998,1,LSP-0999,1,LSP-1000,1,LSP-1001,1,LSP-1002,1,LSP-1003,1,LSP-1004,1,LSP-1005,1,LSP-1006,1,LSP-1007,1,LSP-1008,1,LSP-1009,1,LSP-1010,1,LSP-1011,1,LSP-1012,1,LSP-1013,1,LSP-1014,1,LSP-1015,1,LSP-1016,1,LSP-1017,1,LSP-1018,1,LSP-1019,1,LSP-1020,1,LSP-1021,1,LSP-1022,1,LSP-1023,1,LSP-1024,1,LSP-1025,1,LSP-1026,1,LSP-1027,1,LSP-1028,1,LSP-1029,1,LSP-1030,1,LSP-1031,1,LSP-1032,1,LSP-1033,1,LSP-1034,1,LSP-1035,1,LSP-1036,1,LSP-1037,1,LSP-1038,1,LSP-1039,1,LSP-1040,1,LSP-1041,1,LSP-1042,1,LSP-1043,1,LSP-1044,1,LSP-1045,1,LSP-1046,1,LSP-1047,1,LSP-1048,1,LSP-1049,1,LSP-1050,1,LSP-1051,1,LSP-1052,1,LSP-1053,1,LSP-1054,1,LSP-1055,1,LSP-1056,1,LSP-1057,1,LSP-1058,1,LSP-1059,1,LSP-1060,1,LSP-1061,1,LSP-1062,1,LSP-1063,1,LSP-1064,1,LSP-1065,1,LSP-1066,1,LSP-1067,1,LSP-1068,1,LSP-1069,1,LSP-1070,1,LSP-1071,1,LSP-1072,1,LSP-1073,1,LSP-1074,1,LSP-1075,1,LSP-1076,1,LSP-1077,1,LSP-1078,1,LSP-1079,1,LSP-1080,1,LSP-1081,1,LSP-1082,1,LSP-1083,1,LSP-1084,1,LSP-1085,1,LSP-1086,1,LSP-1087,1,LSP-1088,1,LSP-1089,1,LSP-1090,1,LSP-1091,1,LSP-1092,1,LSP-1093,1,LSP-1094,1,LSP-1095,1,LSP-1096,1,LSP-1097,1,LSP-1098,1,LSP-1099,1,LSP-1100,1,LSP-1101,1,LSP-1102,1,LSP-1103,1,LSP-1104,1,LSP-1105,1,LSP-1106,1,LSP-1107,1,LSP-1108,1,LSP-1109,1,LSP-1110,1,LSP-1111,1,LSP-1112,1,LSP-1113,1,LSP-1114,1,LSP-1115,1,LSP-1116,1,LSP-1117,1,LSP-1118,1,LSP-1119,1,LSP-1120,1,LSP-1121,1,LSP-1122,1,LSP-1123,1,LSP-1124,1,LSP-1125,1,LSP-1126,1,LSP-1127,1,LSP-1128,1,LSP-1129,1,LSP-1130,1,LSP-1131,1,LSP-1132,1,LSP-1133,1,LSP-1134,1,LSP-1135,1,LSP-1136,1,LSP-1137,1,LSP-1138,1,LSP-1139,1,LSP-1140,1,LSP-1141,1,LSP-1142,1,LSP-1143,1,LSP-1144,1,LSP-1145,1,LSP-1146,1,LSP-1147,1,LSP-1148,1,LSP-1149,1,LSP-1150,1,LSP-1151,1,LSP-1152,1,LSP-1153,1,LSP-1154,1,LSP-1155,1,LSP-1156,1,LSP-1157,1,LSP-1158,1,LSP-1159,1,LSP-1160,1,LSP-1161,1,LSP-1162,1,LSP-1163,1,LSP-1164,1,LSP-1165,1,LSP-1166,1,LSP-1167,1,LSP-1168,1,LSP-1169,1,LSP-1170,1,LSP-1171,1,LSP-1172,1,LSP-1173,1,LSP-1174,1,LSP-1175,1,LSP-1176,1,LSP-1177,1,LSP-1178,1,LSP-1179,1,LSP-1180,1,LSP-1181,1,LSP-1182,1,LSP-1183,1,LSP-1184,1,LSP-1185,1,LSP-1186,1,LSP-1187,1,LSP-1188,1,LSP-1189,1,LSP-1190,1,LSP-1191,1,LSP-1192,1,LSP-1193,1,LSP-1194,1,LSP-1195,1,LSP-1196,1,LSP-1197,1,LSP-1198,1,LSP-1199,1,LSP-1200,1,LSP-1201,1,LSP-1202,1,LSP-1203,1,LSP-1204,1,LSP-1205,1,LSP-1206,1,LSP-1207,1,LSP-1208,1,LSP-1209,1,LSP-1210,1,LSP-1211,1,LSP-1212,1,LSP-1213,1,LSP-1214,1,LSP-1215,1,LSP-1216,1,LSP-1217,1,LSP-1218,1,LSP-1219,1,LSP-1220,1,LSP-1221,1,LSP-1222,1,LSP-1223,1,LSP-1224,1,LSP-1225,1,LSP-1226,1,LSP-1227,1,LSP-1228,1,LSP-1229,1,LSP-1230,1,LSP-1231,1,LSP-1232,1,LSP-1233,1,LSP-1234,1,LSP-1235,1,LSP-1236,1,LSP-1237,1,LSP-1238,1,LSP-1239,1,LSP-1240,1,LSP-1241,1,LSP-1242,1,LSP-1243,1,LSP-1244,1,LSP-1245,1,LSP-1246,1,LSP-1247,1,LSP-1248,1,LSP-1249,1,LSP-1250,1,LSP-1251,1,LSP-1252,1,LSP-1253,1,LSP-1254,1,LSP-1255,1,LSP-1256,1,LSP-1257,1,LSP-1258,1,LSP-1259,1,LSP-1260,1,LSP-1261,1,LSP-1262,1,LSP-1263,1,LSP-1264,1,LSP-1265,1,LSP-1266,1,LSP-1267,1,LSP-1268,1,LSP-1269,1,LSP-1270,1,LSP-1271,1,LSP-1272,1,LSP-1273,1,LSP-1274,1,LSP-1275,1,LSP-1276,1,LSP-1277,1,LSP-1278,1,LSP-1279,1,LSP-1280,1,LSP-1281,1,LSP-1282,1,LSP-1283,1,LSP-1284,1,LSP-1285,1,LSP-1286,1,LSP-1287,1,LSP-1288,1,LSP-1289,1,LSP-1290,1,LSP-1291,1,LSP-1292,1,LSP-1293,1,LSP-1294,1,LSP-1295,1,LSP-1296,1,LSP-1297,1,LSP-1298,1,LSP-1299,1,LSP-1300,1,LSP-1301,1,LSP-1302,1,LSP-1303,1,LSP-1304,1,LSP-1305,1,LSP-1306,1,LSP-1307,1,LSP-1308,1,LSP-1309,1,LSP-1310,1,LSP-1311,1,LSP-1312,1,LSP-1313,1,LSP-1314,1,LSP-1315,1,LSP-1316,1,LSP-1317,1,LSP-1318,1,LSP-1319,1,LSP-1320,1,LSP-1321,1,LSP-1322,1,LSP-1323,1,LSP-1324,1,LSP-1325,1,LSP-1326,1,LSP-1327,1,LSP-1328,1,LSP-1329,1,LSP-1330,1,LSP-1331,1,LSP-1332,1,LSP-1333,1,LSP-1334,1,LSP-1335,1,LSP-1336,1,LSP-1337,1,LSP-1338,1,LSP-1339,1,LSP-1340,1,LSP-1341,1,LSP-1342,1,LSP-1343,1,LSP-1344,1,LSP-1345,1,LSP-1346,1,LSP-1347,1,LSP-1348,1,LSP-1349,1,LSP-1350,1,LSP-1351,1,LSP-1352,1,LSP-1353,1,LSP-1354,1,LSP-1355,1,LSP-1356,1,LSP-1357,1,LSP-1358,1,LSP-1359,1,LSP-1360,1,LSP-1361,1,LSP-1362,1,LSP-1363,1,LSP-1364,1,LSP-1365,1,LSP-1366,1,LSP-1367,1,LSP-1368,1,LSP-1369,1,LSP-1370,1,LSP-1371,1,LSP-1372,1,LSP-1373,1,LSP-1374,1,LSP-1375,1,LSP-1376,1,LSP-1377,1,LSP-1378,1,LSP-1379,1,LSP-1380,1,LSP-1381,1,LSP-1382,1,LSP-1383,1,LSP-1384,1,LSP-1385,1,LSP-1386,1,LSP-1387,1,LSP-1388,1,LSP-1389,1,LSP-1390,1,LSP-1391,1,LSP-1392,1,LSP-1393,1,LSP-1394,1,LSP-1395,1,LSP-1396,1,LSP-1397,1,LSP-1398,1,LSP-1399,1,LSP-1400,1,LSP-1401,1,LSP-1402,1,LSP-1403,1,LSP-1404,1,LSP-1405,1,LSP-1406,1,LSP-1407,1,LSP-1408,1,LSP-1409,1,LSP-1410,1,LSP-1411,1,LSP-1412,1,LSP-1413,1,LSP-1414,1,LSP-1415,1,LSP-1416,1,LSP-1417,1,LSP-1418,1,LSP-1419,1,LSP-1420,1,LSP-1421,1,LSP-1422,1,LSP-1423,1,LSP-1424,1,LSP-1425,1,LSP-1426,1,LSP-1427,1,LSP-1428,1,LSP-1429,1,LSP-1430,1,LSP-1431,1,LSP-1432,1,LSP-1433,1,LSP-1434,1,LSP-1435,1,LSP-1436,1,LSP-1437,1,LSP-1438,1,LSP-1439,1,LSP-1440,1,LSP-1441,1,LSP-1442,1,LSP-1443,1,LSP-1444,1,LSP-1445,1,LSP-1446,1,LSP-1447,1,LSP-1448,1,LSP-1449,1,LSP-1450,1,LSP-1451,1,LSP-1452,1,LSP-1453,1,LSP-1454,1,LSP-1455,1,LSP-1456,1,LSP-1457,1,LSP-1458,1,LSP-1459,1,LSP-1460,1,LSP-1461,1,LSP-1462,1,LSP-1463,1,LSP-1464,1,LSP-1465,1,LSP-1466,1,LSP-1467,1,LSP-1468,1,LSP-1469,1,LSP-1470,1,LSP-1471,1,LSP-1472,1,LSP-1473,1,LSP-1474,1,LSP-1475,1,LSP-1476,1,LSP-1477,1,LSP-1478,1,LSP-1479,1,LSP-1480,1,LSP-1481,1,LSP-1482,1,LSP-1483,1,LSP-1484,1,LSP-1485,1,LSP-1486,1,LSP-1487,1,LSP-1488,1,LSP-1489,1,LSP-1490,1,LSP-1491,1,LSP-1492,1,LSP-1493,1,LSP-1494,1,LSP-1495,1,LSP-1496,1,LSP-1497,1,LSP-1498,1,LSP-1499,1,LSP-1500,1,LSP-1501,1,LSP-1502,1,LSP-1503,1,LSP-1504,1,LSP-1505,1,LSP-1506,1,LSP-1507,1,LSP-1508,1,LSP-1509,1,LSP-1510,1,LSP-1511,1,LSP-1512,1,LSP-1513,1,LSP-1514,1,LSP-1515,1,LSP-1516,1,LSP-1517,1,LSP-1518,1,LSP-1519,1,LSP-1520,1,LSP-1521,1,LSP-1522,1,LSP-1523,1,LSP-1524,1,LSP-1525,1,LSP-1526,1,LSP-1527,1,LSP-1528,1,LSP-1529,1,LSP-1530,1,LSP-1531,1,LSP-1532,1,LSP-1533,1,LSP-1534,1,LSP-1535,1,LSP-1536,1,LSP-1537,1,LSP-1538,1,LSP-1539,1,LSP-1540,1,LSP-1541,1,LSP-1542,1,LSP-1543,1,LSP-1544,1,LSP-1545,1,LSP-1546,1,LSP-1547,1,LSP-1548,1,LSP-1549,1,LSP-1550,1,LSP-1551,1,LSP-1552,1,LSP-1553,1,LSP-1554,1,LSP-1555,1,LSP-1556,1,LSP-1557,1,LSP-1558,1,LSP-1559,1,LSP-

Lorem 79, ea dolorsitamet,eiusmodtempor, incididunt,ut labore,et dolore magna aliqua. Ut enim ad minim veniam,quis nostrud exercitation ullamco laboris nisi ut aliquip ex ea commodo consequat. Duis aute irure dolor in reprehenderit in voluptate velit esse cillum dolore eu fugiat nulla pariatur. Excepteur sint occaecat cupidatat non proident, sunt in culpa qui officia deserunt mollit anim id est laborum.

Accidentes	Estacionamiento	Nuevo Nivel	Nuevo Cruce	Cruce
2014	Calle/Avd	Nuevo Leon Mexico Mexico DF 5 6 8 9 10 11 12 13 14 15 16 17 18 19 20 21 22 23 24 25 26 27 28 29 30 31	0.000	0.000
2014	Calle/Avd	Nuevo Leon Mexico Mexico DF 5 6 8 9 10 11 12 13 14 15 16 17 18 19 20 21 22 23 24 25 26 27 28 29 30 31	0.000	0.000
2014	Calle/Avd	Calle/Avd	0.000	0.000
2014	Calle/Avd	Nuevo Leon Mexico Mexico DF 5 6 8 9 10 11 12 13 14 15 16 17 18 19 20 21 22 23 24 25 26 27 28 29 30 31	0.000	0.000
2014	Calle/Avd	Calle/Avd	0.000	0.000
2014	Calle/Avd	Calle/Avd	0.000	0.000
2014	Calle/Avd	Calle/Avd	0.000	0.000
2014	Calle/Avd	Calle/Avd	0.000	0.000
2014	Calle/Avd	Nuevo Leon Mexico Mexico DF 5 6 8 9 10 11 12 13 14 15 16 17 18 19 20 21 22 23 24 25 26 27 28 29 30 31	0.000	0.000
2014	Calle/Avd	Nuevo Leon Mexico Mexico DF 5 6 8 9 10 11 12 13 14 15 16 17 18 19 20 21 22 23 24 25 26 27 28 29 30 31	0.000	0.000
2014	Calle/Avd	Calle/Avd

| Lorem | Ipsum | Dolor | Sit | Amet | Consectetur | Adipiscing | Elit | Sed | Eiusmod | Tempor | Incididunt | Ut | Labore | Et | Dolore | Magna | Aliqua | Ut | Enim | Ad | Minim | Veniam | Quis | Nostrud | Exercitation | Ullamco | Laboris | Nisi | Ut | Aliquip | Ex | Ea | Commodo | Consequat | Duis | Aute | Irure | Dolor | In | Reprehenderit | In | Voluptate | Velit | Esse | Cillum | Dolore | Eu | Fugiat | Nulla | Pariatur | Excepteur | Sint | Occaecat | Cupidatat | Non | Proident | Sunt | In | Culpa | Qui | Officia | Deserunt | Mollit | Anim | Id | Est | Laborum |
|---|---|---

Table S7. Minimal media used to quantify the proportion of the microbiota that can use sole carb			
Component	**Amount/L**	**Concentration**	
KH_2PO4	100 mL	100 mM	
$NaHCO_3$	0.4 g	4.8 mM	
$NaCl_2$	0.08 g	1.37 mM	
CaCl2	1 mL	0.80%	0.8g/100mL stock; autoclave
Vitamin K (menadione)	1 mL	5.8 mM	1 mg/mL stock solution; protect from light; autoclave
$FeSO_4$	1 mL	1.44 mM	0.4 mg $FeSO_4$/mL stock solution; filter sterilize
Histidine Hematin Solution	1 mL	0.1%	1.2 mg hematin/mL in 0.2M histidine; filter sterilize after preparation of stock; protect from light; store at 4C
NH4Cl	1 g		
Tween 80	2 mL	0.05%	
$MgSO_4$-$7H_20$***	1 mL	0.008 mM	
ATCC Vitamin Mix***	10 mL	1%	
ATCC Trace Mineral Mix***	10 mL	1%	
For sole C&E media, add one of the following to Media A			
Aspartic acid	0.02g		
Mannose	0.9g		
Galactose	1.8g		
Sodium acetate	6g	0.60%	
Sodium formate	4g	0.40%	Requires sodium sulfate
D-glucose	0.4 g	2.2 mM	Add to 10ml DI H2O and filter sterilize
Fructose	1 g	2.2 mM	Add to 10ml DI H2O and filter sterilize
Sucrose	1.71g		Add to 10ml DI H2O and filter sterilize
Methylvaleric acid	561ul		Add both methylvaeric and methylbutyric
Methylbutyric acid	517ul		
Oxalate	6.75g	50mM	
pH to 7			
Filter sterilize and bring into anaerobic chamber			
Cysteine***	0.5g		Add to 10ml DI H2O and filter sterilize in anaerobic chamber
sodium sulfate	2g	0.20%	Only add if adding sodium formate
**Let media sit in anaerobic chamber for at least 24hrs to be fully reduced before inoculation			

1615

1616

Table S8. Microorganisms used in the taxonomic cohort. 1617

Species	**Commercial source**	**Isolation source** 1618
Oxalobacter formgienes	ATCC 35274	human
Desulfovibrio piger	DSMZ749	Sheep rumen
Methanobrevibacter smithii	DSMZ11975	animal feces
Ruminococcus gnavus	ATCC 29149	human
Coprococcus comes	ATCC 27758	human
Bacteroides thetaiotaomicron	ATCC 700349	human
Lactobacillus helveticus	ATCC 55796	Unknown
Lactobacillus plantarum	ATCC 700210	Unknown

Supplemental references

1. Kohl, K.D., and Dearing, M.D. (2014). Wild-caught rodents retain a majority of their natural gut microbiota upon entrance into captivity. Environmental microbiology reports *6*, 191-195.
2. Miller, A.W., Oakeson, K.F., Dale, C., and Dearing, M.D. (2016). Effect of Dietary Oxalate on the Gut Microbiota of the Mammalian Herbivore Neotoma albigula. Applied and environmental microbiology *82*, 2669-2675.
3. Belenguer, A., Bati, M.B., Hervás, G., Toral, P.G., Yáñez-Ruiz, D.R., and Frutos, P. (2013). Impact of oxalic acid on rumen function and bacterial community in sheep. animal *7*, 940-947.
4. Miller, A.W., Dale, C., and Dearing, M.D. (2017). Microbiota Diversification and Crash Induced by Dietary Oxalate in the Mammalian Herbivore Neotoma albigula. mSphere *2*. 10.1128/mSphere.00428-17.
5. Miller, A.W., Orr, T., Dearing, D., and Monga, M. (2019). Loss of function dysbiosis associated with antibiotics and high fat, high sugar diet. The ISME journal *13*, 1379-1390.
6. Hatch, M., Gjymishka, A., Salido, E.C., Allison, M.J., and Freel, R.W. (2011). Enteric oxalate elimination is induced and oxalate is normalized in a mouse model of primary hyperoxaluria following intestinal colonization with Oxalobacter. American Journal of Physiology-Gastrointestinal and Liver Physiology *300*, G461-G469.
7. Miller, A.W., Dale, C., and Dearing, M.D. (2017). The Induction of Oxalate Metabolism In Vivo Is More Effective with Functional Microbial Communities than with Functional Microbial Species. MSystems *2*, e00088-00017.
8. Miller, A.W., Oakeson, K.F., Dale, C., and Dearing, M.D. (2016). Microbial community transplant results in increased and long-term oxalate degradation. Microbial ecology *72*, 470-478.
9. Vijay-Kumar, M., Aitken, J.D., Carvalho, F.A., Cullender, T.C., Mwangi, S., Srinivasan, S., Sitaraman, S.V., Knight, R., Ley, R.E., and Gewirtz, A.T. (2010). Metabolic syndrome and altered gut microbiota in mice lacking Toll-like receptor 5. Science *328*, 228-231.
10. Batagello, C.A., Monga, M., and Miller, A.W. (2018). Calcium oxalate urolithiasis: a case of missing microbes? Journal of endourology *32*, 995-1005.
11. Le Naour, J., Montégut, L., Joseph, A., Garbin, K., Vacchelli, E., Kroemer, G., Pol, J.G., and Maiuri, M.C. (2022). Improved Swiss-rolling method for histological analyses of colon tissue. MethodsX *9*, 101630.
12. Koelink, P.J., Wildenberg, M.E., Stitt, L.W., Feagan, B.G., Koldijk, M., van ‘t Wout, A.B., Atreya, R., Vieth, M., Brandse, J.F., and Duijst, S. (2018). Development of reliable, valid and responsive scoring systems for endoscopy and histology in animal models for inflammatory bowel disease. Journal of Crohn's and Colitis *12*, 794-803.
13. Rungby, J., Kassem, M., Eriksen, E.F., and Danscher, G. (1993). The von Kossa reaction for calcium deposits: silver lactate staining increases sensitivity and reduces background. The Histochemical Journal *25*, 446-451.
14. Bankhead, P., Loughrey, M.B., Fernández, J.A., Dombrowski, Y., McArt, D.G., Dunne, P.D., McQuaid, S., Gray, R.T., Murray, L.J., and Coleman, H.G. (2017).

QuPath: Open source software for digital pathology image analysis. Scientific reports *7*, 1-7.

15. Miller, A.W., Kohl, K.D., and Dearing, M.D. (2014). The gastrointestinal tract of the white-throated woodrat (Neotoma albigula) harbors distinct consortia of oxalate-degrading bacteria. Applied and environmental microbiology *80*, 1595-1601.
16. Goodman, A.L., Kallstrom, G., Faith, J.J., Reyes, A., Moore, A., Dantas, G., and Gordon, J.I. (2011). Extensive personal human gut microbiota culture collections characterized and manipulated in gnotobiotic mice. Proceedings of the National Academy of Sciences *108*, 6252-6257.
17. Mak, T.D., Laiakis, E.C., Goudarzi, M., and Fornace Jr, A.J. (2013). Metabolyzer: A novel statistical workflow for analyzing postprocessed lc–ms metabolomics data. Analytical chemistry *86*, 506-513.
18. Okuda, S., Yamada, T., Hamajima, M., Itoh, M., Katayama, T., Bork, P., Goto, S., and Kanehisa, M. (2008). KEGG Atlas mapping for global analysis of metabolic pathways. Nucleic acids research *36*, W423-W426.
19. Wishart, D.S., Feunang, Y.D., Marcu, A., Guo, A.C., Liang, K., Vázquez-Fresno, R., Sajed, T., Johnson, D., Li, C., and Karu, N. (2017). HMDB 4.0: the human metabolome database for 2018. Nucleic acids research *46*, D608-D617.
20. O'Donnell, V.B., Dennis, E.A., Wakelam, M.J., and Subramaniam, S. (2019). LIPID MAPS: Serving the next generation of lipid researchers with tools, resources, data, and training. Science signaling *12*, eaaw2964.
21. Karp, P.D., Billington, R., Caspi, R., Fulcher, C.A., Latendresse, M., Kothari, A., Keseler, I.M., Krummenacker, M., Midford, P.E., and Ong, Q. (2019). The BioCyc collection of microbial genomes and metabolic pathways. Briefings in bioinformatics *20*, 1085-1093.
22. Qi, Z., and Voit, E.O. (2016). Strategies for comparing metabolic profiles: Implications for the inference of biochemical mechanisms from metabolomics data. IEEE/ACM transactions on computational biology and bioinformatics *14*, 1434-1445.
23. Oksanen, J., Blanchet, F.G., Kindt, R., Legendre, P., O'hara, R., Simpson, G.L., Solymos, P., Stevens, M.H.H., and Wagner, H. (2010). Vegan: community ecology package. R package version 1.17-4. http://cran. r-project. org>. Acesso em *23*, 2010.
24. Delhomme, N., Mähler, N., Schiffthaler, B., Sundell, D., Mannapperuma, C., Hvidsten, T.R., and Street, N.R. (2014). Guidelines for RNA-Seq data analysis. Epigenesys Protoc *67*, 1-24.
25. Kopylova, E., Noé, L., and Touzet, H. (2012). SortMeRNA: fast and accurate filtering of ribosomal RNAs in metatranscriptomic data. Bioinformatics *28*, 3211-3217.
26. Andrews, S., Krueger, F., Segonds-Pichon, A., Biggins, L., Krueger, C., and Wingett, S. (2010). FastQC. A quality control tool for high throughput sequence data *370*.
27. Bolger, A.M., Lohse, M., and Usadel, B. (2014). Trimmomatic: a flexible trimmer for Illumina sequence data. Bioinformatics *30*, 2114-2120.

28. Karolchik, D., Barber, G.P., Casper, J., Clawson, H., Cline, M.S., Diekhans, M., Dreszer, T.R., Fujita, P.A., Guruvadoo, L., and Haeussler, M. (2014). The UCSC genome browser database: 2014 update. Nucleic acids research *42*, D764-D770.
29. Pertea, M., Kim, D., Pertea, G.M., Leek, J.T., and Salzberg, S.L. (2016). Transcript-level expression analysis of RNA-seq experiments with HISAT, StringTie and Ballgown. Nature protocols *11*, 1650-1667.
30. Team, R.C. (2013). R: A language and environment for statistical computing.
31. Trapnell, C., Hendrickson, D.G., Sauvageau, M., Goff, L., Rinn, J.L., and Pachter, L. (2013). Differential analysis of gene regulation at transcript resolution with RNA-seq. Nature biotechnology *31*, 46-53.
32. Bult, C.J., Blake, J.A., Smith, C.L., Kadin, J.A., and Richardson, J.E. (2019). Mouse genome database (MGD) 2019. Nucleic acids research *47*, D801-D806.
33. Watts, S.C., Ritchie, S.C., Inouye, M., and Holt, K.E. (2019). FastSpar: rapid and scalable correlation estimation for compositional data. Bioinformatics *35*, 1064-1066.
34. Shannon, P., Markiel, A., Ozier, O., Baliga, N.S., Wang, J.T., Ramage, D., Amin, N., Schwikowski, B., and Ideker, T. (2003). Cytoscape: a software environment for integrated models of biomolecular interaction networks. Genome research *13*, 2498-2504.
35. Bushnell, B., Rood, J., and Singer, E. (2017). BBMerge–accurate paired shotgun read merging via overlap. PLoS One *12*, e0185056.
36. Campbell, M., Oakeson, K.F., Yandell, M., Halpert, J.R., and Dearing, D. (2016). The draft genome sequence and annotation of the desert woodrat Neotoma lepida. Genomics Data *9*, 58-59.
37. Li, H. (2013). Aligning sequence reads, clone sequences and assembly contigs with BWA-MEM. arXiv preprint arXiv:1303.3997.
38. Nurk, S., Meleshko, D., Korobeynikov, A., and Pevzner, P.A. (2017). metaSPAdes: a new versatile metagenomic assembler. Genome research *27*, 824-834.
39. Seemann, T. (2014). Prokka: rapid prokaryotic genome annotation. Bioinformatics *30*, 2068-2069.
40. Consortium, U. (2015). UniProt: a hub for protein information. Nucleic acids research *43*, D204-D212.
41. Pedruzzi, I., Rivoire, C., Auchincloss, A.H., Coudert, E., Keller, G., De Castro, E., Baratin, D., Cuche, B.A., Bougueleret, L., and Poux, S. (2015). HAMAP in 2015: updates to the protein family classification and annotation system. Nucleic acids research *43*, D1064-D1070.
42. Fu, L., Niu, B., Zhu, Z., Wu, S., and Li, W. (2012). CD-HIT: accelerated for clustering the next-generation sequencing data. Bioinformatics *28*, 3150-3152.
43. Love, M.I., Huber, W., and Anders, S. (2014). Moderated estimation of fold change and dispersion for RNA-seq data with DESeq2. Genome biology *15*, 1.
44. Miller, I.J., Rees, E.R., Ross, J., Miller, I., Baxa, J., Lopera, J., Kerby, R.L., Rey, F.E., and Kwan, J.C. (2019). Autometa: automated extraction of microbial genomes from individual shotgun metagenomes. Nucleic acids research *47*, e57-e57.

45. Kachroo, N., Monga, M., and Miller, A.W. (2022). Comparative functional analysis of the urinary tract microbiome for individuals with or without calcium oxalate calculi. Urolithiasis *50*, 303-317. 10.1007/s00240-022-01314-5.
46. Chen, K.-T., Liu, C.-L., Huang, S.-H., Shen, H.-T., Shieh, Y.-K., Chiu, H.-T., and Lu, C.L. (2018). CSAR: a contig scaffolding tool using algebraic rearrangements. Bioinformatics *34*, 109-111.
47. Simpson, J.T., Wong, K., Jackman, S.D., Schein, J.E., Jones, S.J., and Birol, I. (2009). ABySS: a parallel assembler for short read sequence data. Genome research *19*, 1117-1123.
48. Asnicar, F., Thomas, A.M., Beghini, F., Mengoni, C., Manara, S., Manghi, P., Zhu, Q., Bolzan, M., Cumbo, F., and May, U. (2020). Precise phylogenetic analysis of microbial isolates and genomes from metagenomes using PhyloPhlAn 3.0. Nature communications *11*, 1-10.
49. Bowers, R.M., Kyrpides, N.C., Stepanauskas, R., Harmon-Smith, M., Doud, D., Reddy, T., Schulz, F., Jarett, J., Rivers, A.R., and Eloe-Fadrosh, E.A. (2017). Minimum information about a single amplified genome (MISAG) and a metagenome-assembled genome (MIMAG) of bacteria and archaea. Nature biotechnology *35*, 725-731.
50. Kanehisa, M., Sato, Y., Furumichi, M., Morishima, K., and Tanabe, M. (2018). New approach for understanding genome variations in KEGG. Nucleic acids research *47*, D590-D595.
51. Callahan, B.J., McMurdie, P.J., Rosen, M.J., Han, A.W., Johnson, A.J.A., and Holmes, S.P. (2016). DADA2: high-resolution sample inference from Illumina amplicon data. Nature methods *13*, 581.
52. Balvočiūtė, M., and Huson, D.H. (2017). SILVA, RDP, Greengenes, NCBI and OTT—how do these taxonomies compare? BMC genomics *18*, 114.
53. Bodenhofer, U., Bonatesta, E., Horejš-Kainrath, C., and Hochreiter, S. (2015). msa: an R package for multiple sequence alignment. Bioinformatics *31*, 3997-3999.
54. Schliep, K.P. (2011). phangorn: phylogenetic analysis in R. Bioinformatics *27*, 592-593.
55. McMurdie, P.J., and Holmes, S. (2013). phyloseq: an R package for reproducible interactive analysis and graphics of microbiome census data. PloS one *8*, e61217.
56. Lozupone, C., Hamady, M., and Knight, R. (2006). UniFrac–an online tool for comparing microbial community diversity in a phylogenetic context. BMC bioinformatics *7*, 1.